AD-A057 443 ARMY AVIATION ENGINEERING FLIGHT ACTIVITY EDWARDS AF--ETC F/G 20/4
AH-1G HELICOPTER MAIN ROTOR FLOW SURVEY.(U)
APR 78 B H BOIRUN, E E BAILES, R P JEFFERIS

UNCLASSIFIED USAAFFA-74-02 NL

1 OF 1
AD A057443

END
DATE FILMED
9-78
DDC

(14) USAAEFA [redacted]-74-02

LEVEL II

AH-1G HELICOPTER MAIN ROTOR FLOW SURVEY.

(9) FINAL REPORT. May-Oct 75,

(10) BARCLAY H. BOIRUN, [redacted]

EDWARD E. BAILES, [redacted]

ROBERT P. JEFFERIS, [redacted]

JAMES A. ARNOLD [redacted]

JOSEPH C. MEISS [redacted]

(12) 90p

(11) APR[redacted]78

Approved for public release; distribution unlimited.

UNITED STATES ARMY AVIATION ENGINEERING FLIGHT ACTIVITY
EDWARDS AIR FORCE BASE, CALIFORNIA 93523

DISCLAIMER NOTICE

The findings of this report are not to be construed as an official Department of the Army position unless so designated by other authorized documents.

DISPOSITION INSTRUCTIONS

Destroy this report when it is no longer needed. Do not return it to the originator.

TRADE NAMES

The use of trade names in this report does not constitute an official endorsement or approval of the use of the commercial hardware and software.

UNCLASSIFIED

SECURITY CLASSIFICATION OF THIS PAGE (When Data Entered)

REPORT DOCUMENTATION PAGE		READ INSTRUCTIONS BEFORE COMPLETING FORM
1. REPORT NUMBER USAAEFA PROJECT NO. 74-02	2. GOVT ACCESSION NO.	3. RECIPIENT'S CATALOG NUMBER
4. TITLE (and Subtitle) AH-1G HELICOPTER MAIN ROTOR FLOW SURVEY		5. TYPE OF REPORT & PERIOD COVERED MAY - OCT 1975 6. PERFORMING ORG. REPORT NUMBER USAAEFA PROJECT NO. 74-02
7. AUTHOR(s) BARCLAY H. BOIRUN, EDWARD E. BAILES, ROBERT P. JEFFERIS, MAJ JAMES A. ARNOLD, CW3 JOSEPH C. MEISS		8. CONTRACT OR GRANT NUMBER(s)
9. PERFORMING ORGANIZATION NAME AND ADDRESS US ARMY AVIATION ENGINEERING FLIGHT ACTIVITY EDWARDS AIR FORCE BASE, CALIFORNIA 93523		10. PROGRAM ELEMENT, PROJECT, TASK AREA & WORK UNIT NUMBERS DI-4-RR263-04-DI-EC
11. CONTROLLING OFFICE NAME AND ADDRESS US ARMY AVIATION ENGINEERING FLIGHT ACTIVITY EDWARDS AIR FORCE BASE, CALIFORNIA 93523		12. REPORT DATE APRIL 1978 13. NUMBER OF PAGES 92
14. MONITORING AGENCY NAME & ADDRESS(if different from Controlling Office)		15. SECURITY CLASS. (of this report) UNCLASSIFIED 15a. DECLASSIFICATION/DOWNGRADING SCHEDULE NA

16. DISTRIBUTION STATEMENT (of this Report)

Approved for public release; distribution unlimited.

17. DISTRIBUTION STATEMENT (of the abstract entered in Block 20, if different from Report)

18. SUPPLEMENTARY NOTES

19. KEY WORDS (Continue on reverse side if necessary and identify by block number)

Airflow data
Rotor flow environment
Unguided missile firing
AH-1G helicopter

20. ABSTRACT (Continue on reverse side if necessary and identify by block number)

The Army requirement to fire unguided missiles from attack helicopters in hover and low-speed flight conditions has generated a need to accurately predict the rotor flow environment through which the missile must travel. The United States Army Aviation Engineering Flight Activity was requested by the United States Army Missile Command to provide representative flight

→ next page

(continued)

DD FORM 1 JAN 73 1473 EDITION OF 1 NOV 65 IS OBSOLETE

UNCLASSIFIED

SECURITY CLASSIFICATION OF THIS PAGE (When Data Entered)

20. Abstract

is presented
test airflow data with which to determine the launch behavior of missiles and assess the accuracy of theoretical flow field prediction models. A UH-1M helicopter was previously used to develop instrumentation and test methodology for conducting the airflow survey which were applied to the AH-1G test program. The general test objective was to define the rotor wake boundary and three-dimensional airflow velocity components as a function of forward speed.

A total of 32 test flights were conducted for a total of 20 hours of productive test time. Flight tests were conducted from May through October 1975. Airflow measurements were made on the left side of the AH-1G helicopter for the volume of air immediately ahead of the wing store mounts to the nose of the aircraft with total vector split-film anemometers. Six of these airflow probes were mounted on an airflow rake which was moved forward in increments to encompass the total test volume. Measurements were taken during stabilized level flight and hover test conditions. The rotor blade azimuth position was correlated with the transient airflow data to determine the effects of blade passage. Low airspeed and hover test conditions were established with the LORAS II low airspeed system. Due to the fragile nature of this type of anemometer, and an unusually complex data recording and reduction system, only about 63 percent of the target data matrix was successfully recorded. The data were presented in terms of time-averaged and transient local flow velocity and direction as a function of probe position and airspeed. The transient data were recorded at a rate of 1000 samples per second for a period of 1 second (5.4 rotor revolutions). The anemometers provided consistent and instantaneous three-dimensional velocity component data, and the sample rate was sufficient for accurate wave-form reproduction at frequencies up to 200 hertz. The overall accuracy of the velocity data was estimated to be ±5 percent of reading. The airflow data were reduced and stored on magnetic tapes and have been forwarded to the Army Missile Command for further analysis.

TABLE OF CONTENTS

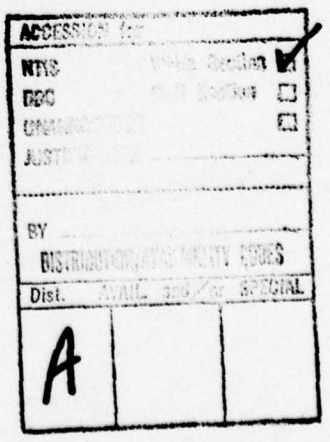

INTRODUCTION

BACKGROUND

1. The Army requirement to fire unguided missiles from attack helicopters in hover and low-speed flight conditions has generated a need to accurately establish the airflow environment through which the missile must travel. The Aeroballistics Directorate of the United States Army Missile Research and Development Command (MIRADCOM) requested the United States Army Aviation Systems Command (AVSCOM), since redesignated the Army Aviation Research and Development Command (AVRADCOM) (ref 1, app A), to provide measured flight test airflow data. These data were required to determine the initial flight behavior of the missiles, and to assess the accuracy of the theoretical flow field prediction models. AVRADCOM directed the United States Army Aviation Engineering Flight Activity (USAAEFA) to conduct a flow field survey to meet the MIRADCOM requirements (ref 2). The measured flow data will be analyzed by MIRADCOM to aid in improving the design of the missile system and for comparison with analytical airflow prediction methods.

2. USAAEFA Project No. 72-05 (ref 3, app A) developed instrumentation and test methodology for the flow field survey using a UH-1M helicopter. The airflow measurements were obtained from total vector split-film anemometers which were mounted on a support structure specifically designed to reduce the failures caused by vibration during the UH-1M testing. The AH-1G rake structure was designed and tested by the MIRADCOM Structural Dynamics Laboratory through a contract with Sperry-Rand Corporation.

TEST OBJECTIVES

3. The general test objective was to determine the instantaneous flow field in a test volume adjacent to the AH-1G helicopter as specified in reference 1, appendix A. The specific objectives were as follows:

a. Determine the rotor wake boundary position in the vicinity of the weapons mount location as a function of forward airspeed.

b. Determine instantaneous three-dimensional velocity components of airflow in the test volume as a function of forward airspeed.

c. Determine the effect of aircraft sideslip and angle of attack on the velocity components at a given forward airspeed.

d. Determine the effects of rotor blade position on the instantaneous velocity components.

e. Determine the reliability and assess the accuracy of the flow measurement instrumentation.

DESCRIPTION

4. The testing was conducted on an AH-1G helicopter, SN 67-15844, manufactured by Bell Helicopter Company. A detailed description of the AH-1G is contained in the operator's manual (ref 4, app A). An external structure designed to reduce anemometer vibration levels was attached to the AH-1G wing store mount to support an airflow instrumentation rake. The structure and mounting allowed longitudinal adjustments of the rake fore and aft, and vertical adjustment by inverting the rake structure. The structure could be mounted on either side of the helicopter, but only the left side was used in these tests. The test volume encompassed by the rake structure is shown by figure A. Six airflow sensors were supported by the rake structure, as shown in figure B. The sensors were split-film total vector anemometers, manufactured by Thermo-Systems, Inc., of Bloomington, Minnesota (ref 5, app A), and are described in detail in appendix B. These airflow sensors are capable of measuring instantaneous velocity vectors with a frequency response which is flat to 1 kHz. The spatial resolution of the hot-film probe is approximately 0.027 inch, which is much smaller than any multiaxis pressure probe. This type of sensor also has the ability to measure flow direction over the full solid angle (4 π steradians). For laboratory conditions, the specified accuracy over a 300 feet per second (ft/sec) velocity range is ±3 percent of reading in magnitude, and ±1.5 percent in direction.

TEST SCOPE

5. The flow field under the main rotor of the AH-1G was defined primarily during stabilized level flight and hover. The conditions shown in table 1 were flown at a constant thrust coefficient (C_T) of .00475 and repeated for each of the 16 rake positions required to define the test volume shown in figure A. Additional tests were made with the variations of hover height and sideslip angle and climbing and descending flight.

FIGURE A
AIRFLOW INSTRUMENTATION INSTALLATION
ON THE AH-1G HELICOPTER

● DATA PROBE LOCATION

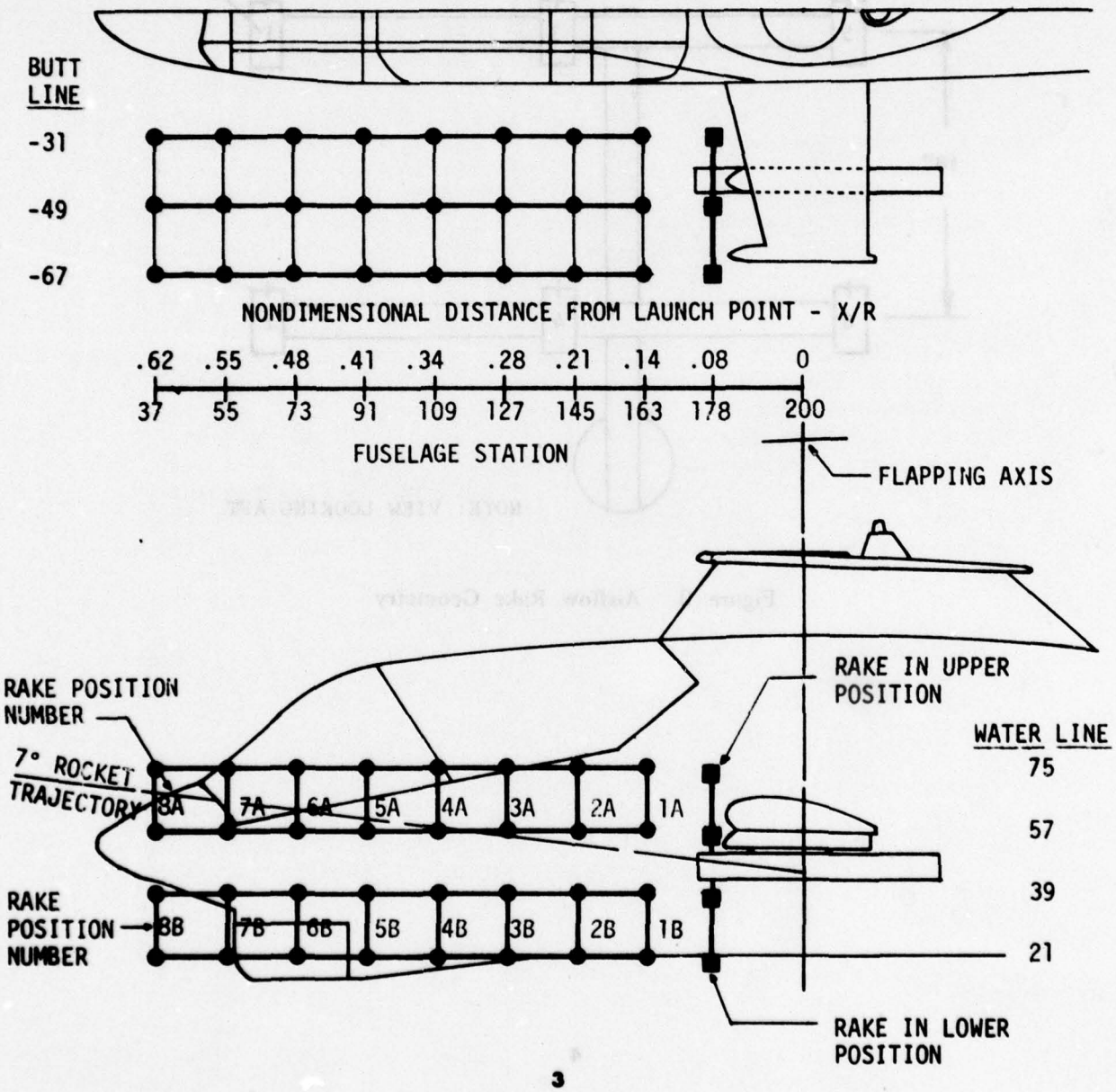

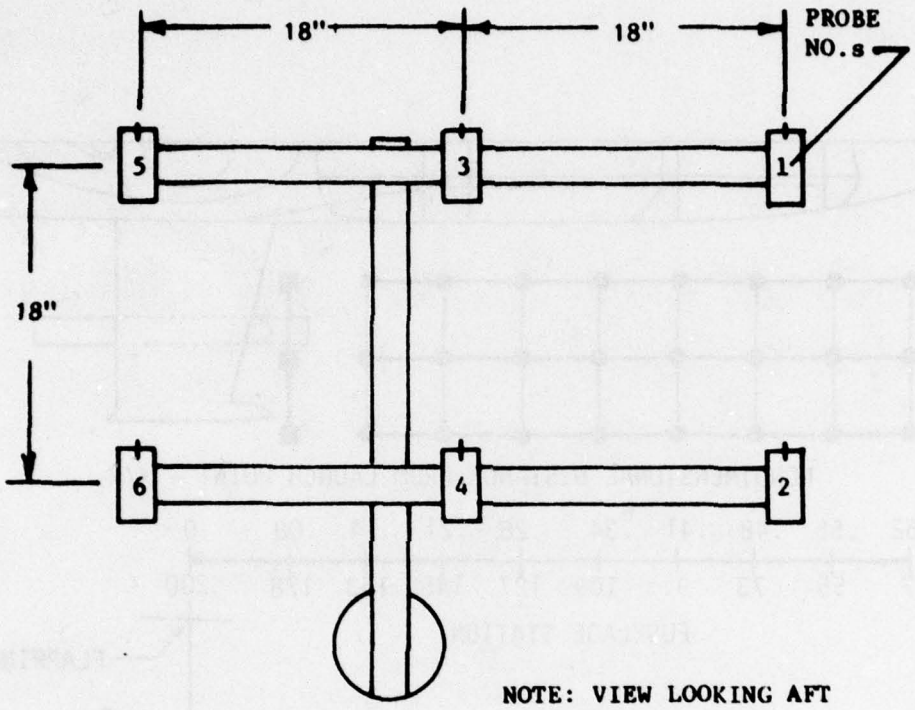

Figure B. Airflow Rake Geometry

Table 1. AH-1G Airflow Survey Test Conditions.[1]

True Airspeed (kt)	Advance Ratio (μ)	Forward Velocity (ft/sec)
Zero (hover)	Zero	Zero
5.9	.0134	10
11.8	.0268	20
17.8	.0402	30
23.7	.0536	40
30.0	.068	50
35.5	.0804	60
59.2	.1340	100
71.0	.1608	120
88.8	.201	150
118.5	.268	200

[1]Average test conditions:
Gross weight: 8250 pounds.
Density altitude: 5000 feet.
Rotor speed: 324 rpm.
Thrust coefficient: .00475.
Longitudinal center of gravity (cg): fuselage station (FS) 196.
Lateral cg: buttline zero.

6. A total of 32 flights were completed, requiring 35 flight hours, of which 20 hours were productive test time. Due to the fragile nature of the anemometers, some flights had inoperational probes, as shown in table 2. The test schedule did not allow sufficient time to repeat flights when sensor malfunctions occurred.

TEST METHODOLOGY

7. The test aircraft was configured to simulate missile armament, and ballast was added as required to maintain constant gross weight and cg. Prior to commencing the airflow test flights, the LORAS II and the aircraft test boom pitot-static airspeed systems were calibrated using the trailing bomb and ground pace vehicle test methods.

Table 2. Summary of Anemometer Positions.

Rake Position Number	Fuselage Station of Probe 1	Water Line of Probe 1	Anemometer Serial No./Calibration For Probe Location No.[1]					
			1	2	3	4	5	6
1A	163	75	Note[2]	127D	128C	130C	131D	133C
2A	145	75	125D	127D	128C	129D	131D	133C
3A	127	75	125D	127D	128C	Note[3]	131D	133C
4A	109	75	125D	127D	128C	Note[3]	131D	133C
5A	91	75	125D	127D	128C	Note[3]	131D	133C
6A	73	75	125D	127D	128C	Note[3]	131D	133C
7A	55	75	125D	127D	128C	129D	Note[3]	133C
8A	37	75	125D	127D	128C	129D	Note[3]	133C
8B	37	39	125D	127D	128C	129D	Note[3]	133C
7B	55	39	125D	127D	128C	129D	131D	133C
6B	73	39	125D	127D	128C	129D	131D	133C
5B	91	39	125D	127D	128C	129D	131D	133C
4B	109	39	Note[3]	Note[2]	125D	129D	131D	133C
3B	127	39	Note[3]	Note[2]	125D	129D	131D	133C
2B	145	39	Note[3]	Note[2]	125D	129D	131D	133C
1B	163	39	Note[3]	Note[2]	125D	129D	131D	133C

[1]The buttline of Probe Nos.:

1 and 2 = 67
3 and 4 = 49
5 and 6 = 31

[2]Probe position vacant.

[3]Probe provided faulty data.

RESULTS AND DISCUSSION

GENERAL

8. The flow field under the main rotor of the AH-1G was measured in stabilized level flight and hover. The tests were flown at a constant aim C_T of .00475 and repeated for each of the 16 rake positions required to define the test volume. About 63 percent of the target data matrix was achieved, with an estimated error of ±5 percent in total velocity measurements. The measured data are presented in terms of time-averaged local velocity and direction as a function of probe position and aircraft advance ratio. Sample time-variant data for two probe positions are presented, and ground effect variations on a third position are also shown. The time-variant data for all test points were recorded on magnetic data tapes and provided to MICOM for further analysis.

ACCURACY AND RELIABILITY OF AIRFLOW INSTRUMENTATION

9. The fragile nature and electronic complexity of the anemometers led to numerous ground accidents and failures. The time frame for testing did not allow for probe repair, and on some flights, spare probes were not available. This resulted in a number of vacancies in the data matrix shown in table 2. About 20 percent of the probe positions were not measured due to partially inoperative probes or unavailability of spares. Another 17 percent of the target data matrices could not be reduced due to a data timing problem. However, when the system was functioning, the instrumentation provided consistent and instantaneous three-dimensional velocity and directional data. The sample rate of 1000 per second was sufficient for accurate wave-form reproduction to a frequency of 200 Hz.

10. Mass tuning of the AH-1G airflow rake was required to reduce the maximum vibration values at the probe mounts to less than 1g at 10.8 Hz, a frequency of 2-per-rotor-revolution (2/rev). No in-flight anemometer failures were attributed to the vibration during this test. This represents a major improvement over the vibration-related failures which occurred on the UH-1M test (ref 3, app A). The only rake vibration effect noted was at a frequency of 135 Hz, where movement of the probe tip influenced the directional data. A dynamic filter with an upper cut-off frequency of 160 Hz was used to remove this vibration influence during final data processing.

11. The accuracy of the velocity and direction data from the anemometers cannot be stated in absolute terms. However, a reasonable estimate can be obtained from an analysis of test data and a theoretical downwash model (ref 6, app A). The airspeed system calibration showed the nose boom to read 6 to 7 ft/sec lower than the free stream (approximately a 5-percent position error at 100 knots true airspeed (KTAS)). These data agreed well with the prediction for position error on a UH-1B helicopter from the theoretical model discussed in reference 6. The model also predicted a similar position error for the probe locations that measured for the nose boom airspeed system. Figures 1 through 32, appendix D, show a comparison of averaged total probe velocity with free stream velocity obtained from the nose boom airspeed system. The variation in the velocity data in the range of $\mu = 0.12$ to 0.28 is from slightly higher than free stream to approximately 10 percent below the free stream value. Correcting the data for a 5-percent position error would yield results within approximately ±5 percent of the free stream values.

TIME-AVERAGED AIRFLOW CHARACTERISTICS IN LEVEL FLIGHT

12. The variation of the time-averaged airflow velocity and direction data with nondimensional forward airspeed (μ) is shown in figures 1 through 32, appendix D. The velocity components are presented in terms of the air relative to the helicopter. Each figure shows the results for the three horizontal probe locations along the airflow rake (either probe numbers 1, 3, and 5, or 2, 4, and 6). The figures are grouped in order of decreasing fuselage station, starting at the most aft location and moving forward in 18-inch increments. Four figures (one for each water line (WL)) are required to complete one FS location. The rake position number and the corresponding FS, WL, and buttline (BL) of each probe number are provided on the figures. The absence of a probe position symbol or missing velocity point indicates that the data were not available. Figures 18 through 31 show that probes number 4 and 5 provided faulty directional or component velocity data. Occasionally, a probe produced data in excess of free stream values by as much as 5 percent. The bridge balance was set on each split-film sensor prior to each flight. Unfortunately, the bridge balance could change with successive test points so that assuming a constant bias error may not be valid, and no new correction was made.

13. During low-speed flight, the maximum average flow velocity measured was approximately 90 ft/sec at an average local angle of attack (α) of -95 degrees in hover at FS 37 (figs. 29 through 32, app D), which was the most forward rake position. This position also provided the lowest airspeed ($\mu = .02$) where the probe passed

through the rotor flow to free stream conditions (wake transition speed). Generally, the wake transition speed increased as rake position moved aft, reaching $\mu \approx .050$ at rake position 1 (FS = 163). The average flow velocity at this position was the lowest measured in hover, approximately 50 ft/sec at an average α of -75 degrees. Figure 5 shows the effects of a slight rearward velocity ($\mu \approx -.005$). The total airflow velocity in hover is primarily vertical and rapidly changes to a longitudinal direction with a slight increase in rearward speed. Since this rake position is near the rocket launch point, a significant variable flow condition could exist with slight airspeed shifts from hover.

14. Figure C presents the time-averaged vertical velocity in out-of-ground-effect (OGE) hover obtained from the flight test data matrix for the 7-degree rocket trajectory line shown in figure A. The minimum and maximum variation of vertical velocity occurring during a 1-second time period are also shown for each test point. The test data are compared to the analytical data predicted for the AH-1G in reference 7, appendix A. The analytical predictions were projected for a rotor thrust coefficient of 0.00472 and tip speed of 746 ft/sec. The general trends were very similar; however, the measured velocity from the flight test was approximately 20 percent greater. The time-variant oscillations during tests were also generally larger than those obtained from the analytical method. The analytical data of reference 6 were previously found to be in close agreement with model helicopter airflow data obtained in a wind tunnel.

TRANSIENT AIRFLOW CHARACTERISTICS IN LEVEL FLIGHT

15. The airflow data were recorded for a 1-second sampling period in a stabilized flight condition. The data reduction method utilized the rotor azimuth reference to begin the data processing at a known blade position (TIME = 0 at $\psi = 54.2 \pm 2.4$ deg). From this point, the blade azimuth position was obtained by integrating the average rotor speed during the data run. The anemometer data recorded in flight were converted on the ground to engineering units at the rate of 1000 samples per second and recorded on magnetic data tape, as discussed in appendix D. Figures 34 through 56, appendix D, present typical results of the transient airflow characteristics at several selected probe locations. A more detailed analysis will be provided in the MIRADCOM final report.

16. Figures 33 through 37, appendix D, show the results for probe number 3 in rake position number 2 during low-speed flight. Figure 33 shows the flow characteristics in OGE hover, and the forward airspeed for each succeeding figure is about 10 ft/sec higher. Each low-speed data run shows a unique wave-form pattern

VARIATION OF VERTICAL VELOCITY ALONG
ROCKET TRAJECTORY IN OGE HOVER
FOR THE AH-1G HELICOPTER

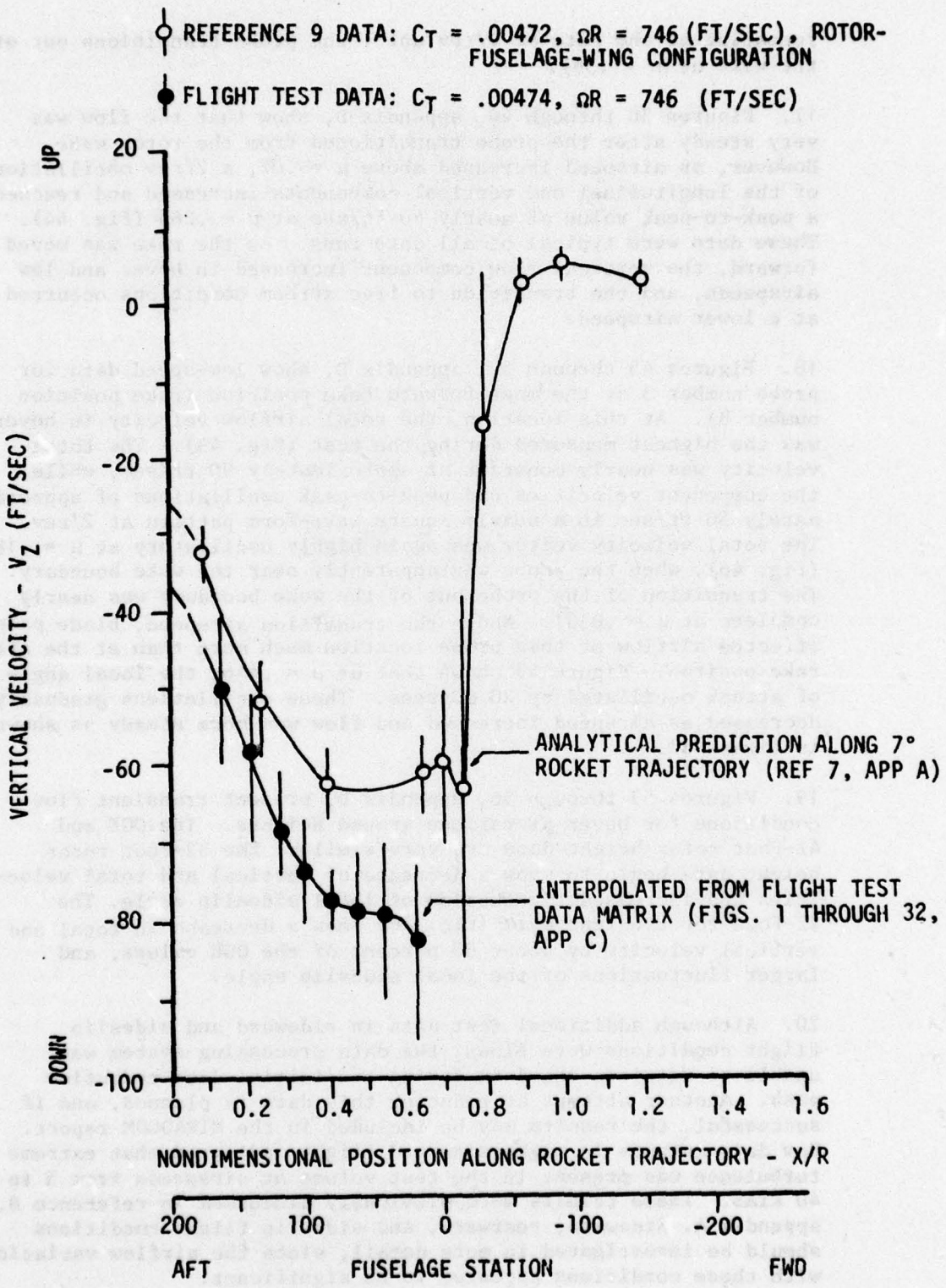

repeating at the rate of 2/rev until the probe transitions out of the wake at (μ = .56).

17. Figures 38 through 44, appendix D, show that the flow was very steady after the probe transitioned from the rotor wake. However, as airspeed increased above μ = .07, a 2/rev oscillation of the longitudinal and vertical components increased and reached a peak-to-peak value of nearly 40 ft/sec at μ = .265 (fig. 44). These data were typical of all data runs. As the rake was moved forward, the vertical flow component increased in hover and low airspeeds, and the transition to free stream conditions occurred at a lower airspeed.

18. Figures 45 through 52, appendix D, show low-speed data for probe number 3 at the most forward rake position (rake position number 8). At this location, the total airflow velocity in hover was the highest measured during the test (fig. 45). The total velocity was nearly constant at approximately 90 ft/sec, while the component velocities had peak-to-peak oscillations of approximately 50 ft/sec in a nearly square wave-form pattern at 2/rev. The total velocity vector was again highly oscillatory at μ = .184 (fig. 46), when the probe was apparently near the wake boundary. The transition of the probe out of the wake boundary was nearly complete at μ = .0337. Above the transition airspeed, blade passage affected airflow at this probe location much more than at the aft rake positon. Figure 49 shows that at μ = .446, the local angle of attack oscillated by 20 degrees. These oscillations gradually decreased as airspeed increased and flow was more steady as shown in figure 52.

19. Figures 53 through 56, appendix D, present transient flow conditions for hover at various ground heights. The OGE and 42-foot rotor height data are very similar. The 32-foot rotor height data begin to show a decrease of vertical and total velocities and increased fluctuation of local sideslip angle. The 22-foot rotor height data (fig. 56) show a decrease in total and vertical velocity by about 60 percent of the OGE values, and larger fluctuations of the local sideslip angle.

20. Although additional test data in sideward and sideslip flight conditions were flown, the data processing system was unable to retrieve the data during the initial data reduction pass. Another attempt at reducing this data is planned, and if successful, the results may be included in the MIRADCOM report. Raw data outputs in right sideward flight indicated that extreme turbulence was present in the test volume at airspeeds from 5 to 40 KTAS. These results were previously discussed in reference 8, appendix A. Sideward, rearward, and sideslip flight conditions should be investigated in more detail, since the airflow variation with these conditions appeared to be significant.

CONCLUSIONS

GENERAL

21. Although approximately 37 percent of the target airflow data matrix were not available, a large volume of transient airflow data in the vicinity of the rocket launch trajectory were successfully obtained. The transient response of the anemometers appeared to be of high quality, and the data should be useful for further analysis.

SPECIFIC

22. The data rate of 1000 samples per second was sufficient for accurate wave-form reproduction up to 210 Hz (para 9).

23. Mass tuning of the AH-1G airflow rake was required to reduce vibration at the probe mounts. The vibration at the primary frequency of 10.8 Hz (2/rev) was reduced to 1g or less for all flight conditions (para 10).

24. No in-flight failures of the anemometers were attributable to excessive vibrations (para 10).

25. A filter with a cut-off of 160 Hz was required to remove the influence of high-frequency vibration from the raw anemometer data (para 10).

26. The time-averaged vertical velocities in OGE hover varied from approximately 50 ft/sec at FS 163 to 90 ft/sec at FS 37. These values were nearly 20 percent higher than predicted for the AH-1G by analytical and wind tunnel results (para 14).

27. Within the rotor wake, the total flow velocity remained relatively constant, although the component velocities had peak-to-peak oscillations as high as 50 ft/sec (para 16).

28. The total flow velocity was highly oscillatory near the rotor wake boundary (para 16).

29. The ground effect at a rotor height of 22 feet reduced the total and vertical flow velocity by 60 percent of the OGE values (para 19).

30. Sideward, rearward, and sideslip flight conditions were observed to significantly affect the airflow in the vicinity of the rocket trajectory (paras 13 and 20).

RECOMMENDATIONS

31. The AH-1G airflow data should be subjected to further analysis and correlated with current wake analysis methods.

32. Future airflow survey tests should include more measurements in sideward, rearward, and sideslip flight conditions.

APPENDIX A. REFERENCES

1. Letter, MICOM, AMSMI-RDK, 18 October 1961, subject: Helicopter Flow Measurement Flight Test.

2. Letter, AVSCOM, AMSAV-EFT, 3 February 1972, subject: Test Directive No. 72-05, Helicopter Flow Field Survey.

3. Final Report, USAAEFA Project No. 72-05, *Rotor Flow Survey Program, UH-1M Helicopter*, May 1974.

4. Technical Manual, TM 55-1520-221-10, *AH-1G Operator's Manual*, April 1967.

5. Technical Manual, Thermo-Systems, Inc., *Operating and Service Manual for Model 2080 and Model 1080D Total Vector Anemometer*, 1973.

6. Report, Cornell Aeronautical Laboratory, Inc. *Theoretical Prediction of the Flow in the Wake of a Helicopter Rotor*, Cal No. BB-1994-S-1, September 1965.

7. Report, United Technologies Research Center, No. R77-912571-15, *Investigation of the Airflow of a Hovering Model Helicopter at Rocket Trajectory and Wind Sensor Locations*, July 1977.

8. Interim Report, USAAEFA Project No. 74-02, *AH-1G Helicopter Flow Field Survey*, presented at the proceedings of the Conference on the Effects of Helicopter Downwash on Free Projectiles, November 1975.

APPENDIX B. INSTRUMENTATION

GENERAL

1. The test instrumentation was installed, calibrated, and maintained by USAAEFA. The split-film anemometers were calibrated and repaired under contract by Thermosystems, Inc. The LORAS II low airspeed sensor was leased from Pacer System, Inc., and installed and calibrated by USAAEFA. A test boom with swiveling pitot-static head was also installed on the nose of the aircraft and was connected to test airspeed and altimeter indicators on both instrument panels and recorded on magnetic tape. All data were obtained from test instrumentation and were displayed on or recorded from the following aircraft sources:

Pilot Panel

Airspeed (boom)
Airspeed (LORAS forward)
Airspeed (LORAS lateral)
Altitude (boom)
Rate of climb (boom)
Angle of sideslip (boom)
Radar altimeter

Engineer Panel

Airspeed (boom)
Altitude (boom)
Outside air temperature
Fuel counter
Data system controls

Digital (PCM) Parameters

Time of day
Engineer event
Run number counter
Rotor blip
Fuel counter
Rotor speed (analog)
Rotor speed (digital)
Altimeter (radar)
Pressure altitude (boom)
Ambient air temperature (boom)

Angle of attack (boom)
Angle of sideslip (boom)
Airspeed low range (boom)
Airspeed (LORAS longitudinal)
Airspeed (lORAS Lateral)
Pitch attitude
Roll attitude
Lateral swashplate angle
Longitudinal swashplate angle

2. The total vector anemometer data were recorded on the frequency modulation (FM) system. There were 6 anemometers, each of which output 6 bridge voltages, requiring 36 separate data channels.

TOTAL VECTOR ANEMOMETERS

3. Figure 1 shows the flow survey anemometer signal flow. Airflow was sensed by six Thermo-Systems, Inc., Model 1080 total vector anemometers. Each anemometer included a Model 1296F probe and a companion 1083 signal conditioning module. A Model-C rack with a 1082 control circuit completed the anemometer system.

4. Each probe (figs. 2 and 3) consists of three sensor rods, a support shaft, a copper-constantan temperature sensor mounted between the rods, and a pneumatic probe-tip shield. The three-dimensional coordinate system is formed by the six independent films (two per rod, separated azimuthally). Each of the film sensors forms one leg of a bridge circuit which is completed by components in the associated 1083 control circuit module. The 1083 module regulates bridge excitation power so that a constant temperature ratio is maintained between each film and a nominal shielded ambient temperature value (actually controlled by bridge completion resistors). The bridge excitation voltage is scaled for a zero- to 5-volt direct current (VDC) output for an airflow scale of zero to 150 ft/sec. In addition to the six-bridge and scaling circuits, each signal conditioning module provides a compensated reference junction for the tip thermocouple. Compensated thermocouple electromotive force (EMF) is amplified and a linear zero- to 5-VDC analog temperature output is provided for correcting flow vectors measured at nonstandard conditions. The tip thermocouples and pneumatic shield actuators were not used. A single Rosemount type 102AU2CK platinum resistance total temperature probe and a Rosemount 510BF signal conditioning amplifier were used for ambient temperature measurements. This subsystem

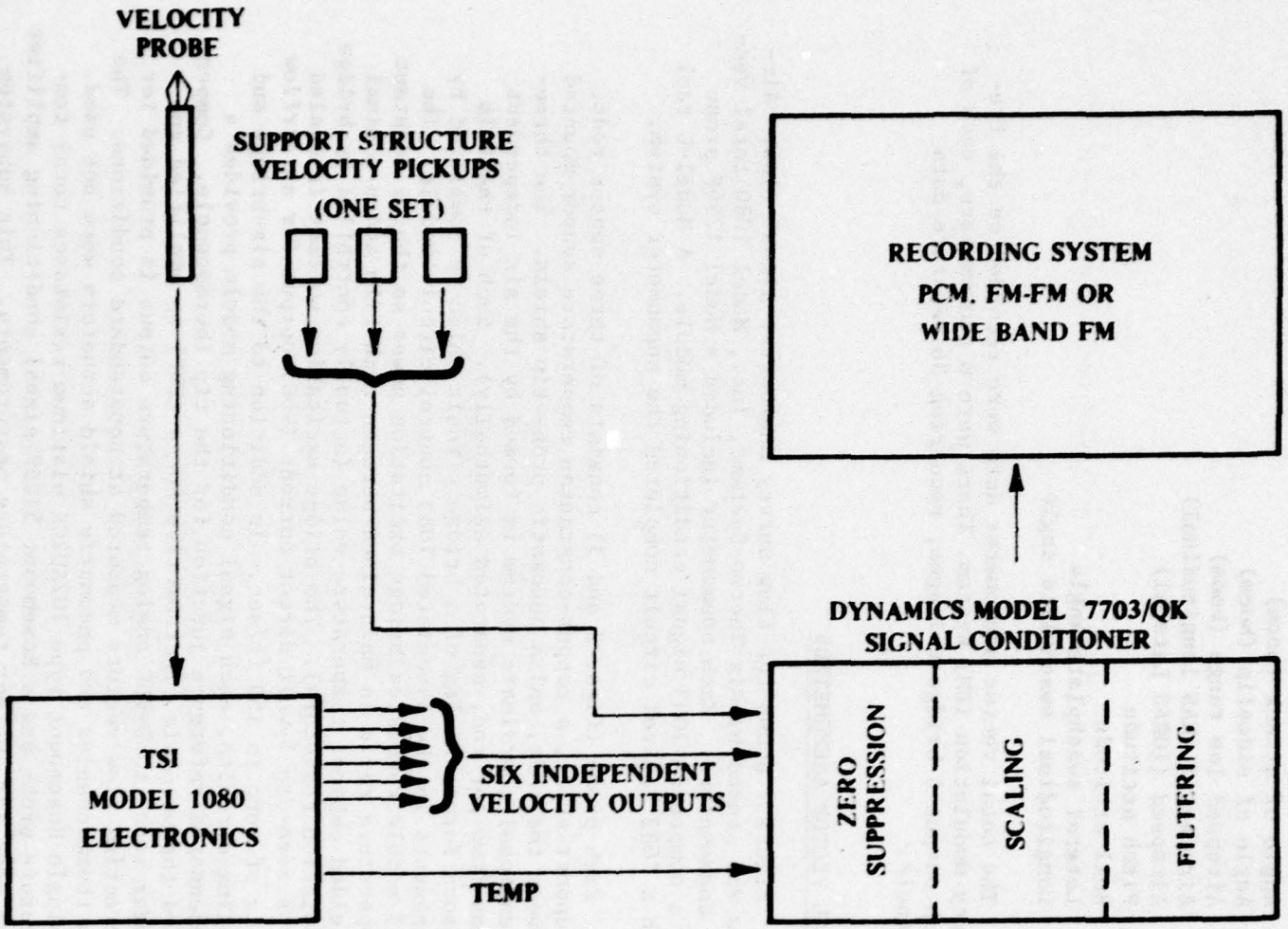

Figure 1. Instrumentation Schematic

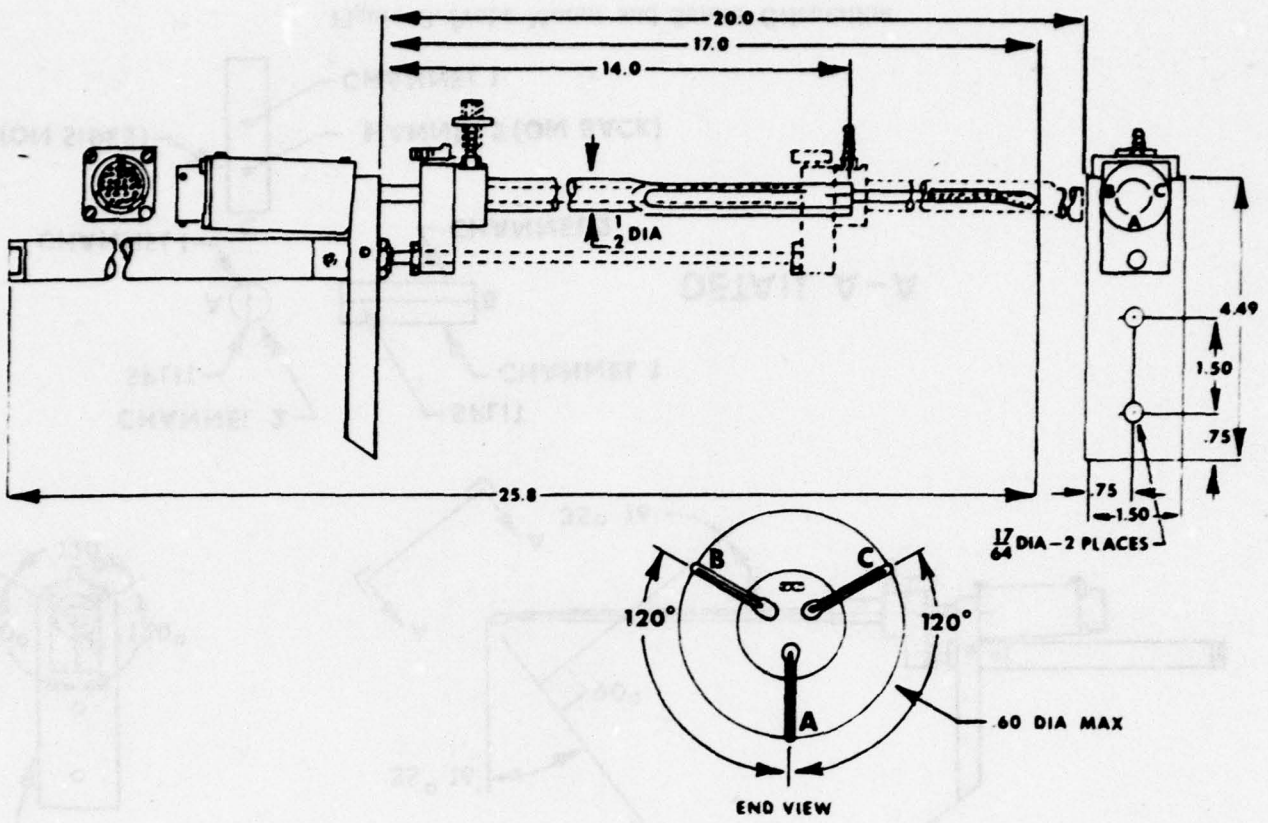

Figure 2. Model 1296F Probe.

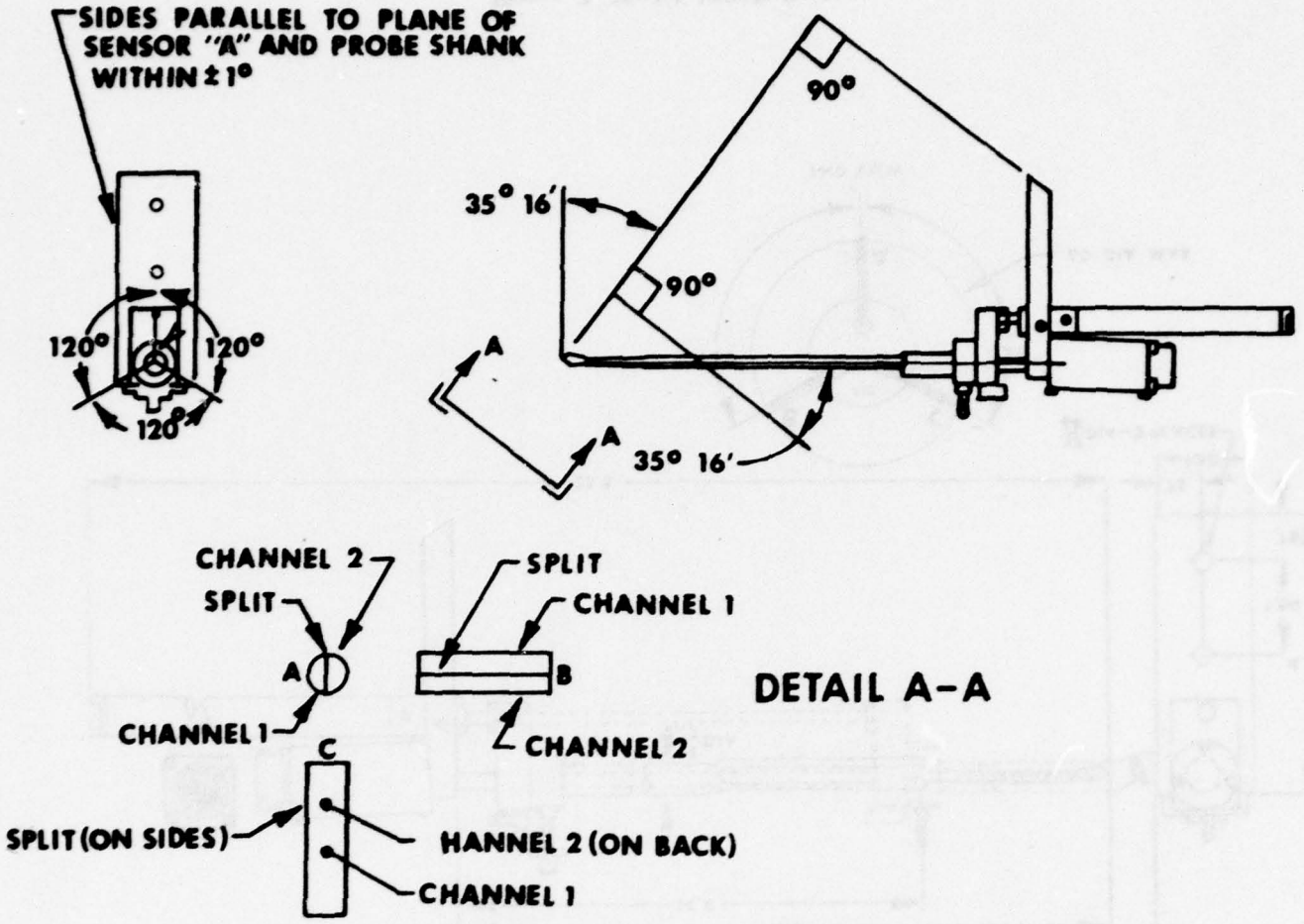

Figure 3. Probe Mount and Sensor Orientation

yielded higher accuracy than the tip thermocouples could have, and only one channel was required. The probe shields were activated manually to eliminate the need for pneumatic valves, plumbing, and gas storage bottles on the aircraft.

5. Six single-ended, high-level velocity signals (from each probe) were routed directly to a Vector, Inc., constant bandwith voltage controlled oscillators (VCOS), a 120 kHz reference oscillator, and a mixer amplifier. VCO deviation was ±4 kHz from a center frequency of 25, 40, 55, 79, 85, or 100 kHz for a zero- to 5-VDC input. The discriminators used for data reduction were EMR Model 4150's. They incorporated low pass output filters with a constant amplitude response (7-pole Butterworth) and a cutoff frequency of 2 kHz. The output of a mixer amplifier was routed directly to a tape track and to a telemetry switch for real time monitor selection. The reference oscillator signals were used to provide tape speed compensation during data reduction.

6. The aircraft parameters were recorded in a PCM format using Spacecraft, Inc., PCM units. Each unit contains a 64-channel, high-level analog multiplexer (tiered groups of 8), a 112-bit discrete bi-level multiplexer (14-transistor logic compatible 8-bit words), an analog buffer/sample and hold amplifier, an 8-bit, zero- to 5-VDC successive approximation analog to digital converter, and all control and formatting circuits required to construct a serial IRIG compatible NRZC PCM bit stream suitable for magnetic tape recording or radio frequency (RF) telemetry. The complete analog portion has been proven to be a monotonic ±0.5 percent full scale system, with a maximum nonlinearity of ±1/2 least significant bit (LSB). Bit rates are hardware programmable in powers of 2 from 32 K-bits per second to 512 K-bits per second, yielding fixed main-frame rates from 50 frames/sec to 800 frames/sec. This test used a frame rate of 100 frames/sec (100 samples/sec/parameter).

7. The airflow data were set up for automatic cueing and synchronization with rotor azimuth by an event pulse in the PCM frame. The flight engineer would turn the tape recorder on while a desired flight condition was being established. When he decided that valid data were available, he activated an event switch on his console to arm the even pulse circuit. An optical proximity sensor mounted on the rotor swashplate defined rotor azimuth once per rotor revolution, and the armed event circuit activated the event pulse as soon as a rotor azimuth pulse was received. The event pulse had a fixed duration of 1 second and was supercommutated in the PCM unit to a sample rate of 800 samples/sec, allowing automatic data cueing to rotor azimuth with an uncertainty of ±2.4 degrees at a rotor speed of 324 rpm.

8. A time code generator provided parallel binary coded decimal (BCD) time-of-day information IRIG-B for in-line timing in the PCM main frame and a modulated 1 = kHz serial code on an independent tape track for automatic tape searching.

9. All of the data were recorded on magnetic tape. An Ampex AR-700 intermediate band recorder was used with a tape speed of 30 in./sec with the following track layout:

Track	Signal	Format
1	Voice (intercom)	Direct
2	Time	1 KHz Mod Code
3	PCM	Serial BCD
4	Probe #1	FM/FM CBW*
5	Probe #2	FM/FM CBW
6	Probe #3	FM/FM CBW
7	Probe #4	FM/FM CBW
8	Probe #5	FM/FM CBW
9	Probe #6	FM/FM CBW
10	Rack vibrations	FM/FM CBW
11	Rack vibrations	FM/FM CBW
12	Tachometer reference	Direct

10. Preflight anemometer performance checks were made at a zero velocity point and at a standard flow setting using the manufacturer-supplied calibration data. Integral to each probe tip shield is a sonic orifice, which serves to establish a self-test flow point when a regulated 50-PSIG gas supply is applied to the rear of the shield. Bridge output ratios were checked against

*CBW: Constant bandwidth

manufacturer-suggested tolerances with a voltage divider and null detector at the test flow point. Manufacturer-supplied airflow data, exact pressure measurements of the test gas source, barometric pressure readings, and ambient temperature readings were put into the probe data reduction equations for these checks.

LORAS II LOW AIRSPEED SYSTEM

11. Low forward airspeeds were measured by the LORAS II airspeed system, which includes a sensor unit mounted above the main rotor head, an airspeed computer, control panel, and longitudinal and lateral airspeed indicators. The sensor unit consists of two rotating venturi tubes oriented on opposite ends of a tubular rotor. The venturis are connected to a differential pressure transducer. The rotating assembly is 13.0 inches in diameter and is driven at a constant rotational speed of 720 rpm. The total velocity at each tube consists of a steady component from the constant rotational speed, and a sinusoidal component at rotational frequency from the translational velocity. The differential pressure transducer converts the sinusoidal velocity component into an electrical signal. To obtain average steady-state values, this signal is resolved into longitudinal and lateral velocity components and then filtered to remove the modulation frequency. Optional outputs, which are selected from the control panel, include total velocity and either true or indicated airspeed. The system is designed to operate from 50 KTAS rearward to 200 KTAS forward, 50 KTAS right and left laterally, and to be insensitive to vertical airspeed.

APPENDIX C. TEST TECHNIQUES AND DATA ANALYSIS METHODS

TEST TECHNIQUES

1. The aircraft was stabilized in zero sideslip level flight conditions for each test point. Altitude was increased between each test point to compensate for fuel burn-off to maintain a constant coefficient of thrust (C_T) on each data set. Airspeed and sideslip information were provided by the LORAS II airspeed system in low-speed flight and by the test boom airspeed system in high-speed flight. Test airspeeds were adjusted to maintain constant aim values of advance ratio (μ) on each test flight. The 100 percent rotor speed of 324 rpm was used for all flights.

DATA ANALYSIS METHODS

2. The nondimensional thrust coefficient (C_T) and advance ratio (μ) were computed for each test point by the relation:

$$C_T = \frac{GW}{\rho A (\Omega R)^2} \quad (1)$$

$$\mu = V_T \; 1.6878/\Omega R \quad (2)$$

Where:

GW = Aircraft gross weight (lb)

ρ = Air density (slug/ft^3)

A = Main rotor disc area (ft^2)

Ω = Main rotor rotational frequency (rad/sec)

R = Main rotor radius (ft)

V_T = True airspeed (kt) = $V_{cal}/\sqrt{\sigma}$

V_{cal} = Calibrated airspeed (kts)

σ = Air density ratio = ρ/ρ_o

Airflow Parameters

3. Each anemometer had six voltage outputs, as discussed in appendix B. These voltages were resolved into three orthogonal axes velocity components by mathematical methods provided by the manufacturer in reference 5, appendix A. This process required the development of an iterative solution software subprogram, which was added to the basic data reduction package. The resultant components (V_A, V_V, and V_C) were aligned with the axes system formed by the 3 split-film rods on each probe, as shown in figure 1.

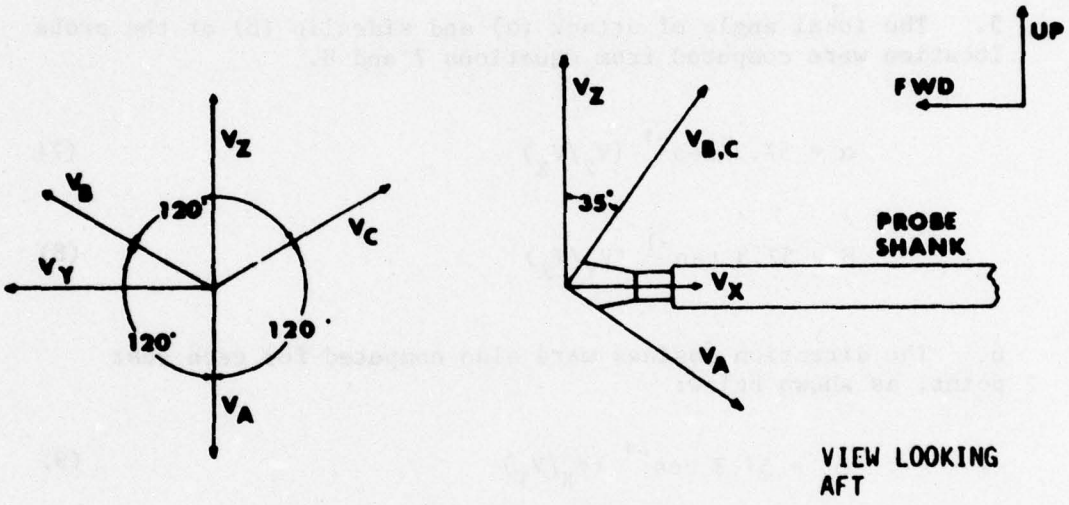

Figure 1. Anemometer Velocity Components

4. Since the probe shank was aligned with the longitudinal axis of the helicopter, the measured components were first rotated into the aircraft body axis system. This was done by applying the transformation equations 3, 4, and 5 to the calculated velocity components. The total velocity was computed from equation 6. The velocity components are shown relative to the helicopter in their positive sense. Positive V_X indicates that the flow is moving aft, positive V_Z indicates that the flow is moving up, and a positive V_Y indicates that the flow is moving right.

$$V_X = \text{Sin } 35° \ (V_A + V_B + V_C) \qquad (3)$$

$$V_Y = \text{Sin } 45^\circ \ (V_B - V_C) \tag{4}$$

$$V_Z = -\text{Cos } 35^\circ \ (V_A) + \sin 45^\circ \tan 30^\circ \ (V_C + V_B) \tag{5}$$

$$V = \sqrt{V_x^2 + V_y^2 + V_z^2} \tag{6}$$

5. The local angle of attack (α) and sideslip (β) at the probe location were computed from equations 7 and 8.

$$\alpha = 57.3 \cos^{-1} (V_Z/V_X) \tag{7}$$

$$\beta = 57.3 \tan^{-1} (V_Y/V_X) \tag{8}$$

6. The direction cosines were also computed for each test point, as shown below:

$$\Theta_x = 57.3 \cos^{-1} (V_X/V_T) \tag{9}$$

$$\Theta_y = 57.3^{-1} (V_Y/V_T) \tag{10}$$

$$\Theta_z = 57.3 \cos^{-1} (V_Z/V_T) \tag{11}$$

Output Data Format

7. The anemometer data were recorded on magnetic tape in frequency modulation (FM) format to allow processing at the desired sample rate of 1000 samples/sec. Hardware limitations allowed only 12 channels or two anemometers to be reduced on one pass of the flight tape. Therefore, three data processing passes were required to reduce the taped information data to velocities.

Probe numbers 1 and 2 were reduced in pass 1, probe numbers 3 and 4 were reduced in pass 2, and probe numbers 5 and 6 were reduced in pass number 3. These separate passes were merged onto magnetic tapes in USAAEFA standard engineering units 01 (SEU01) format. These tapes can only be read by the EMR 6135 computer; therefore, they must be coded into a BCD format to be read by other computer systems. The tapes sent to MIRADCOM were coded into data blocks of 1240 BCD characters of F14.8 format. Each data run was identified by the flight, pass, and run number and stored in the data blocks in the word number order shown in table 1. Normally, there were 1000 time points per data run followed by an average, minimum, maximum, standard deviation, start frame, event frame, and slope of each word during the run.

Table 1. Airflow Data Format on Engineering Unit Tape.

Constant Parameters		
Word	Parameter	Unit
1	Basic weight	lb
2	Basic FS cg	in.
3	Basic BL cg	in.
4	Basic WL cg	in.
5	Initial fuel volume	gal
6	Initial fuel temperature	deg
7	Initial fuel specific weight	lb/gal
8	Blank	
9	Fuselage station of probe 1 attach point	in.
10	Buttline of probe 1 attach point	in.
11	Water line of probe 1 attach point	in.
12	Blank	
13	Blank	
14	Rotor speed	rpm
15	Ambient air temperature	°C
16	Pressure ratio	—
17	Thrust coefficient ($C_T \times 10^4$)	—
18	Advance ratio ($\mu \times 10^3$)	—
19	Theoretical induced velocity in hover (v_o)	ft/sec
20	Forward velocity	ft/sec

Transient Parameters		
Word	Parameter	Unit
1	Time of day	hr, min sec, ms
2	Time of day in seconds	sec
3	Seconds from start of data run	sec
4	Frame number of data run	--
5	Probe 1, voltage 1	volts
6	Probe 1, voltage 2	volts
7	Probe 1, voltage 3	volts
8	Probe 1, voltage 4	volts
9	Probe 1, voltage 5	volts
10	Probe 1, voltage 6	volts
11	Probe 2, voltage 1	volts
12	Probe 2, voltage 2	volts
13	Probe 2, voltage 3	volts
14	Probe 2, voltage 4	volts
15	Probe 2, voltage 5	volts
16	Probe 2, voltage 6	volts
17	Total rotor azimuth from start of data run	deg
18	Rotor azimuth (zero to 360 deg)	deg
19	Probe 1, total velocity (V)	ft/sec
20	Probe 1, longitudinal velocity (V_x)	ft/sec
21	Probe 1, lateral velocity (V_y)	ft/sec
22	Probe 1, vertical velocity (V_z)	ft/sec
23	Probe 1, and of attack (α)	deg
24	Probe 1, angle of sideslip (β)	deg
25	Probe 1, direction cosine (θ_x)	deg
26	Probe 1, direction cosine (θ_y)	deg
27	Probe 1, direction cosine (θ_z)	deg
28	Probe 2, total velocity (V)	ft/sec
29	Probe 2, longitudinal velocity (V_x)	ft/sec
30	Probe 2, lateral velocity (V_y)	ft/sec
31	Probe 2, vertical velocity (V_z)	ft/sec
32	Probe 2, angle of attack (α)	deg
33	Probe 2, angle of sideslip (β)	deg
34	Probe 2, direction cosine (θ_x)	deg
35	Probe 2, direction cosine (θ_y)	deg
36	Probe 2, direction cosine (θ_z)	deg

APPENDIX D. TEST DATA

INDEX

FIGURE 1
AVERAGED AIRFLOW CHARACTERISTICS IN LEVEL FLIGHT
AH-1G USA S/N 67-6844
RAKE POSITION NO. 1A (FS = 163, WL = 75)

SYMBOL	PROBE NO.	BL
△	5	31

AVERAGE THRUST COEFFICIENT = .00475
AVERAGE ROTOR SPEED = 323.8 RPM

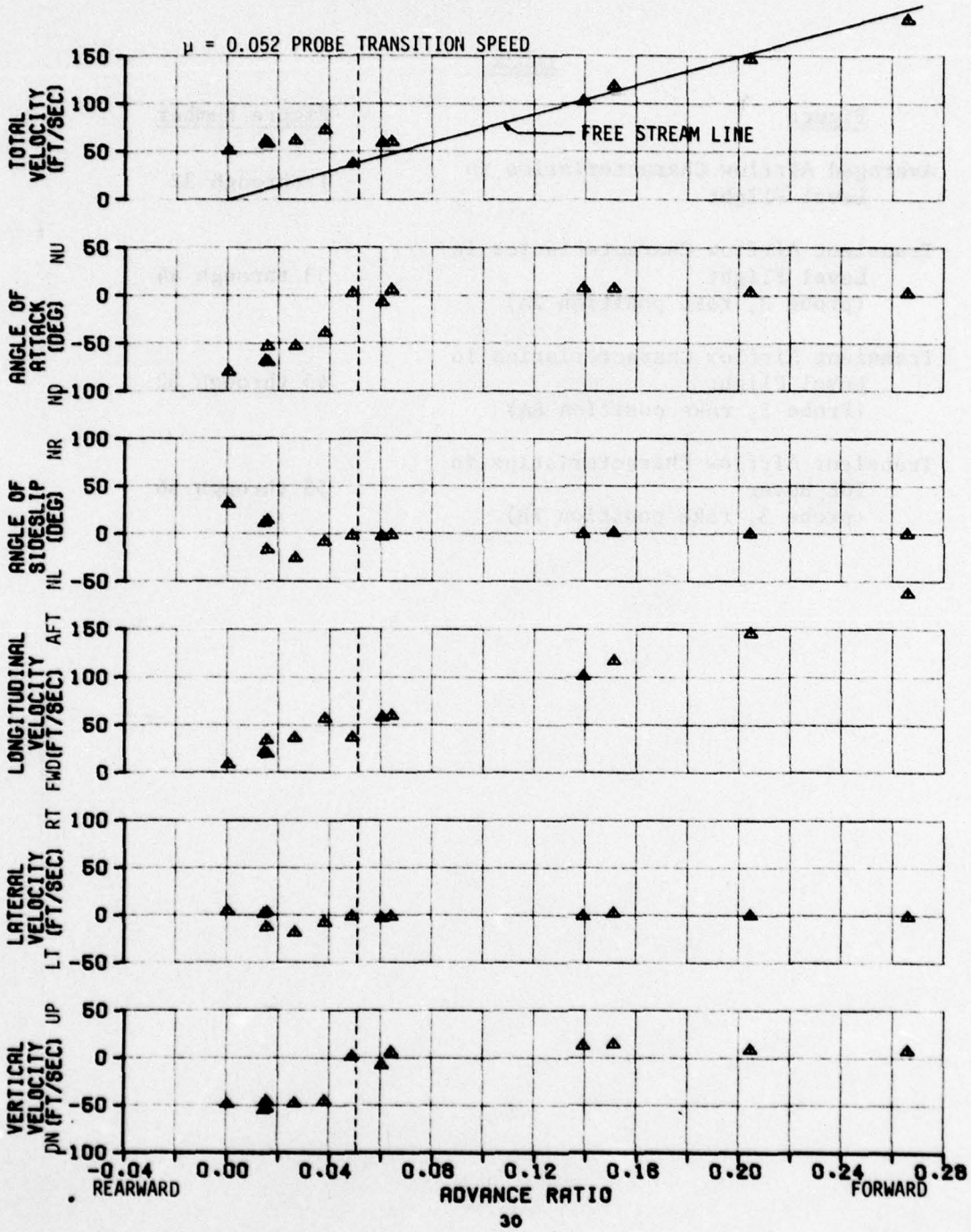

FIGURE 2
AVERAGED AIRFLOW CHARACTERISTICS IN LEVEL FLIGHT
AH-1G USA S/N 67-6844
RAKE POSITION NO. 1A (FS = 163, WL = 57)

SYMBOL	PROBE NO.	BL
Δ	6	31

AVERAGE THRUST COEFFICIENT = .00475
AVERAGE ROTOR SPEED = 323.8 RPM

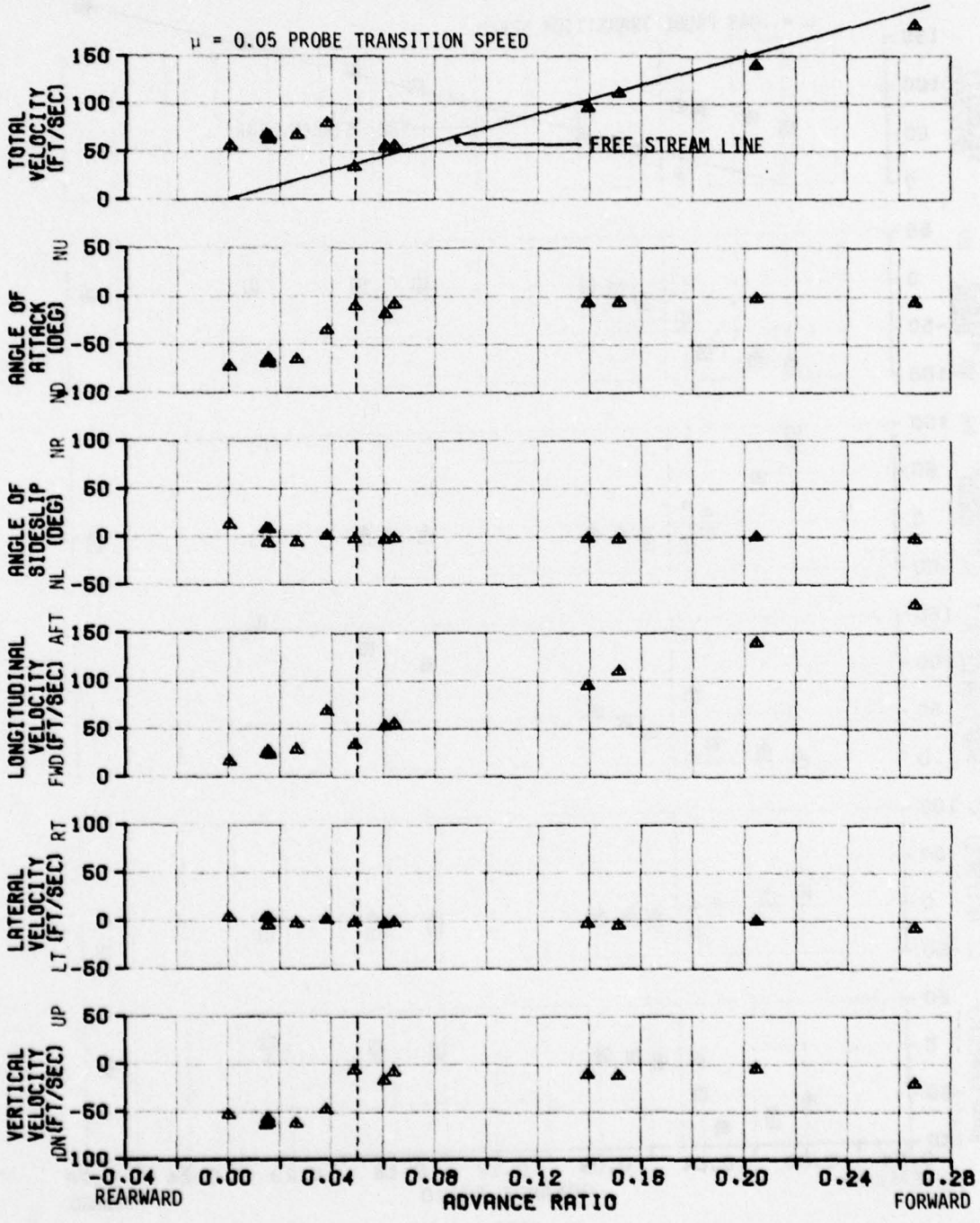

FIGURE 3
AVERAGED AIRFLOW CHARACTERISTICS IN LEVEL FLIGHT
AH-1G USA S/N 67-6844
RAKE POSITION NO. 1B (FS = 163, WL = 39)

SYMBOL	PROBE NO.	BL
□	3	49
△	5	31

AVERAGE THRUST COEFFICIENT = .00473
AVERAGE ROTOR SPEED = 324.0 RPM

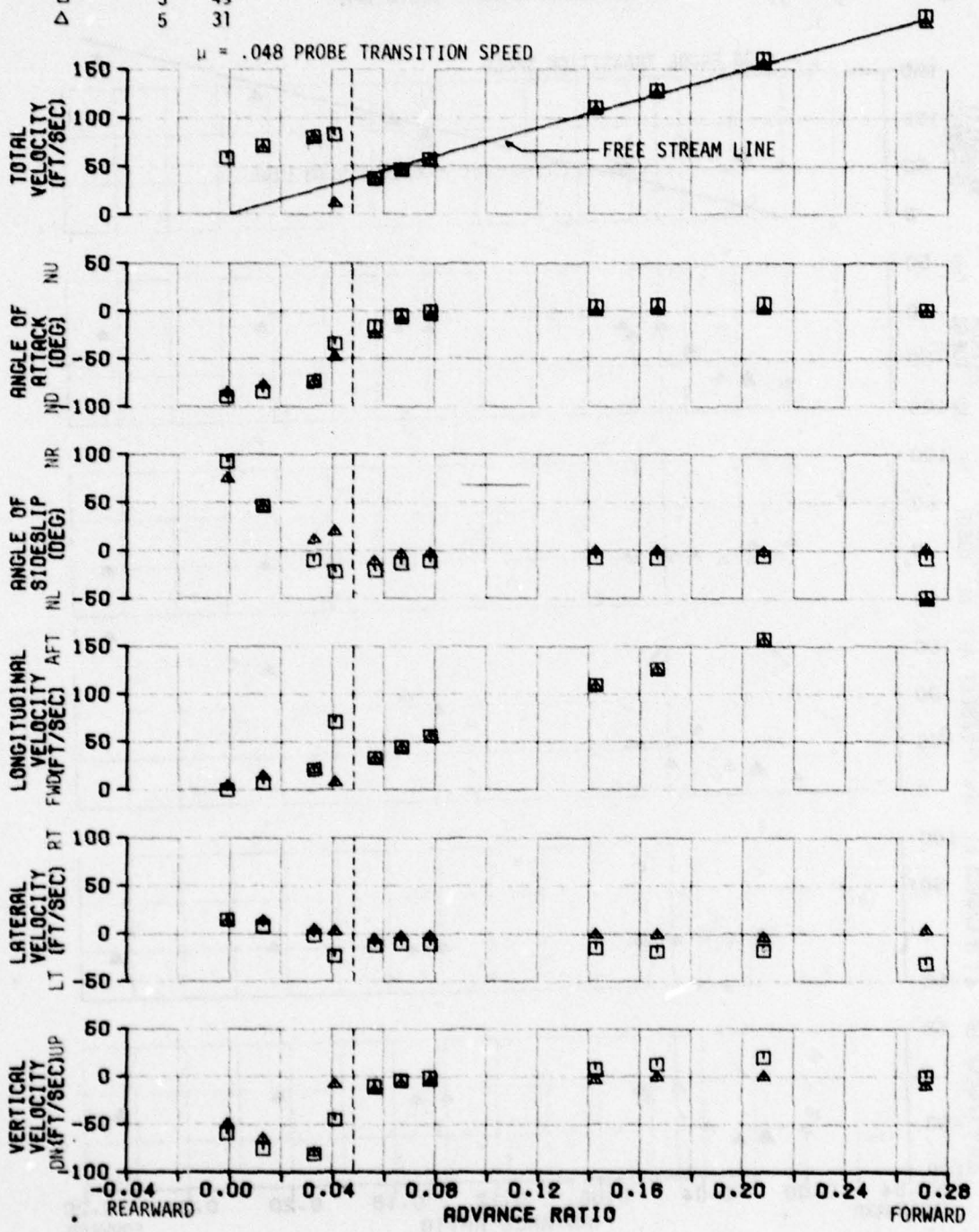

FIGURE 4
AVERAGED AIRFLOW CHARACTERISTICS IN LEVEL FLIGHT
AH-1G USA S/N 67-6844
RAKE POSITION NO. 1B (FS = 163, WL = 21)

SYMBOL	PROBE NO.	BL
□	4	49
△	6	31

AVERAGE THRUST COEFFICIENT = .00473
AVERAGE ROTOR SPEED = 324 RPM

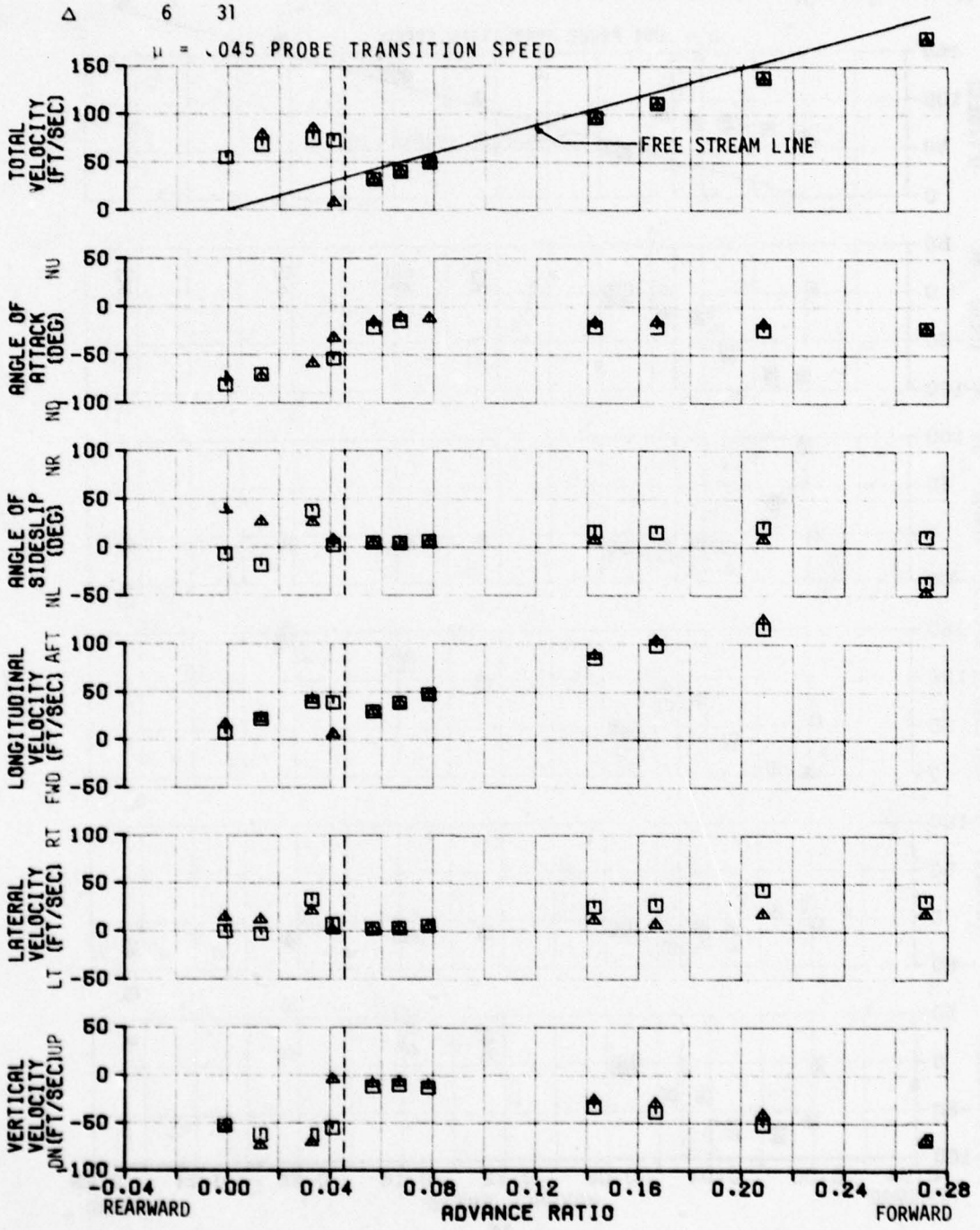

FIGURE 5
AVERAGED AIRFLOW CHARACTERISTICS IN LEVEL FLIGHT
AH-1G USA S/N 67-6844
RAKE POSITION NO. 2A (FS = 145, WL = 75)

SYMBOL	PROBE NO.	BL
□	3	49
△	5	31

AVERAGE THRUST COEFFICIENT = .00475
AVERAGE ROTOR SPEED = 323.8 RPM

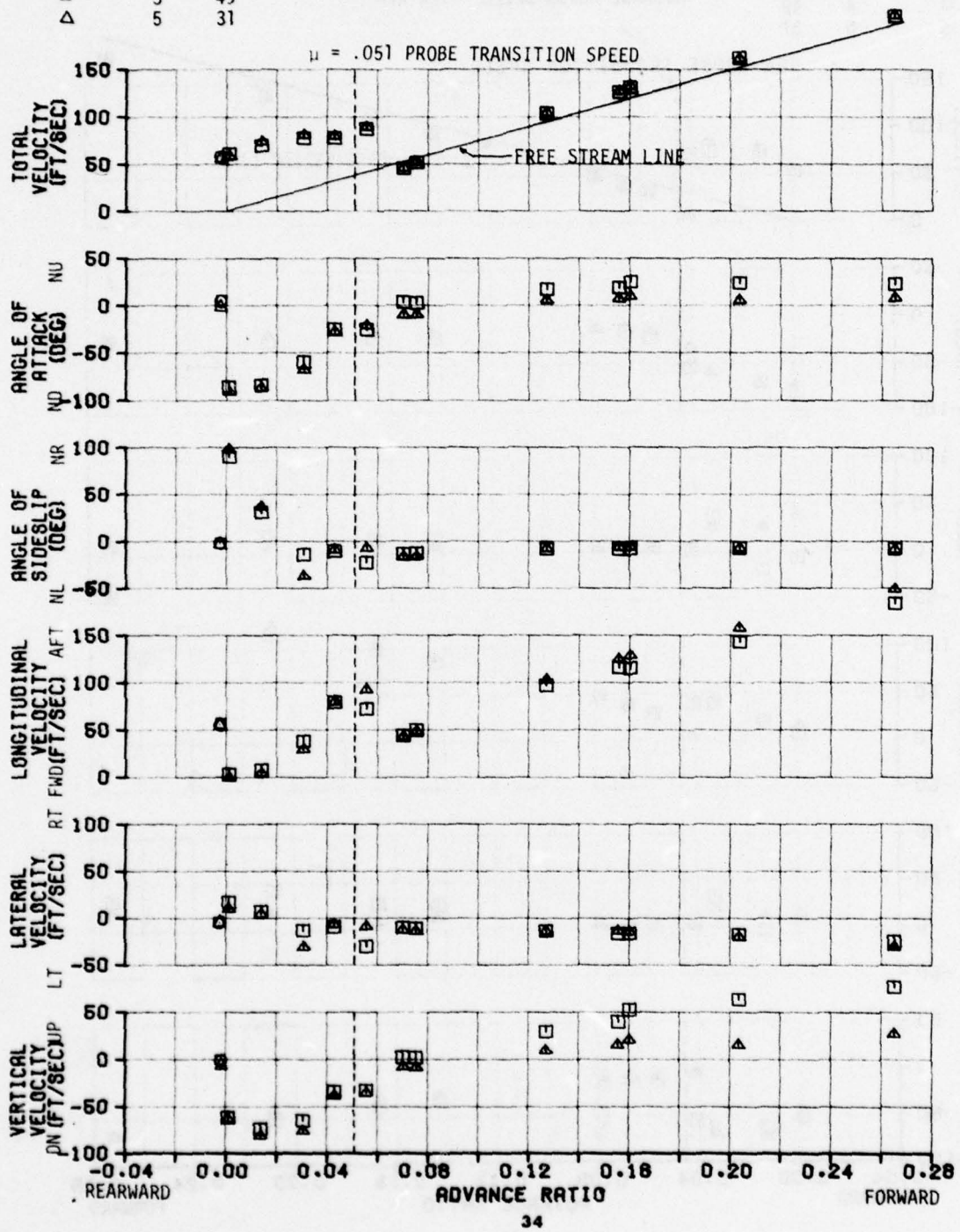

FIGURE 6
AVERAGED AIRFLOW CHARACTERISTICS IN LEVEL FLIGHT
AH-1G USA S/N 67-6844
RAKE POSITION NO. 2A (FS = 145, WL = 57)

SYMBOL	PROBE NO.	BL
□	4	49
△	6	31

AVERAGE THRUST COEFFICIENT = .00475
AVERAGE ROTOR SPEED = 323.8 RPM

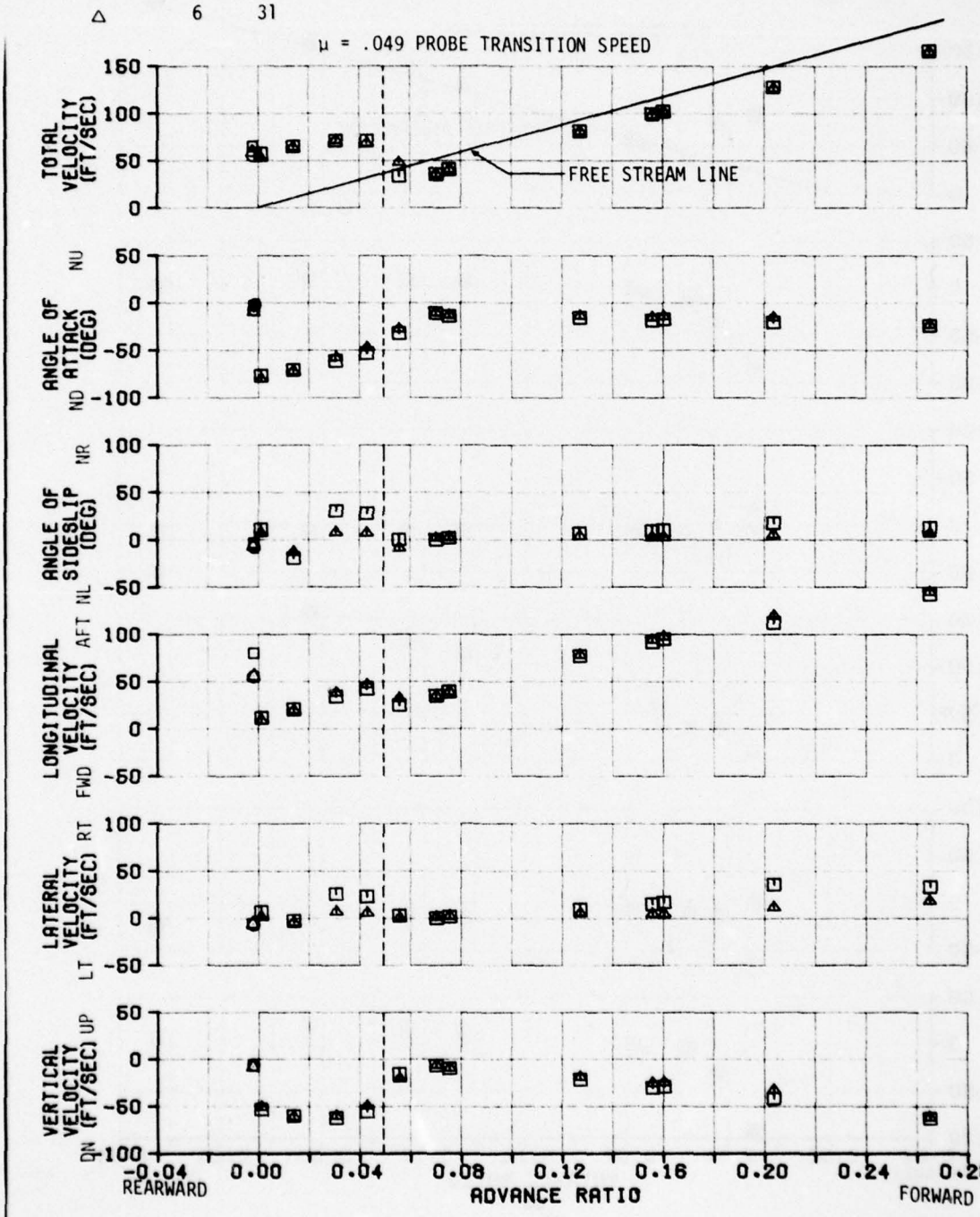

FIGURE 7
AVERAGED AIRFLOW CHARACTERISTICS IN LEVEL FLIGHT
AH-1G USA S/N 67-6844
RAKE POSITION NO. 2B (FS = 145, WL = 39)

SYMBOL	PROBE NO.	BL
□	3	49
△	5	31

AVERAGE THRUST COEFFICIENT = .00473
AVERAGE ROTOR SPEED = 323.9 RPM

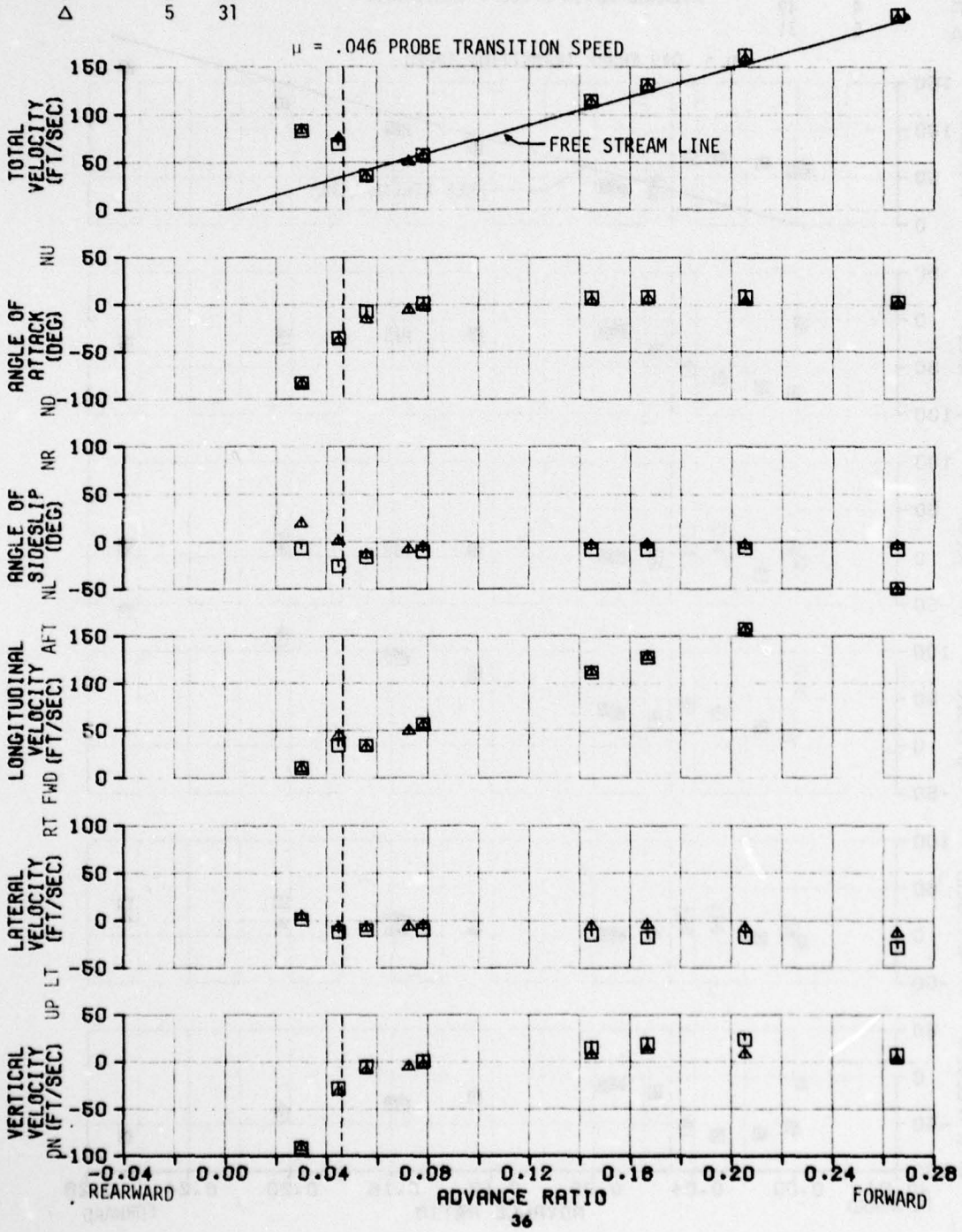

FIGURE 8
AVERAGED AIRFLOW CHARACTERISTICS IN LEVEL FLIGHT
AH-1G USA S/N 67-6844
RAKE POSITION NO.2B (FS = 145, WL = 21)

SYMBOL	PROBE NO.	BL
□	4	49
△	6	31

AVERAGE THRUST COEFFICIENT = .00473
AVERAGE ROTOR SPEED = 323.9 RPM

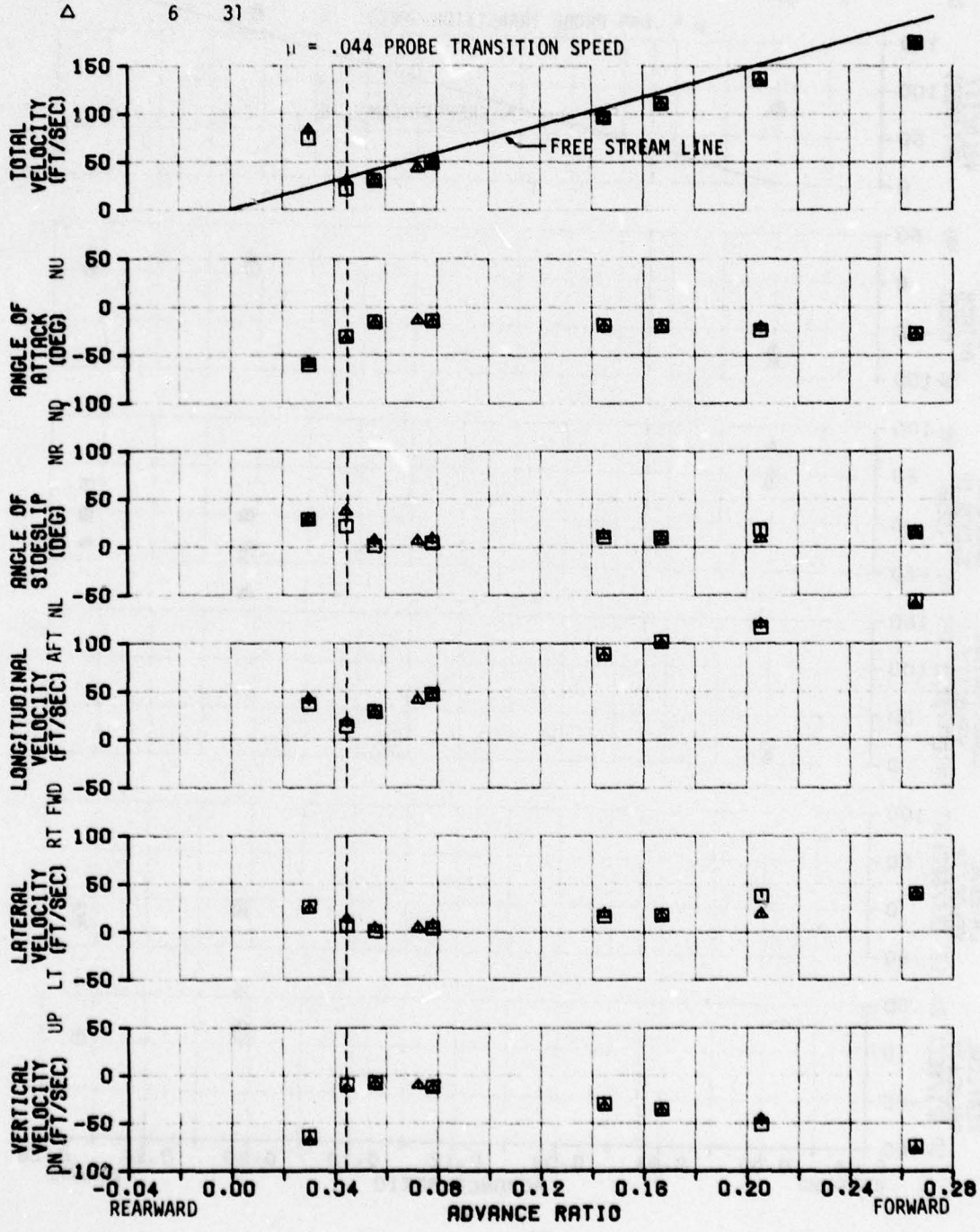

FIGURE 9
AVERAGED AIRFLOW CHARACTERISTICS IN LEVEL FLIGHT
AH-1G USA S/N 67-6844
RAKE POSITION NO. 3A (FS = 127, WL = 75)

AVERAGE THRUST COEFFICIENT = .00469
AVERAGE ROTOR SPEED = 324.4 RPM

SYMBOL	PROBE NO.	BL
○	1	67
△	5	31

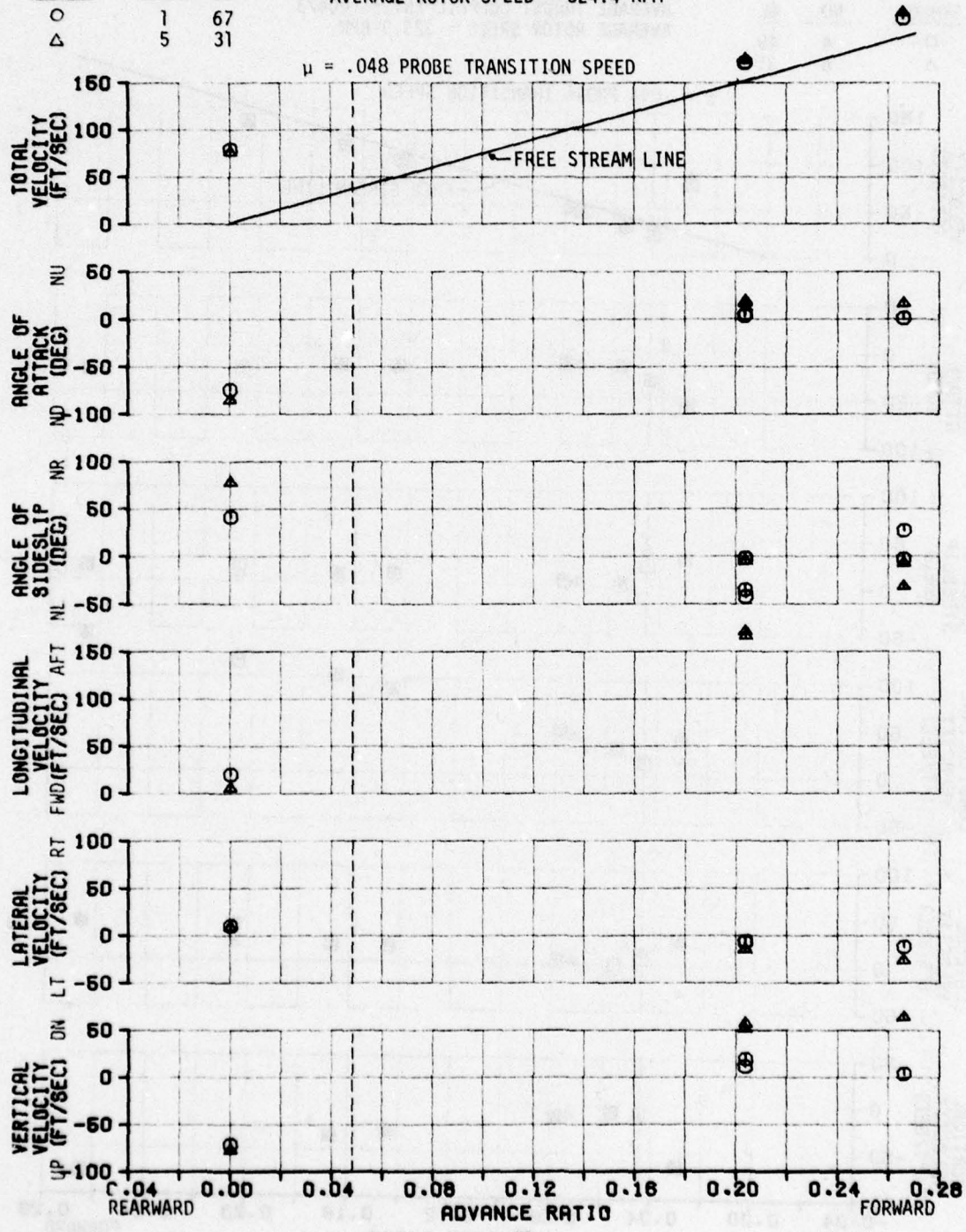

FIGURE 10
AVERAGED AIRFLOW CHARACTERISTICS IN LEVEL FLIGHT
AH-1G USA S/N 67-6844
RAKE POSITION NO. 3A (FS = 127, WL = 57)

SYMBOL	PROBE NO.	BL
○	2	67
△	6	31

AVERAGE THRUST COEFFICIENT = .00469
AVERAGE ROTOR SPEED = 324.4 RPM

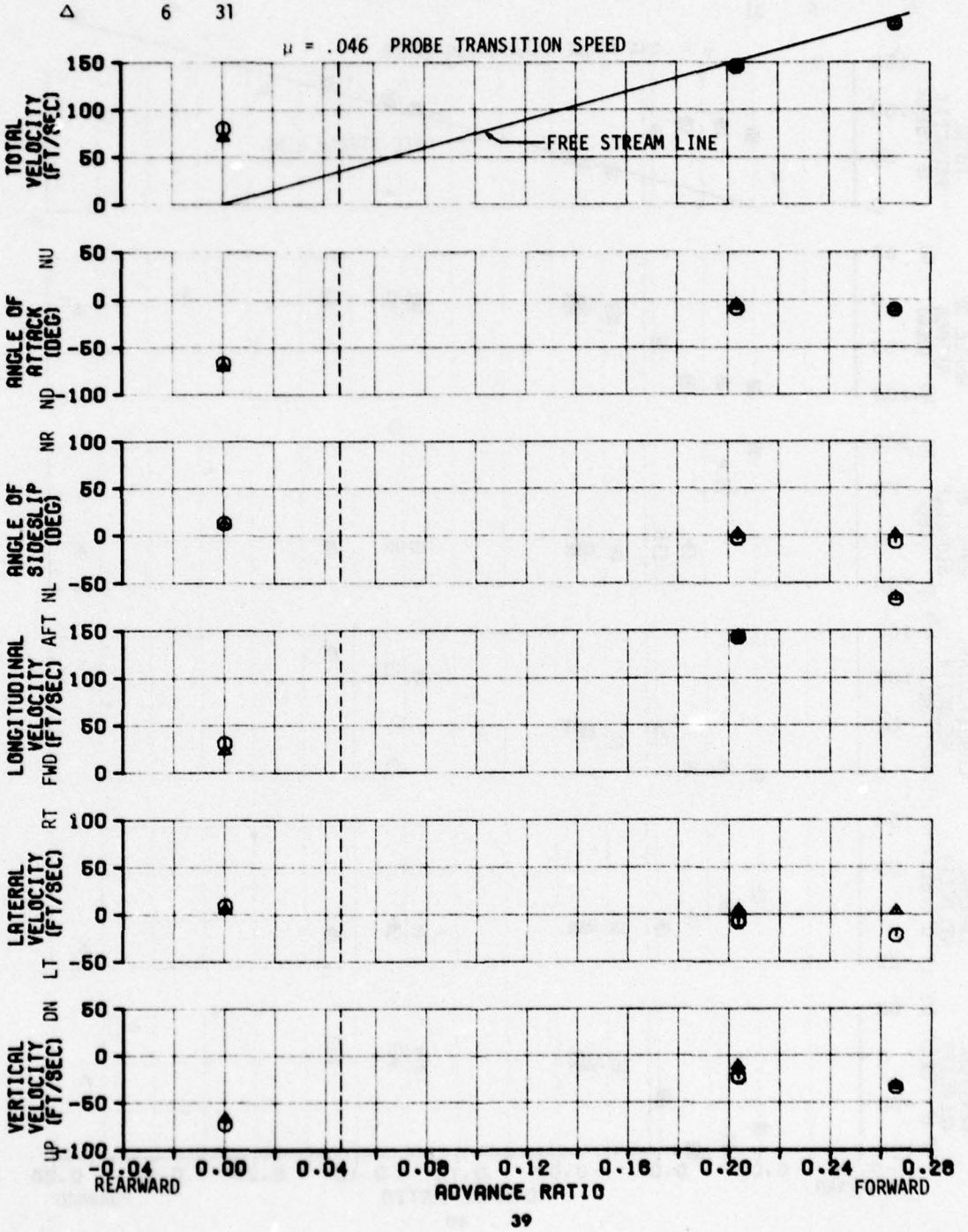

FIGURE 11
AVERAGED AIRFLOW CHARACTERISTICS IN LEVEL FLIGHT
AH-1G USA S/N 67-6844
RAKE POSITION NO. 3B (FS = 127, WL = 39)

SYMBOL	PROBE NO.	BL
□	3	49
△	5	31

AVERAGE THRUST COEFFICIENT = .00473
AVERAGE ROTOR SPEED = 324.1 RPM

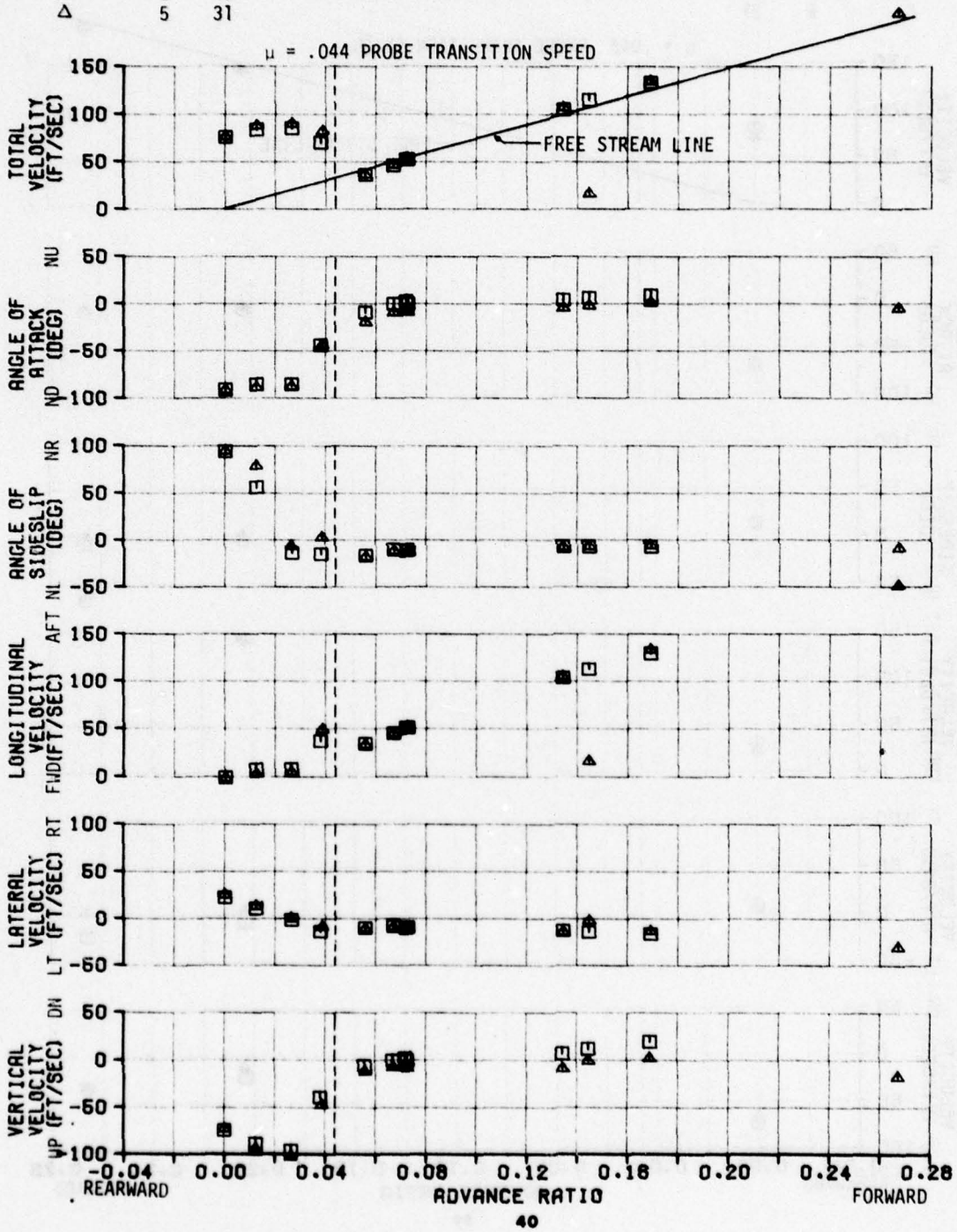

FIGURE 12
AVERAGED AIRFLOW CHARACTERISTICS IN LEVEL FLIGHT
AH-1G USA S/N 67-6844
RAKE POSITION NO. 3B (FS = 127, WL = 21)

SYMBOL	PROBE NO.	BL
□	4	49
△	6	31

AVERAGE THRUST COEFFICIENT = .00473
AVERAGE ROTOR SPEED = 324.1 RPM

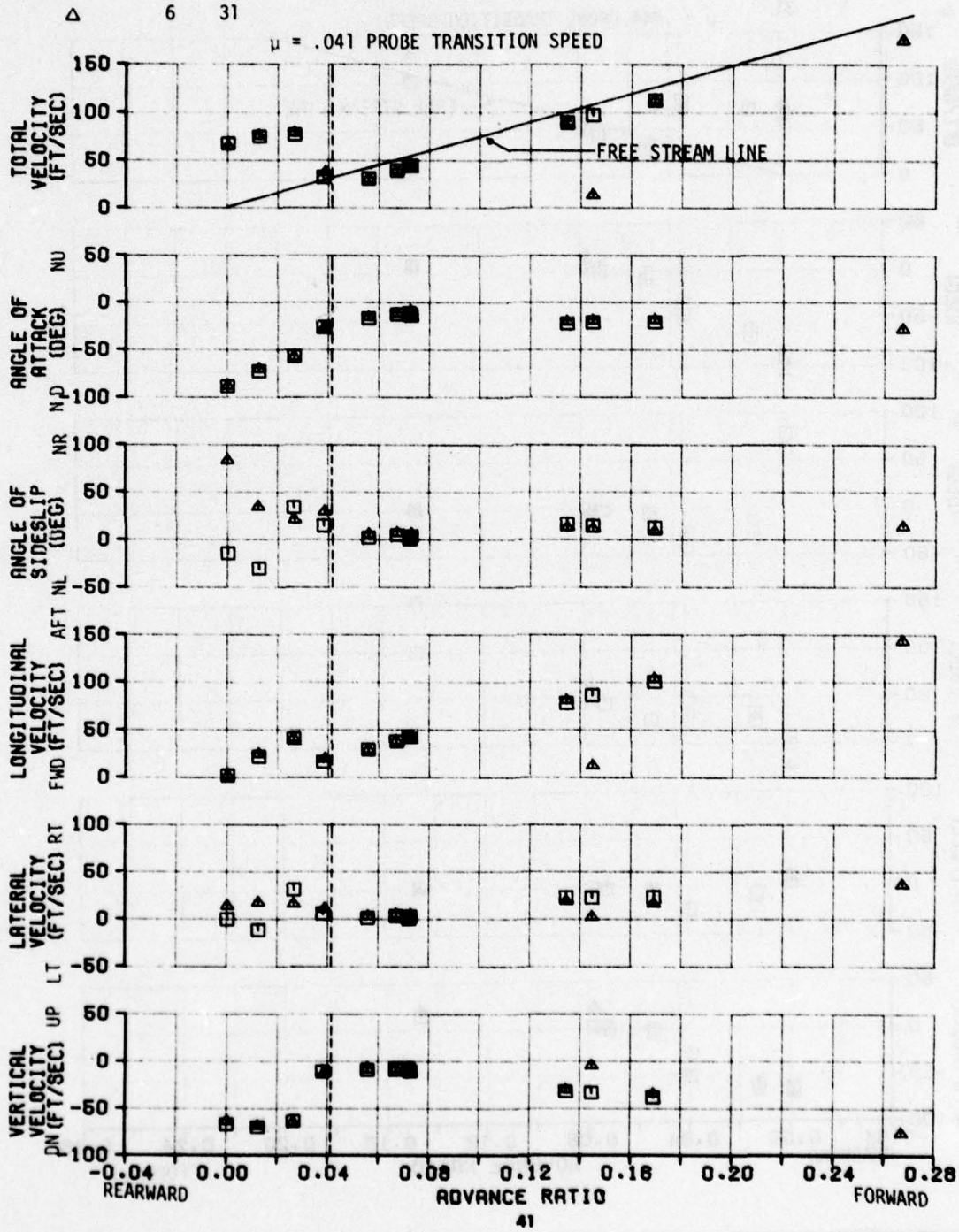

FIGURE 13
AVERAGED AIRFLOW CHARACTERISTICS IN LEVEL FLIGHT
AH-1G USA S/N 67-6844
RAKE POSITION NO. 4A (FS = 109, WL = 75)

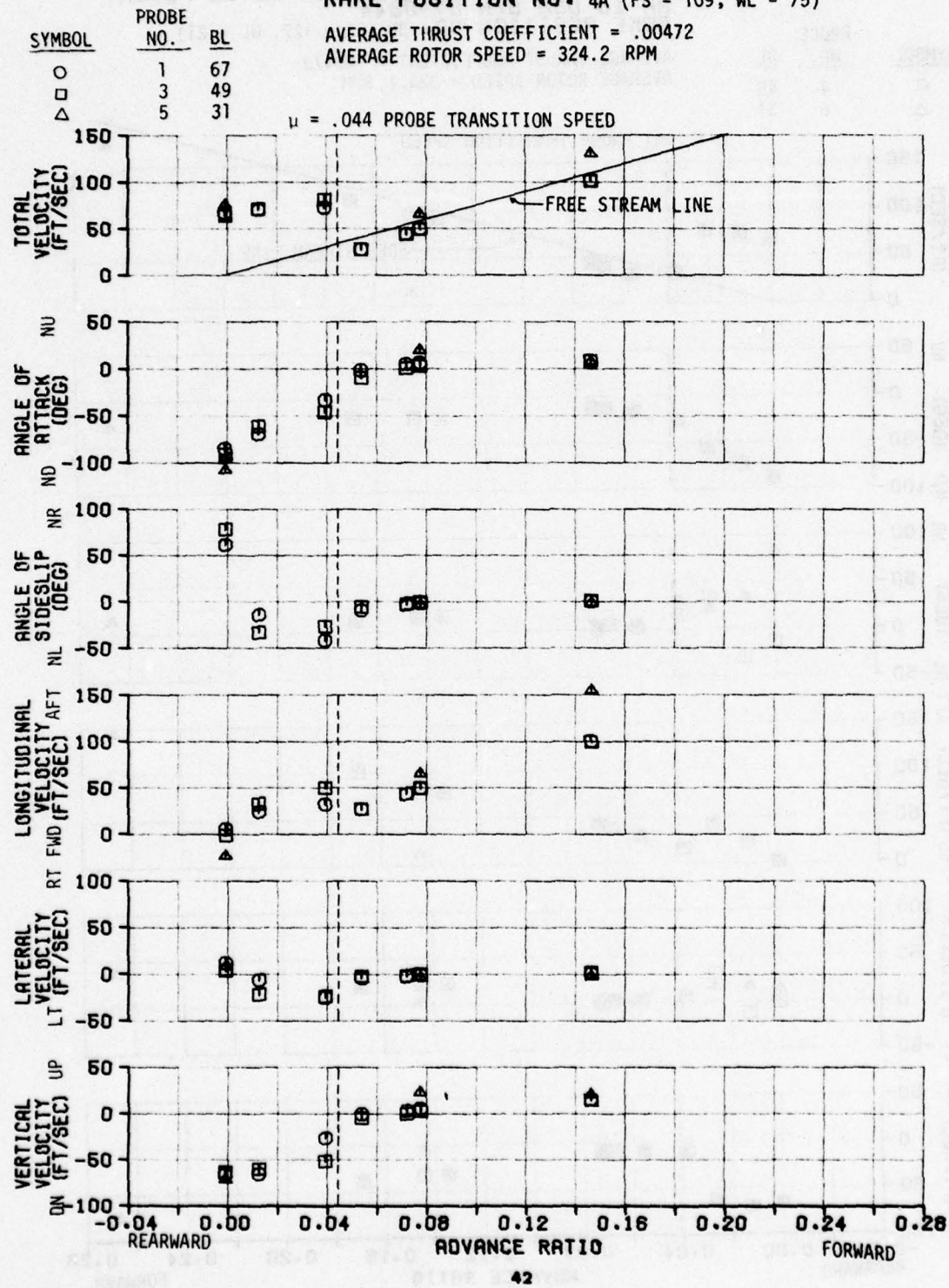

FIGURE 14
AVERAGED AIRFLOW CHARACTERISTICS IN LEVEL FLIGHT
AH-1G USA S/N 67-6844
RAKE POSITION NO. 4A (FS = 109, WL = 75)

SYMBOL	PROBE NO.	BL
○	2	67
□	4	49
△	6	31

AVERAGE THRUST COEFFICIENT = .00472
AVERAGE ROTOR SPEED = 324.2 RPM
(VELOCITY COMPONENTS ARE IN ERROR)

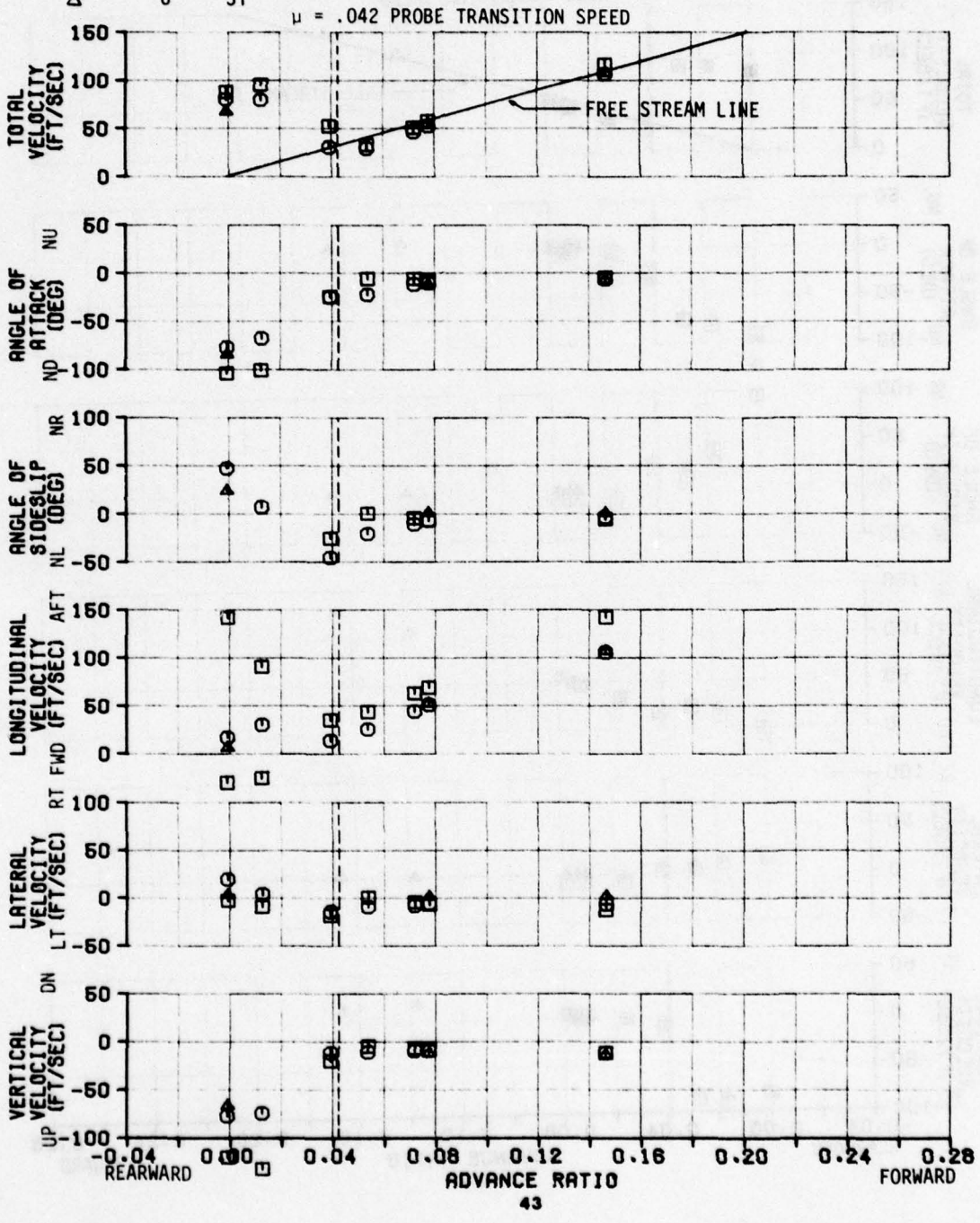

FIGURE 15
AVERAGED AIRFLOW CHARACTERISTICS IN LEVEL FLIGHT
AH-1G USA S/N 67-6844
RAKE POSITION NO. 4B (FS = 109, WL = 39)

SYMBOL	PROBE NO.	BL
□	3	49
△	5	31

AVERAGE THRUST COEFFICIENT = .00471
AVERAGE ROTOR SPEED = 323.9 RPM

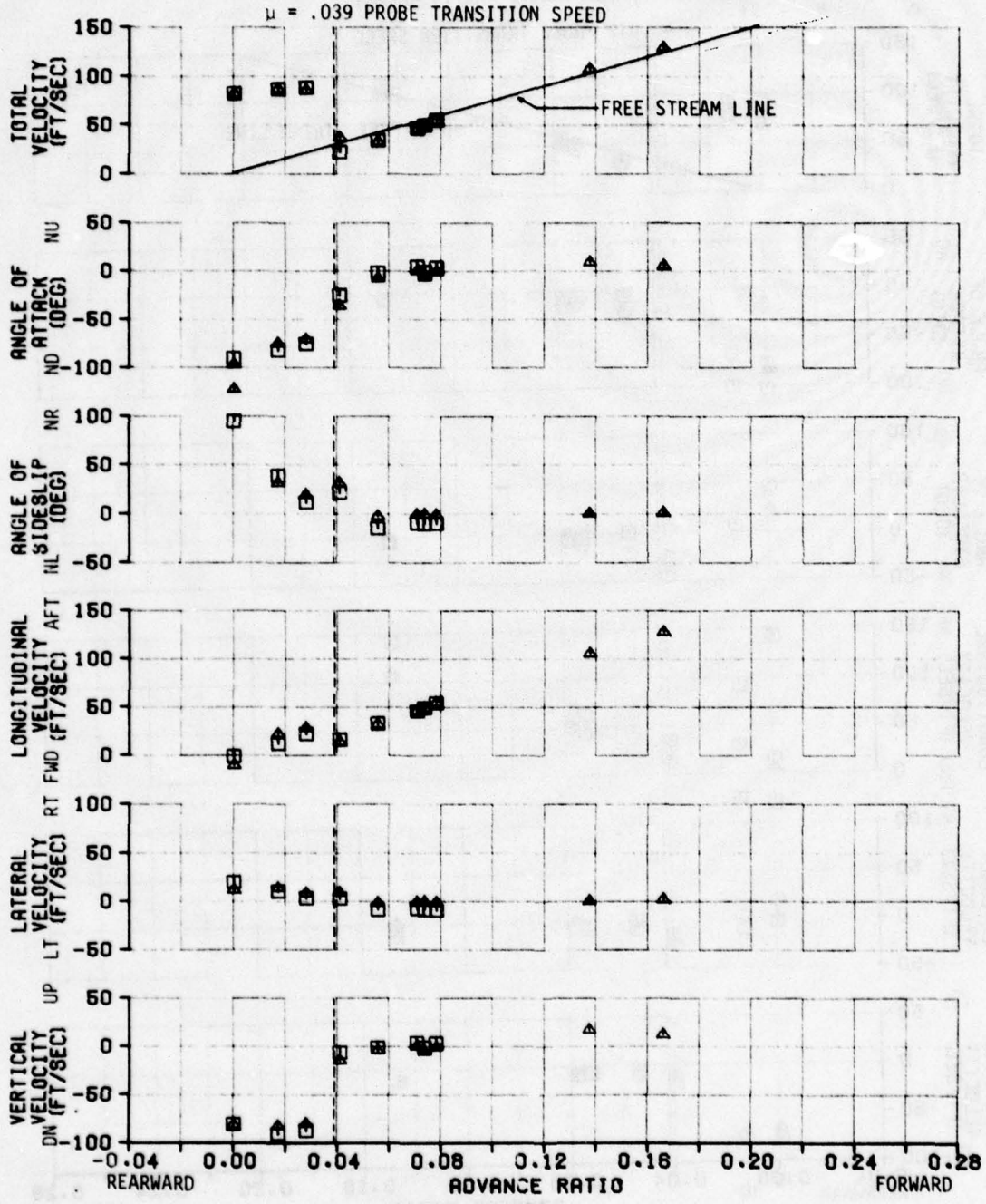

FIGURE 16
AVERAGED AIRFLOW CHARACTERISTICS IN LEVEL FLIGHT
AH-1G USA S/N 67-6844
RAKE POSITION NO. 4B (FS = 109, WL = 21)

SYMBOL	PROBE NO.	BL
□	4	49
△	6	31

AVERAGE THRUST COEFFICIENT = .00471
AVERAGE ROTOR SPEED = 323.9 RPM

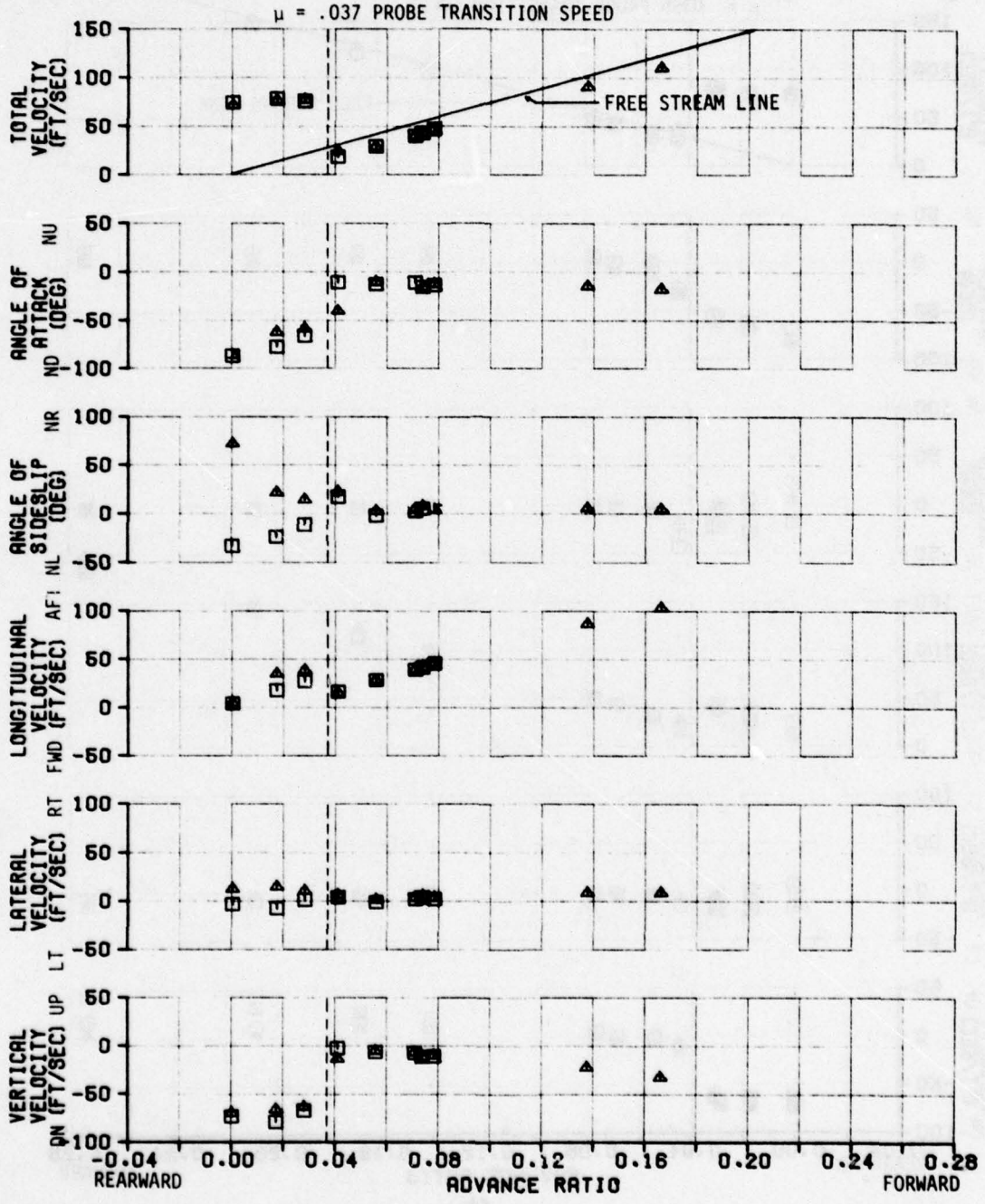

FIGURE 17
AVERAGED AIRFLOW CHARACTERISTICS IN LEVEL FLIGHT
AH-1G USA S/N 67-6844
RAKE POSITION NO. 5A (FS = 91, WL = 75)

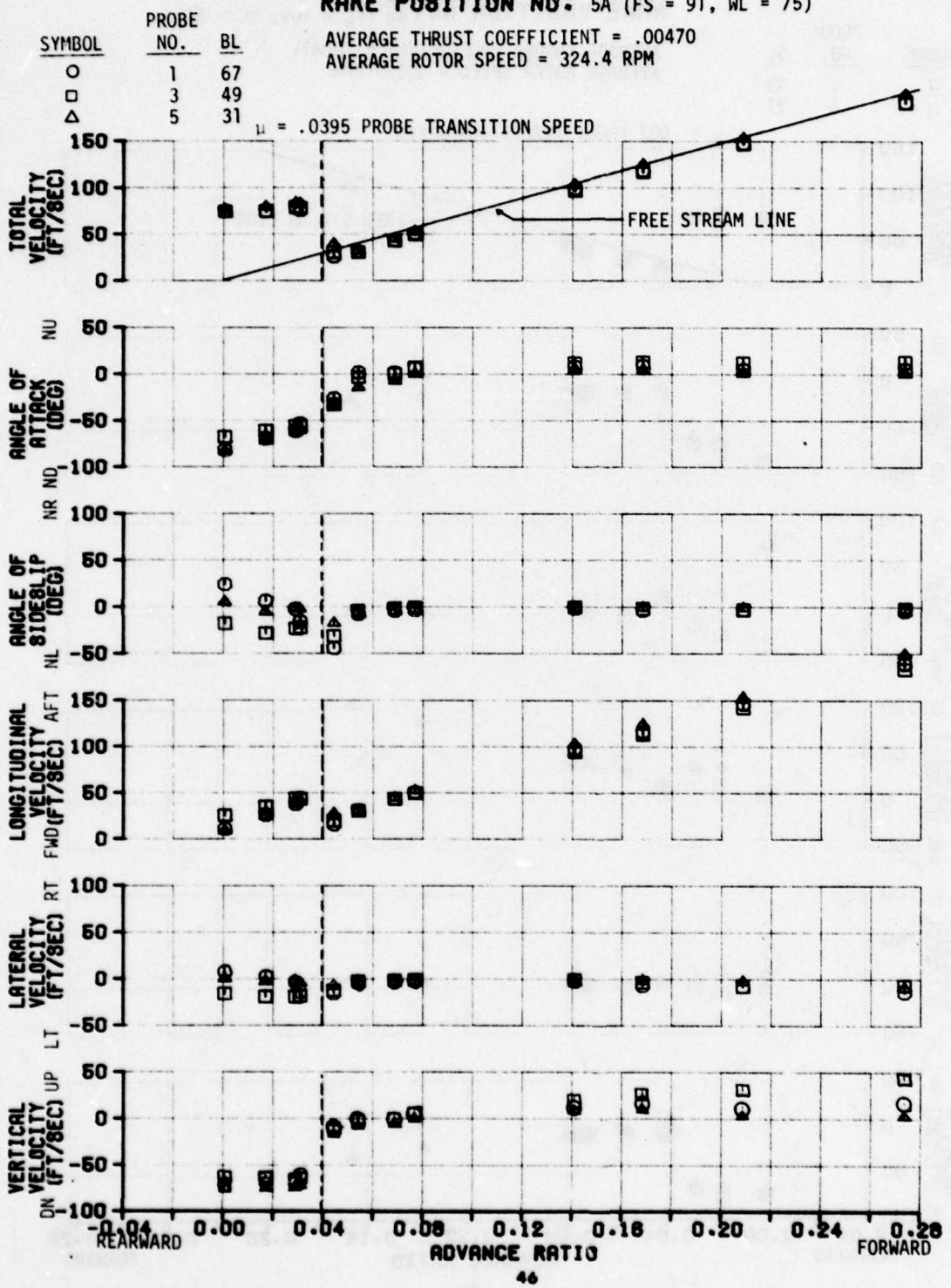

FIGURE 18
AVERAGED AIRFLOW CHARACTERISTICS IN LEVEL FLIGHT
AH-1G USA S/N 67-6844
RAKE POSITION NO. 5A (FS = 91, WL = 57)

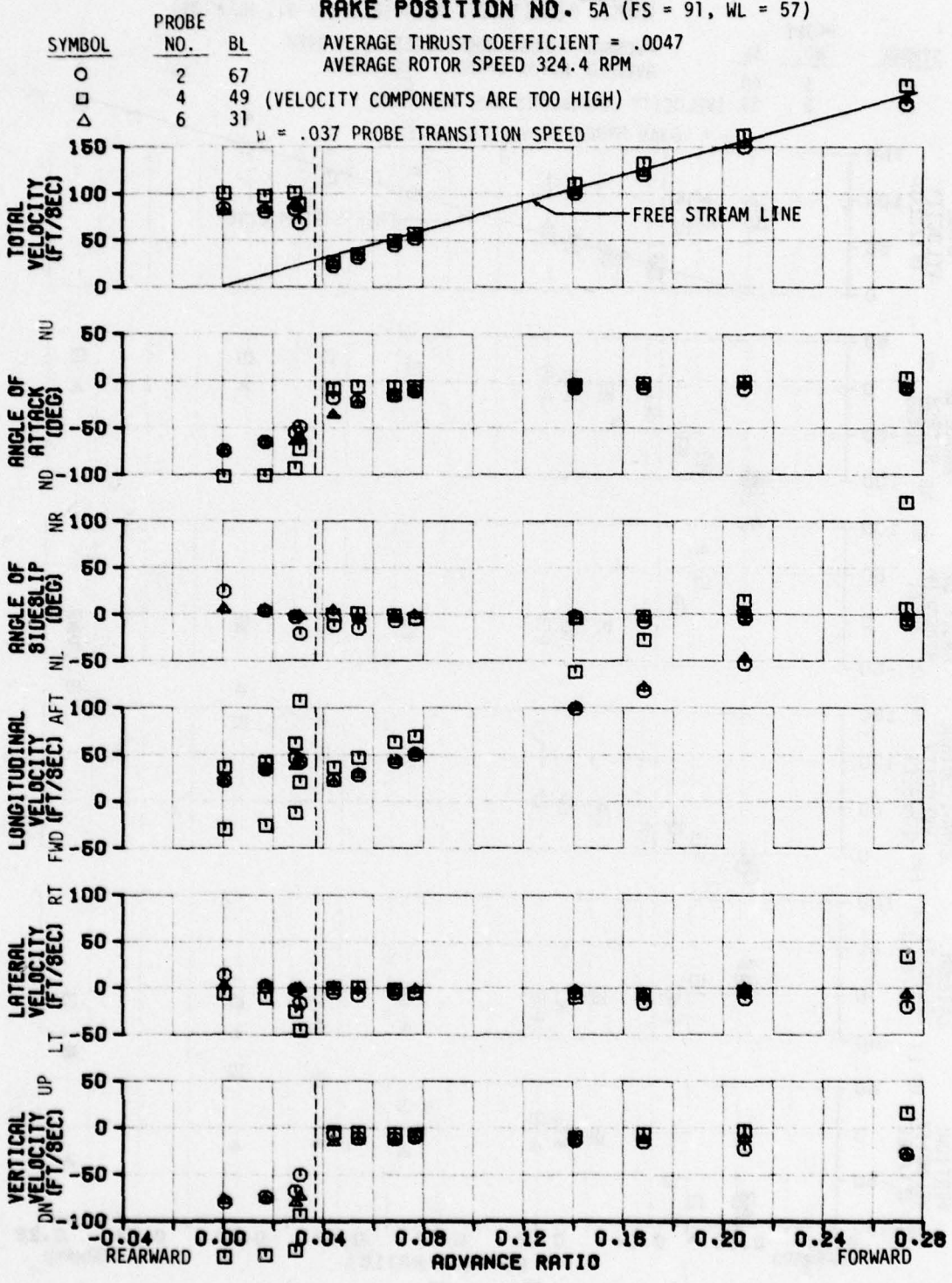

FIGURE 19
AVERAGED AIRFLOW CHARACTERISTICS IN LEVEL FLIGHT
AH-1G USA S/N 67-6844
RAKE POSITION NO. 5B (FS = 91, WL = 39)

SYMBOL	PROBE NO.	BL
□	3	49
△	5	31

AVERAGE THRUST COEFFICIENT = .00472
AVERAGE ROTOR SPEED = 323.9 RPM
(VELOCITY COMPONENTS ARE TOO HIGH)

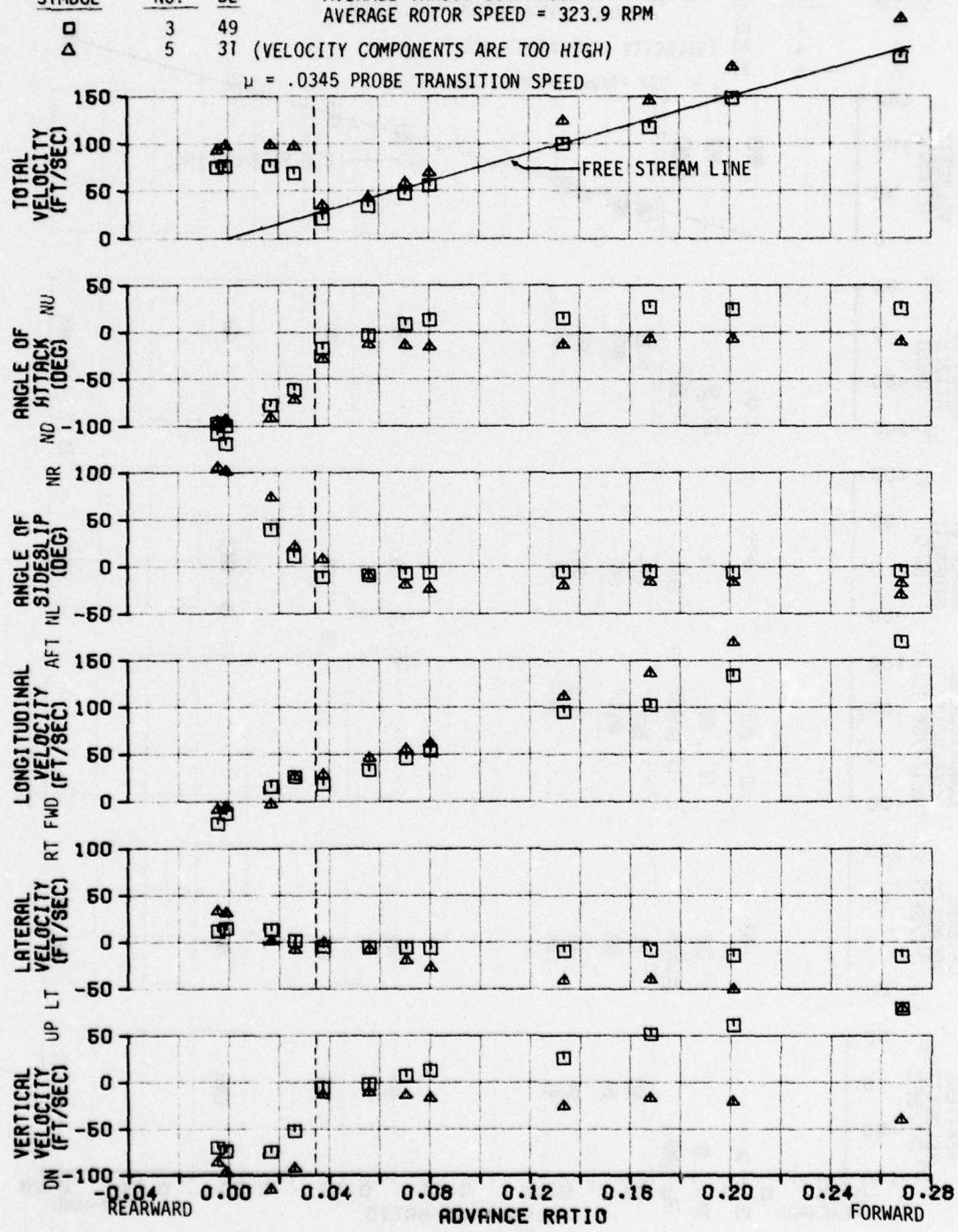

FIGURE 20
AVERAGED AIRFLOW CHARACTERISTICS IN LEVEL FLIGHT
AH-1G USA S/N 67-6844
RAKE POSITION NO. 5B (FS = 91, WL = 21)

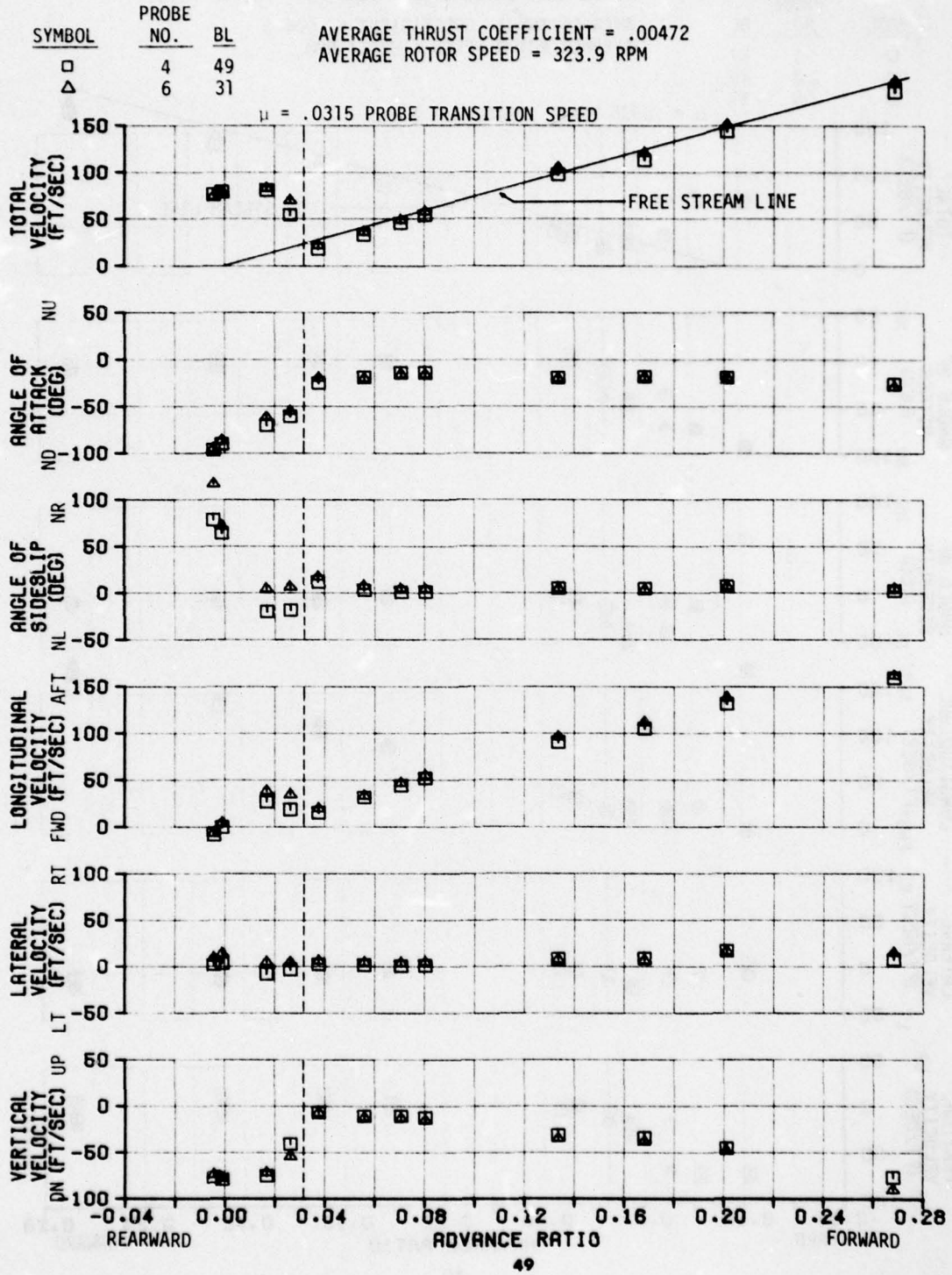

FIGURE 21
AVERAGED AIRFLOW CHARACTERISTICS IN LEVEL FLIGHT
AH-1G USA S/N 67-6844
RAKE POSITION NO. 6A (FS = 73, WL = 75)

SYMBOL	PROBE NO.	BL
○	1	67
□	3	49
△	5	31

AVERAGE THRUST COEFFICIENT = .00473
AVERAGE ROTOR SPEED = 324.1 RPM

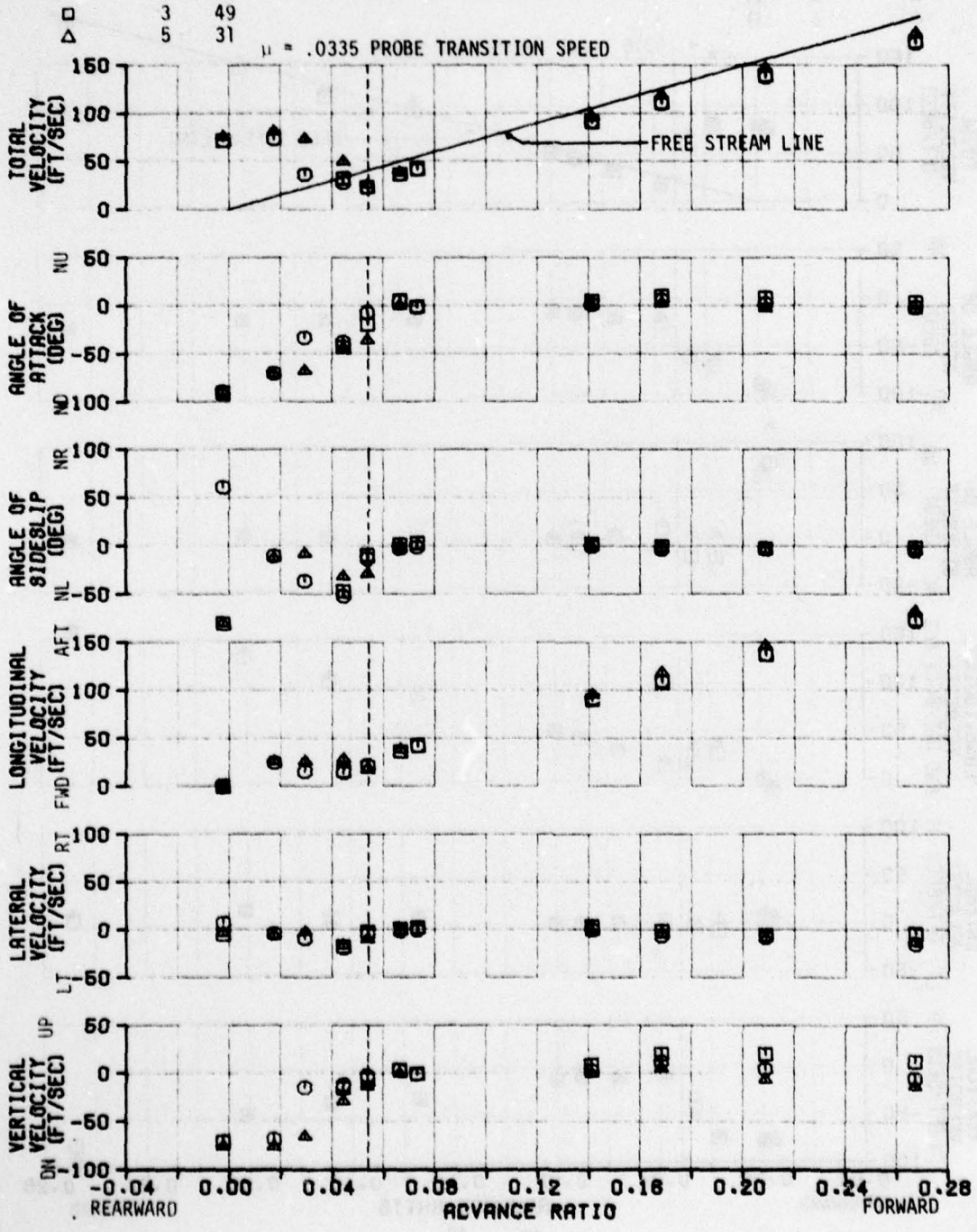

FIGURE 22
AVERAGED AIRFLOW CHARACTERISTICS IN LEVEL FLIGHT
AH-1G USA S/N 67-6844
RAKE POSITION NO. 6A (FS = 73, WL = 57)

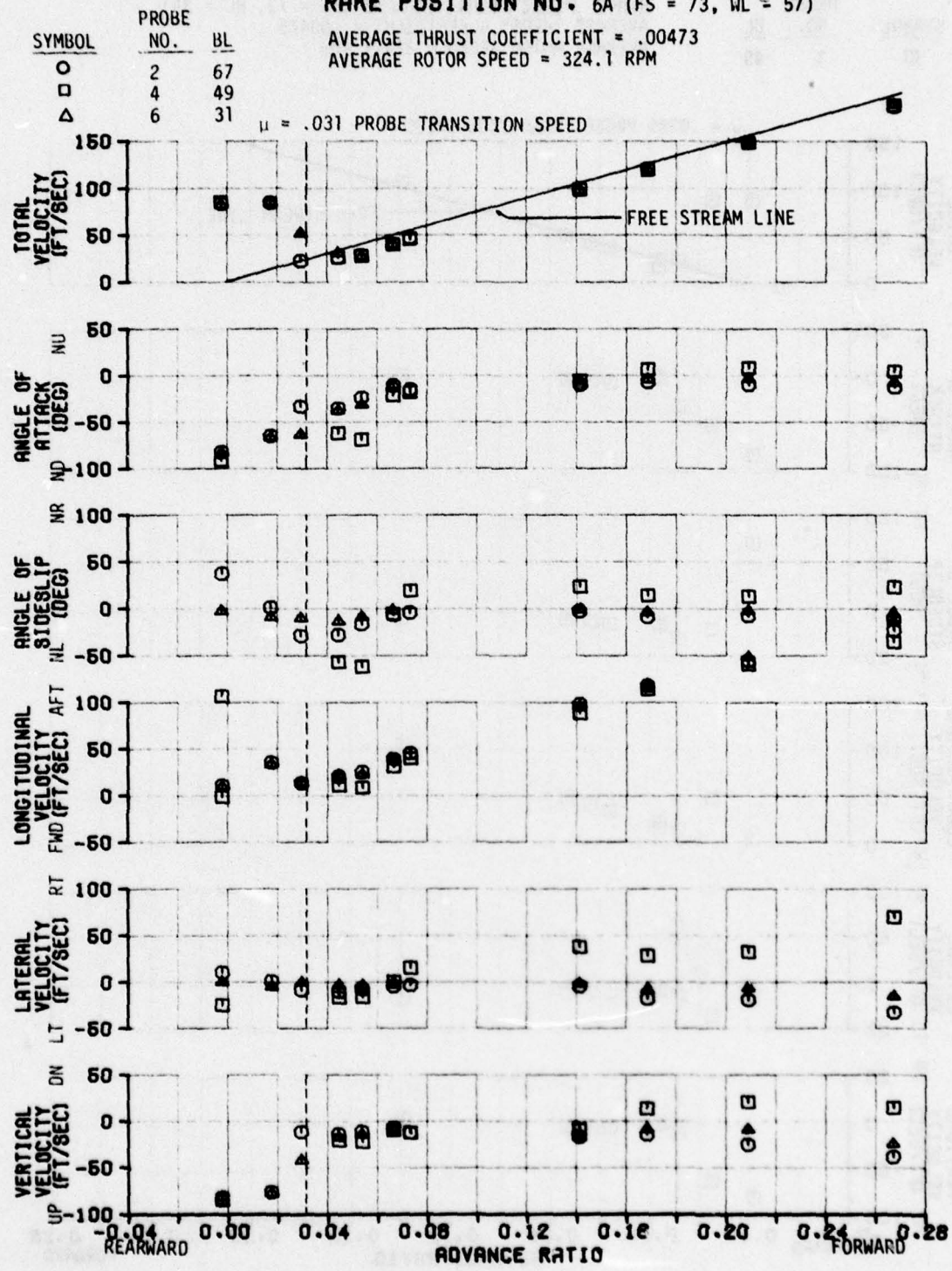

FIGURE 23
AVERAGED AIRFLOW CHARACTERISTICS IN LEVEL FLIGHT
AH-1G USA S/N 67-6844
RAKE POSITION NO. 6B (FS = 73, WL = 39)
AVERAGE THRUST COEFFICIENT = .00475
AVERAGE ROTOR SPEED = 324.1 RPM

SYMBOL	PROBE NO.	BL
□	3	49

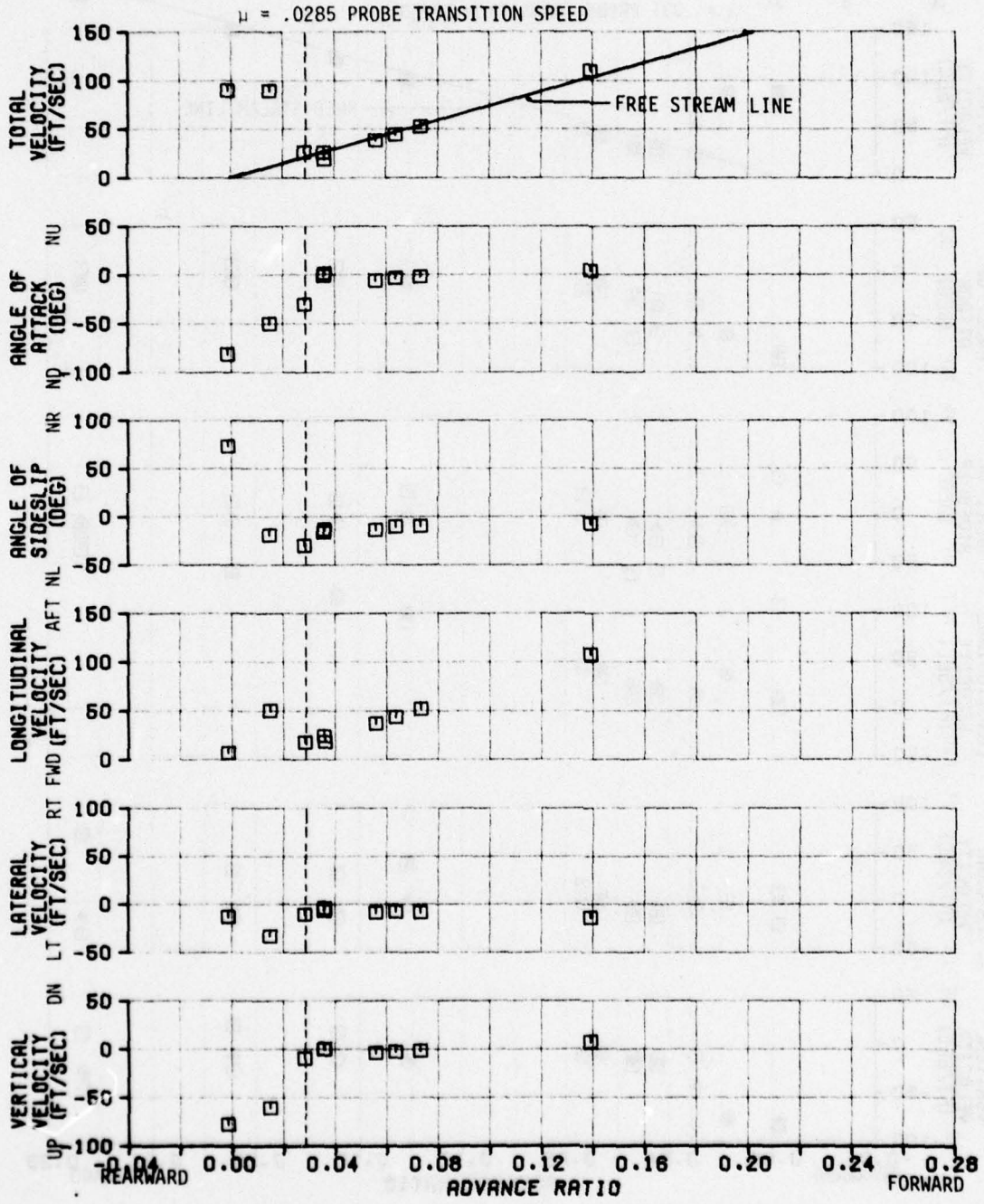

FIGURE 24
AVERAGED AIRFLOW CHARACTERISTICS IN LEVEL FLIGHT
AH-1G USA S/N 67-6844
RAKE POSITION NO. 6B (FS = 73, WL = 39)

SYMBOL	PROBE NO.	BL
□	4	49

AVERAGE THRUST COEFFICIENT = .00475
AVERAGE ROTOR SPEED = 324.1 RPM

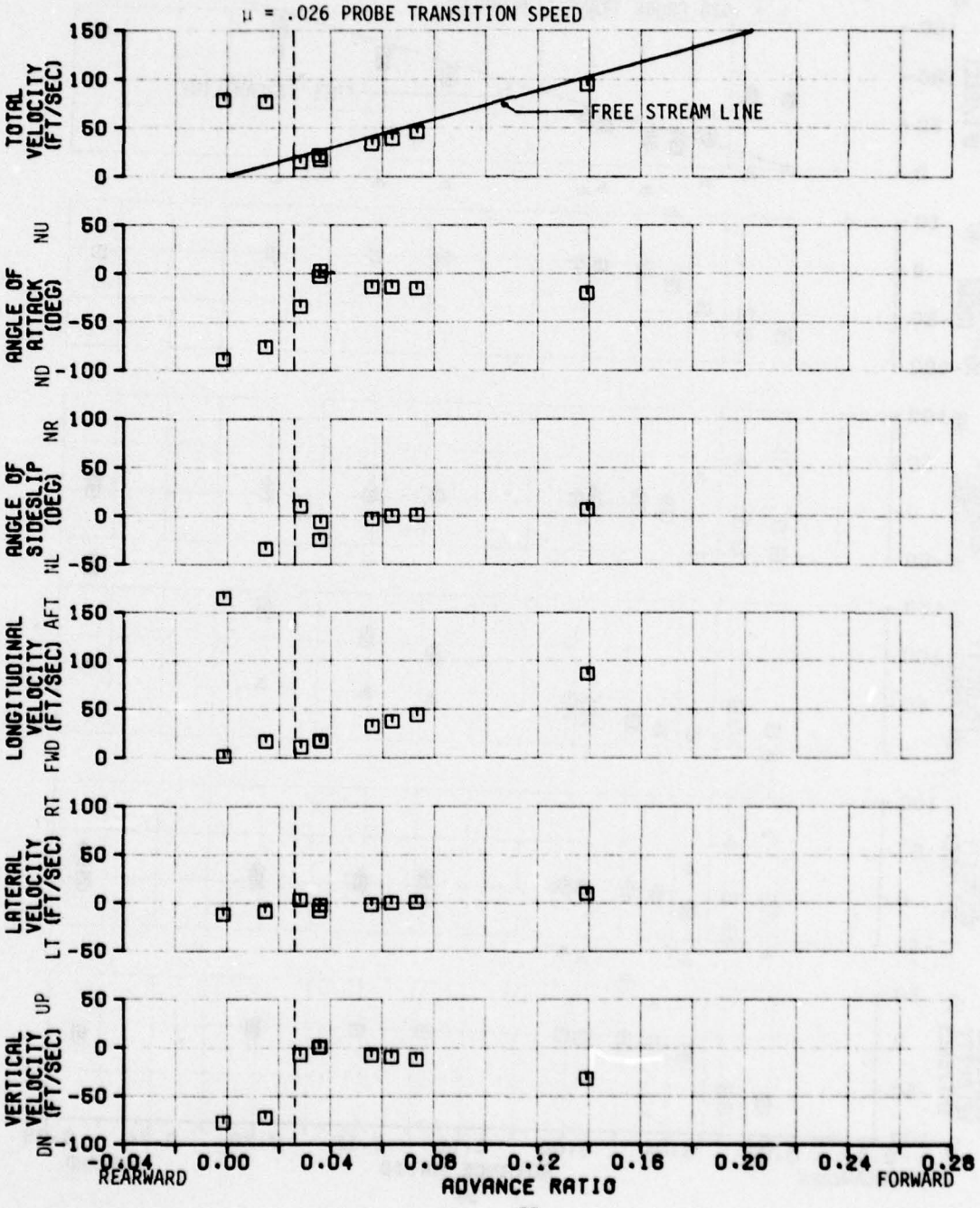

FIGURE 25
AVERAGED AIRFLOW CHARACTERISTICS IN LEVEL FLIGHT
AH-1G USA S/N 67-6844
RAKE POSITION NO. 7A (FS = 55, WL = 75)

SYMBOL	PROBE NO.	BL
○	1	67
□	3	49
△	5	31

AVERAGE THRUST COEFFICIENT = .00472
AVERAGE ROTOR SPEED = 324.0 RPM
(VELOCITY COMPONENTS ARE IN ERROR)
μ = .026 PROBE TRANSITION SPEED

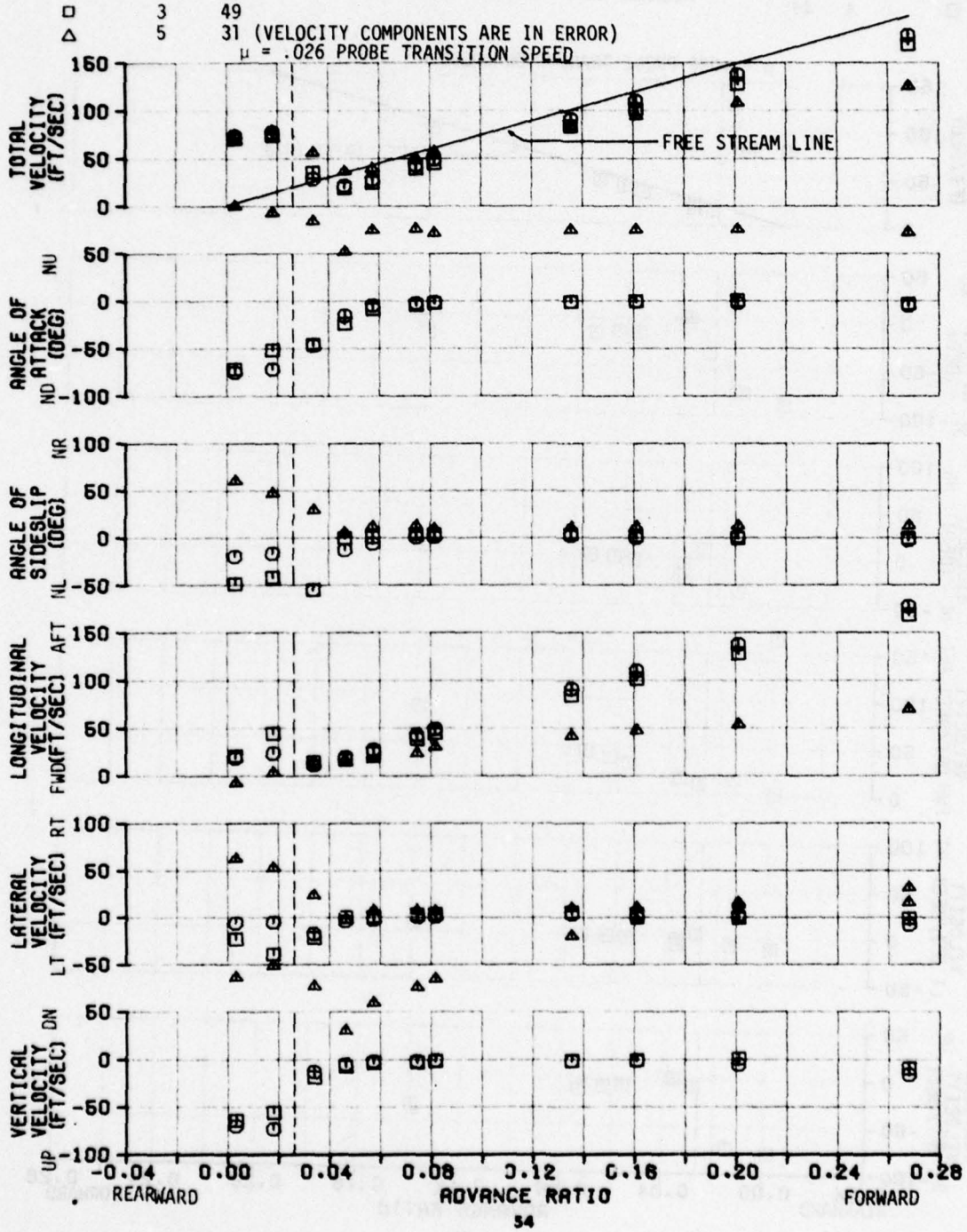

FIGURE 26
AVERAGED AIRFLOW CHARACTERISTICS IN LEVEL FLIGHT
AH-1G USA S/N 67-6844
RAKE POSITION NO. 7A (FS = 55, WL = 57)

SYMBOL	PROBE NO.	BL
○	2	67
□	4	49
△	6	31

AVERAGE THRUST COEFFICIENT = .00472
AVERAGE ROTOR SPEED = 324.0 RPM

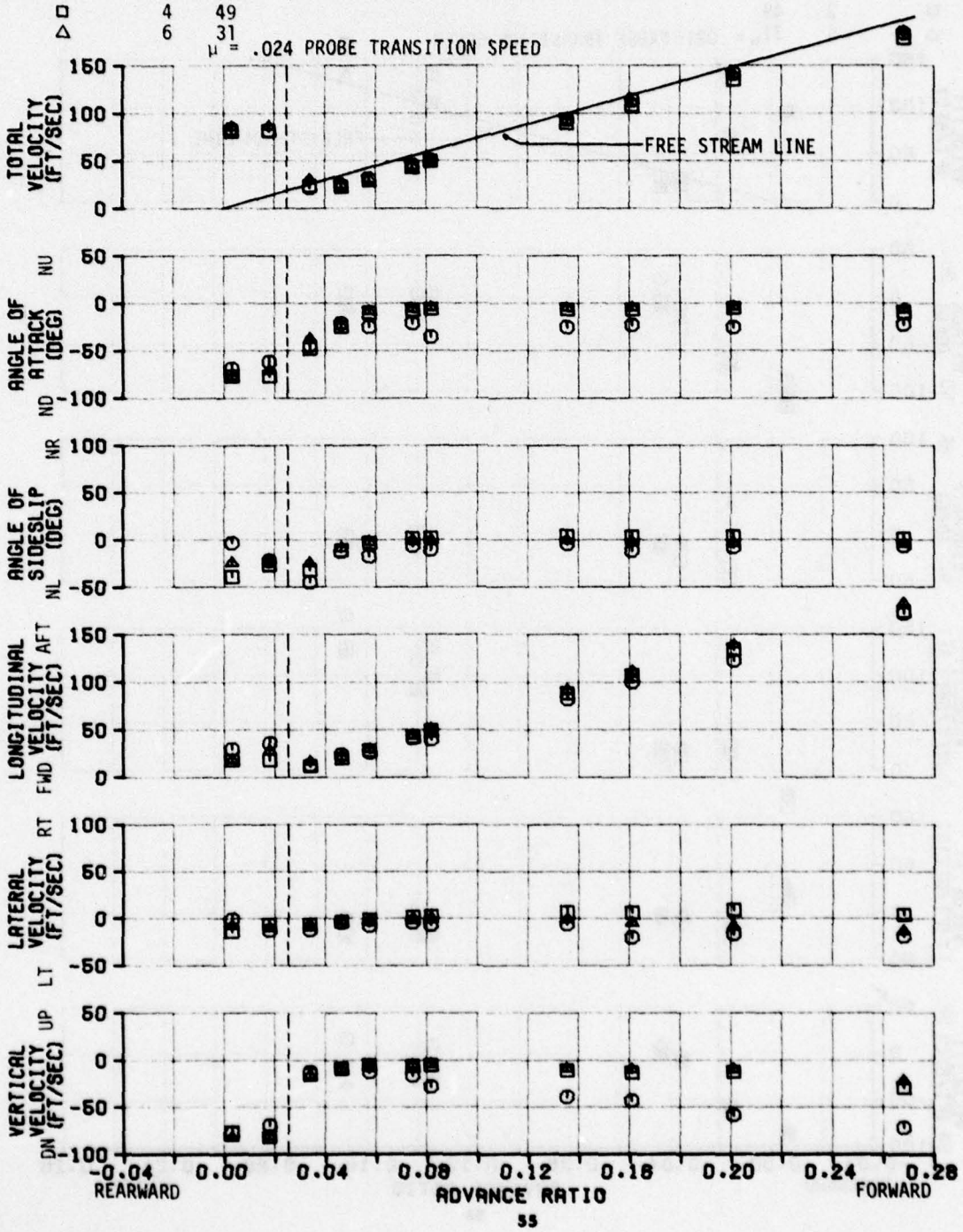

FIGURE 27
AVERAGED AIRFLOW CHARACTERISTICS IN LEVEL FLIGHT
AH-1G USA S/N 67-6844
RAKE POSITION NO. 7B (FS = 55, WL = 39)

SYMBOL	PROBE NO.	BL
○	1	67
□	3	49
△	5	31

AVERAGE THRUST COEFFICIENT = .00475
AVERAGE ROTOR SPEED = 323.9 RPM

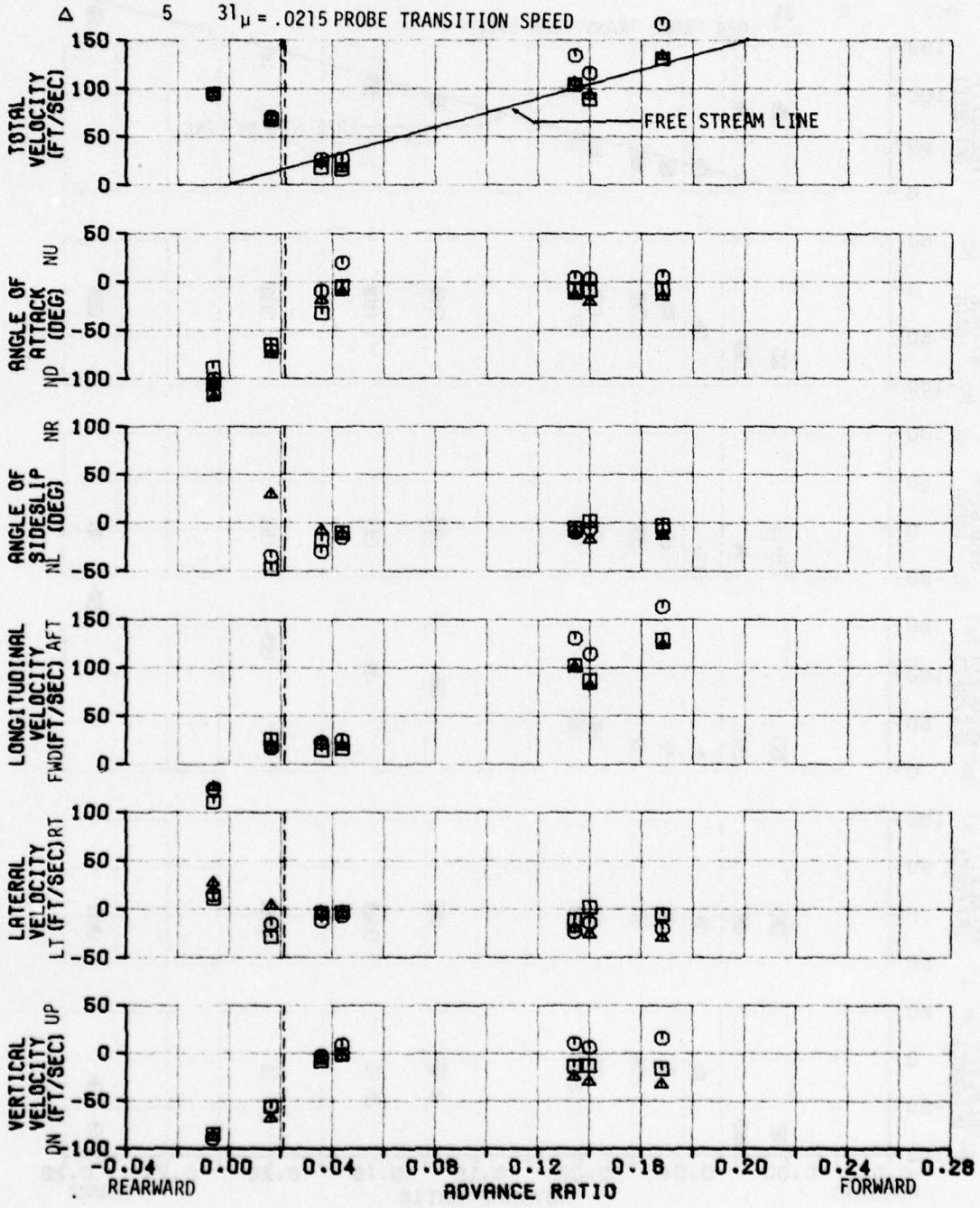

FIGURE 28
AVERAGED AIRFLOW CHARACTERISTICS IN LEVEL FLIGHT
AH-1G USA S/N 67-6844
RAKE POSITION NO. 7B (FS = 55, WL = 21)

SYMBOL	PROBE NO.	BL
○	2	67
□	4	49
△	6	31

AVERAGE THRUST COEFFICIENT = .00475
AVERAGE ROTOR SPEED = 323.9 RPM

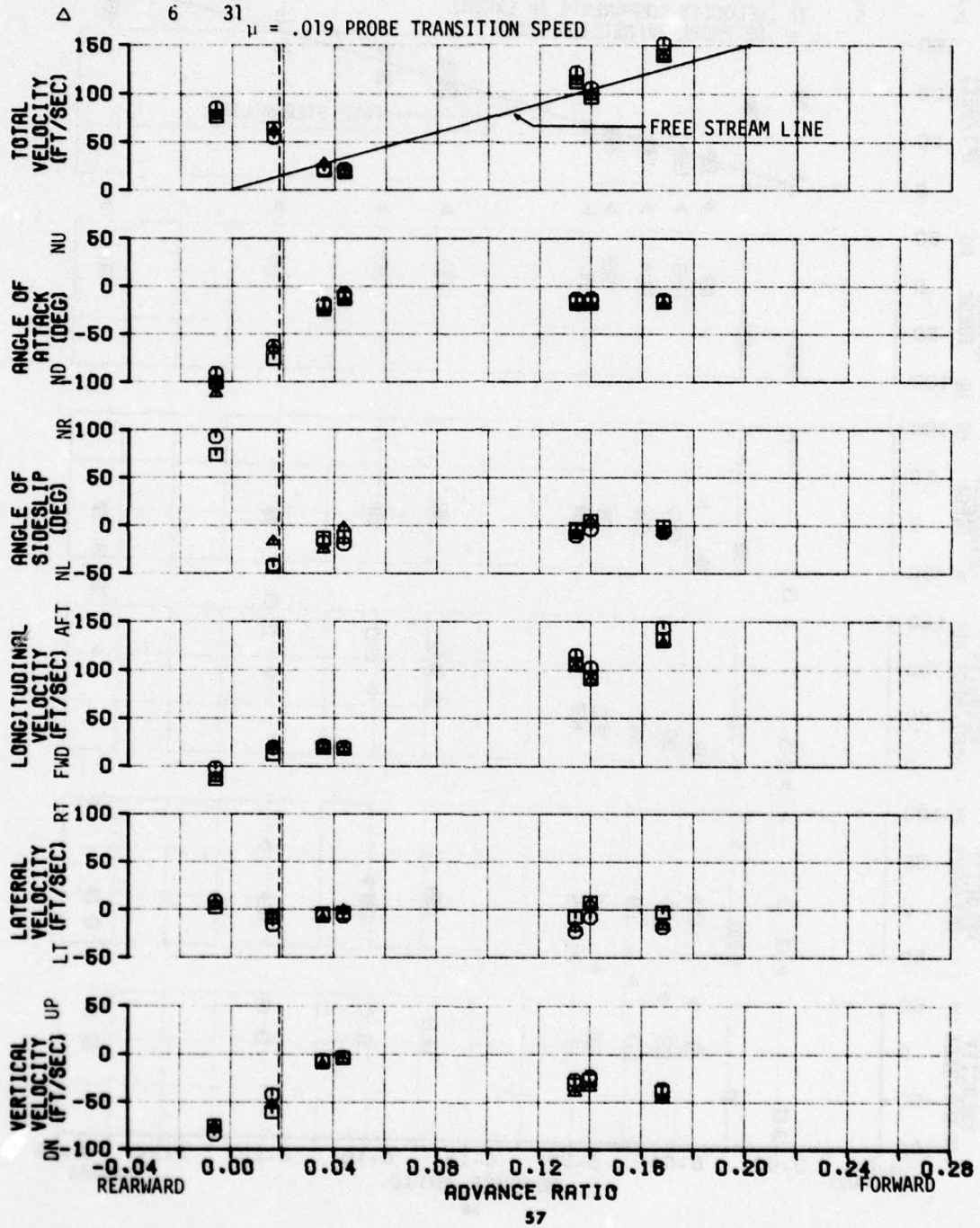

FIGURE 29
AVERAGED AIRFLOW CHARACTERISTICS IN LEVEL FLIGHT
AH-1G USA S/N 67-6844
RAKE POSITION NO. 8A (FS = 37, WL = 75)

SYMBOL	PROBE NO.	BL
○	1	67
□	3	49
△	5	31

AVERAGE THRUST COEFFICIENT = .00475
AVERAGE ROTOR SPEED = 324.7 RPM
(VELOCITY COMPONENTS IN ERROR)
μ = .02 PROBE TRANSITION SPEED

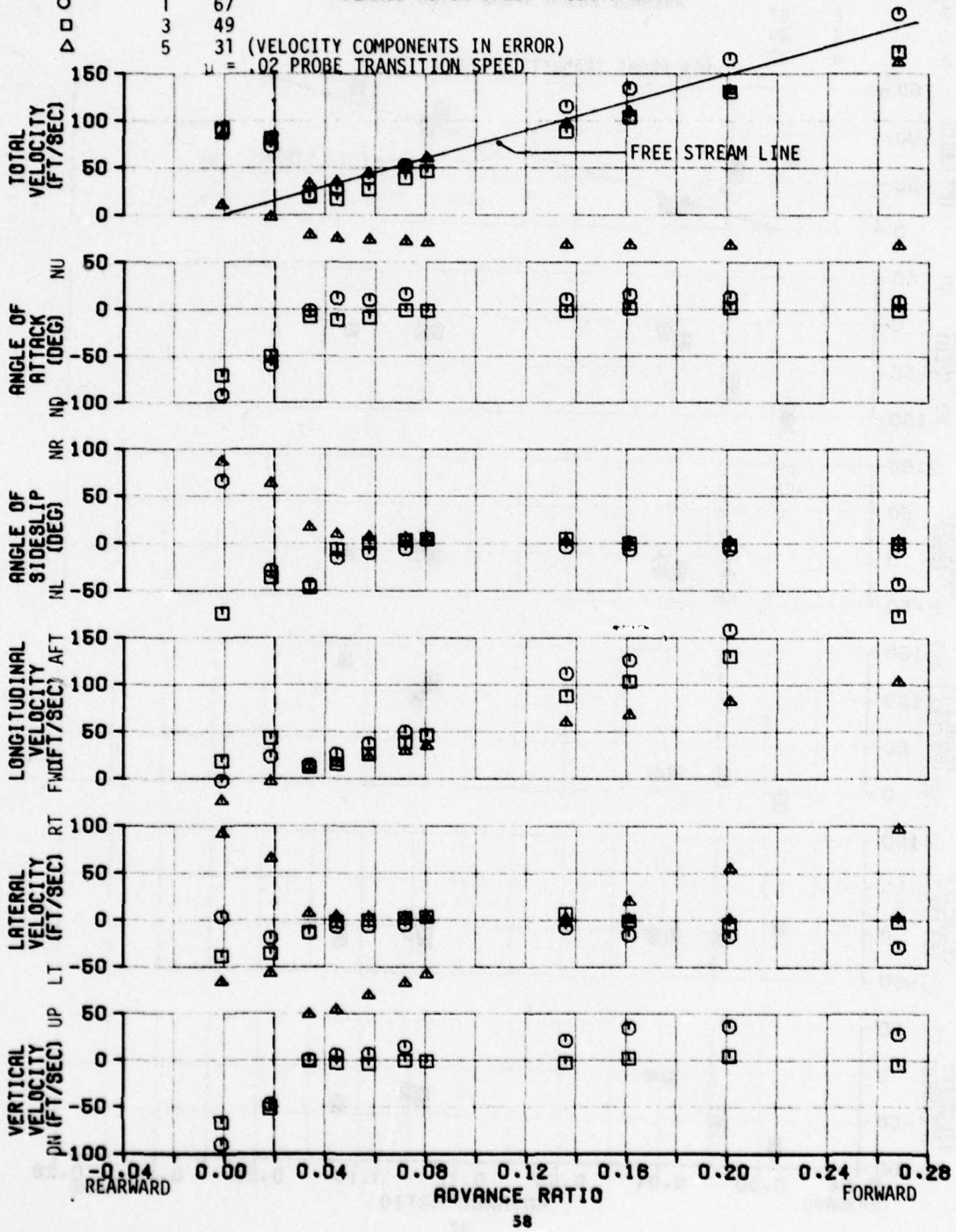

FIGURE 30
AVERAGED AIRFLOW CHARACTERISTICS IN LEVEL FLIGHT
AH-1G USA S/N 67-6844
RAKE POSITION NO. 8A (FS = 37, WL = 57)

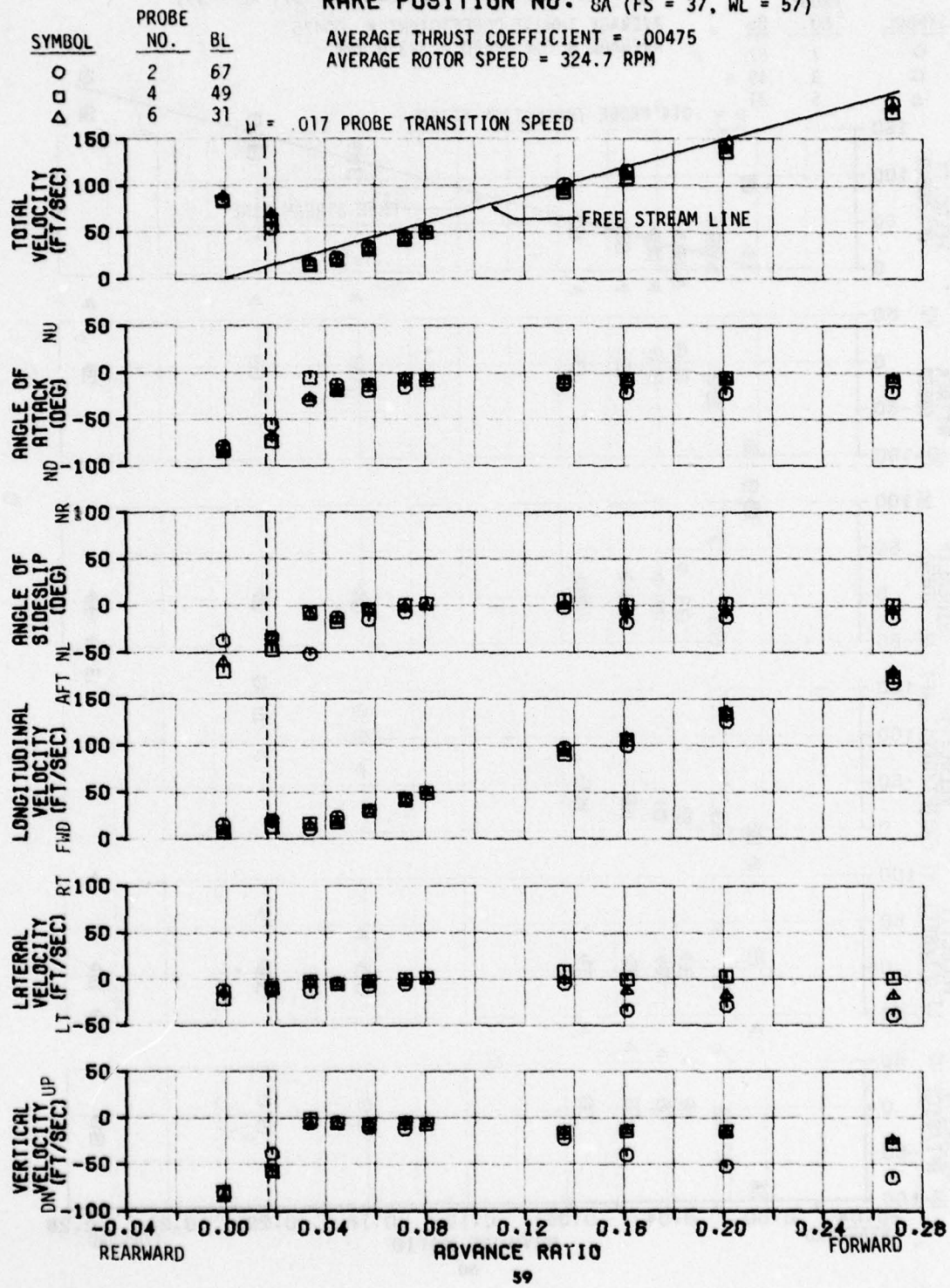

FIGURE 31
AVERAGED AIRFLOW CHARACTERISTICS IN LEVEL FLIGHT
AH-1G USA S/N 67-6844
RAKE POSITION NO. 8B (FS = 37, WL = 39)

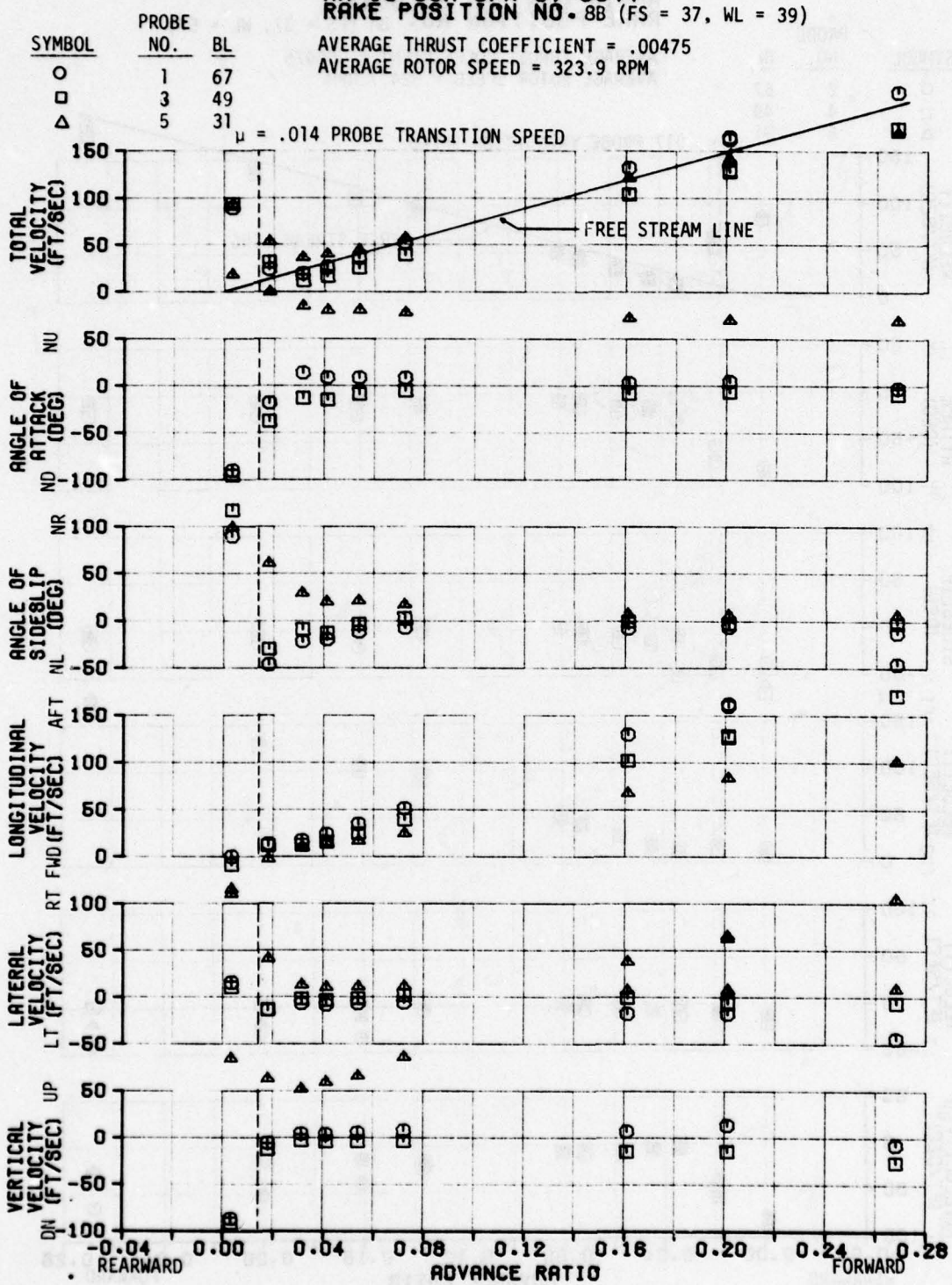

FIGURE 32
AVERAGED AIRFLOW CHARACTERISTICS IN LEVEL FLIGHT
AH-1G USA S/N 67-6844
RAKE POSITION NO. 8B (FS = 37, WL = 21)

SYMBOL	PROBE NO.	BL
○	2	67
□	4	49
△	6	31

AVERAGE THRUST COEFFICIENT = .00475
AVERAGE ROTOR SPEED = 323.9 RPM

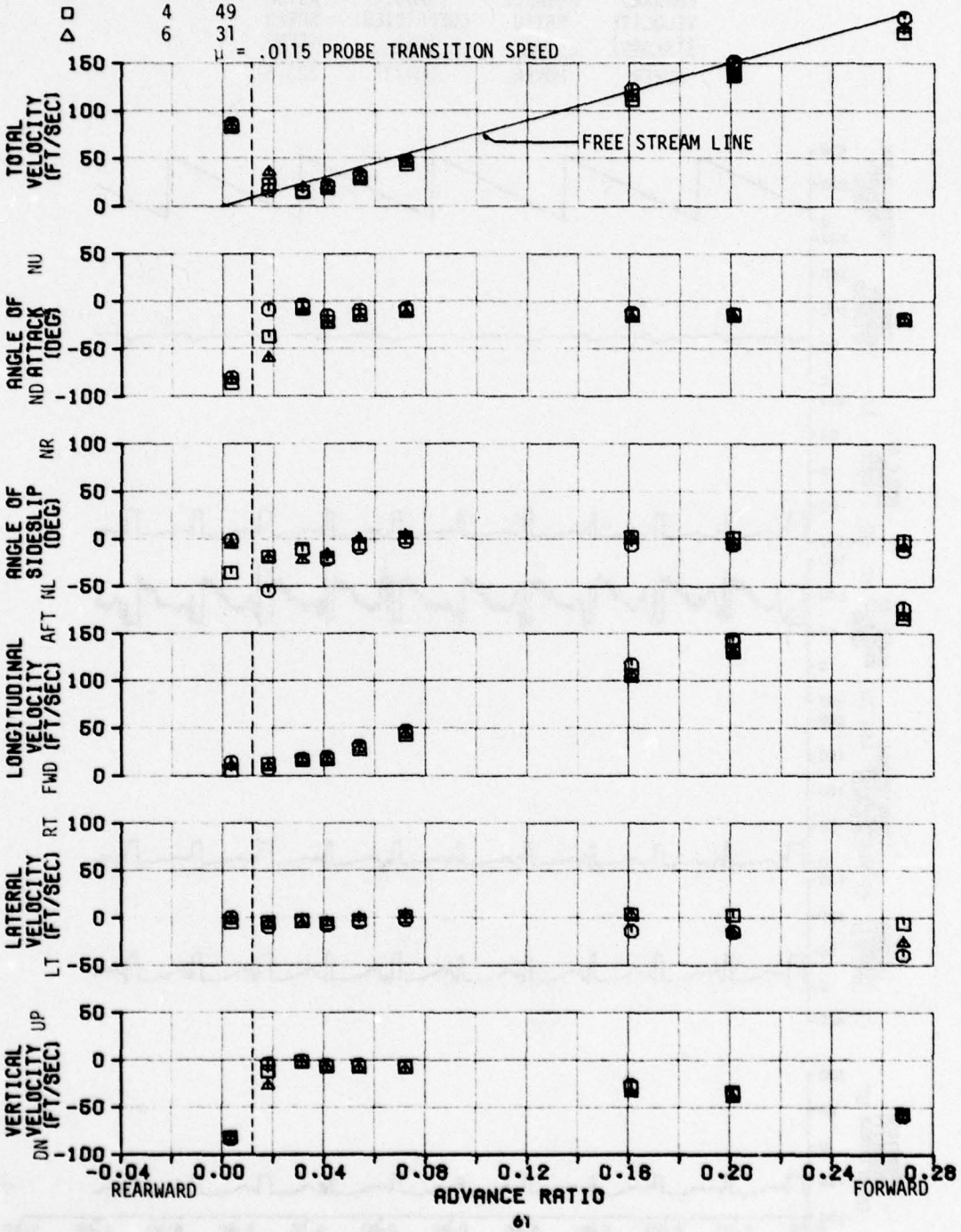

FIGURE 33
TRANSIENT AIRFLOW CHARACTERISTICS IN LEVEL FLIGHT
AH-1G USA S/N 67-8844
RAKE POSITION NO. 2A (FS = 145, WL = 75)

PROBE NO. 3 (BL = 49)

FORWARD VELOCITY (ft/sec)	ADVANCE RATIO (μ)	THRUST COEFFICIENT (C_T)	ROTOR SPEED (RPM)
HOVER	HOVER	.00473	323.5

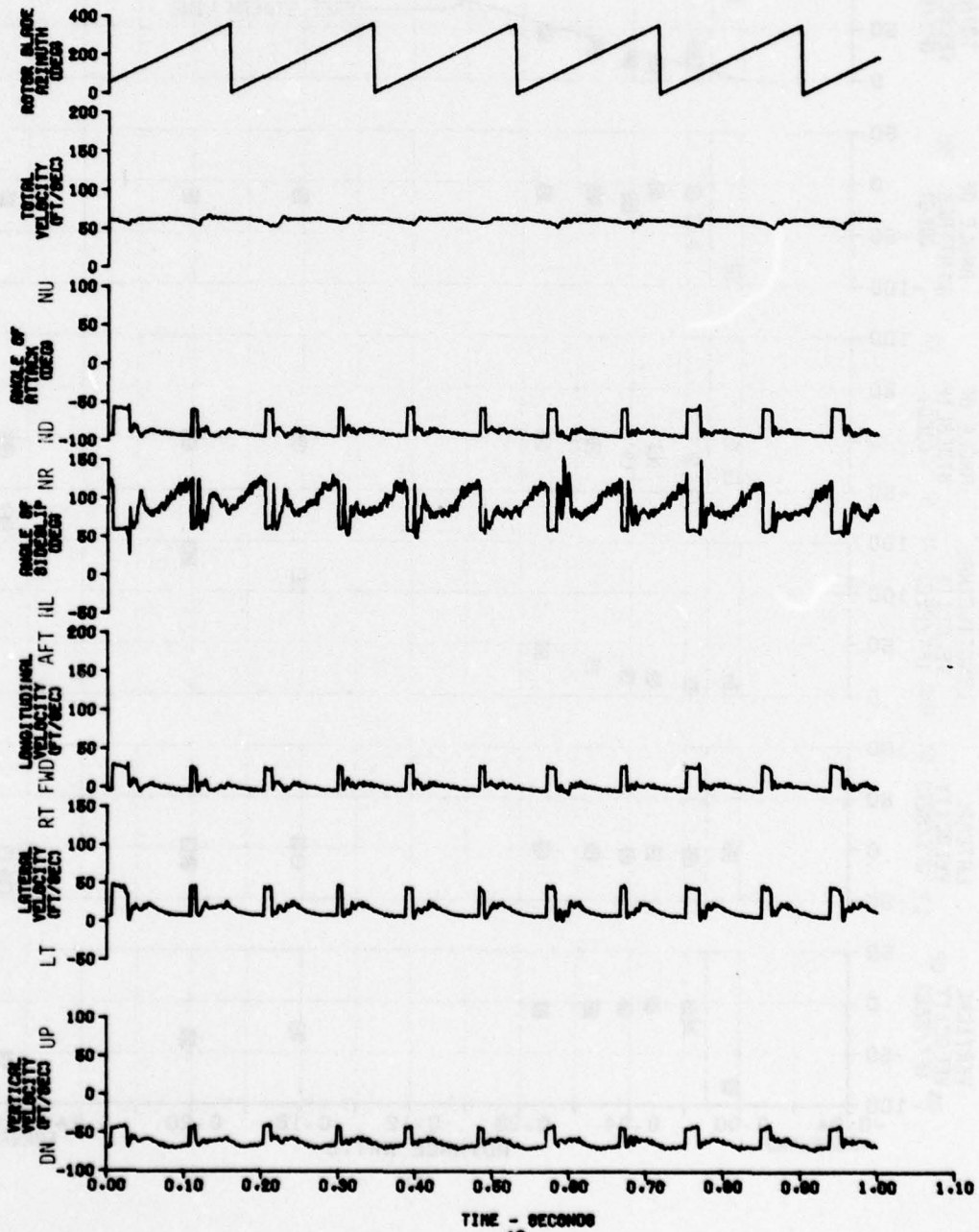

FIGURE 34
TRANSIENT AIRFLOW CHARACTERISTICS IN LEVEL FLIGHT
RH-1G UGR S/N 67-6844
RAKE POSITION NO. 2A (FS = 145, WL = 75)

PROBE NO. 3 (BL = 49)

FORWARD VELOCITY (ft/sec)	ADVANCE RATIO (μ)	THRUST COEFFICIENT (C_T)	ROTOR SPEED (RPM)
10.2	.0138	.00478	323.0

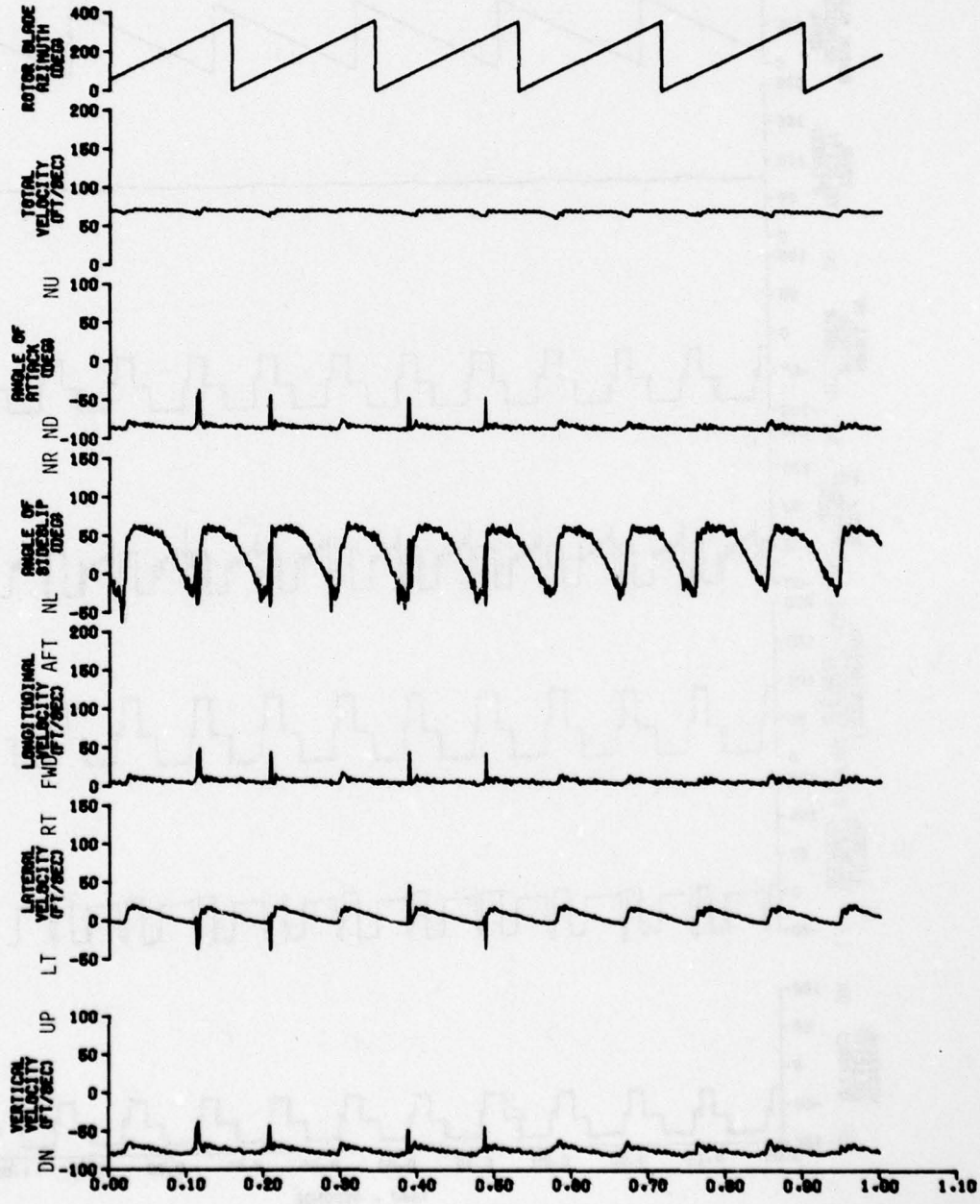

FIGURE 35
TRANSIENT AIRFLOW CHARACTERISTICS IN LEVEL FLIGHT
AH-1G USA S/N 67-6844
RAKE POSITION NO. 2A (FS = 145, WL = 75)

PROBE NO. 3 (BL = 49)

FORWARD VELOCITY (ft/sec)	ADVANCE RATIO (μ)	THRUST COEFFICIENT (C_T)	ROTOR SPEED (RPM)
22.9	.0306	.00475	324.1

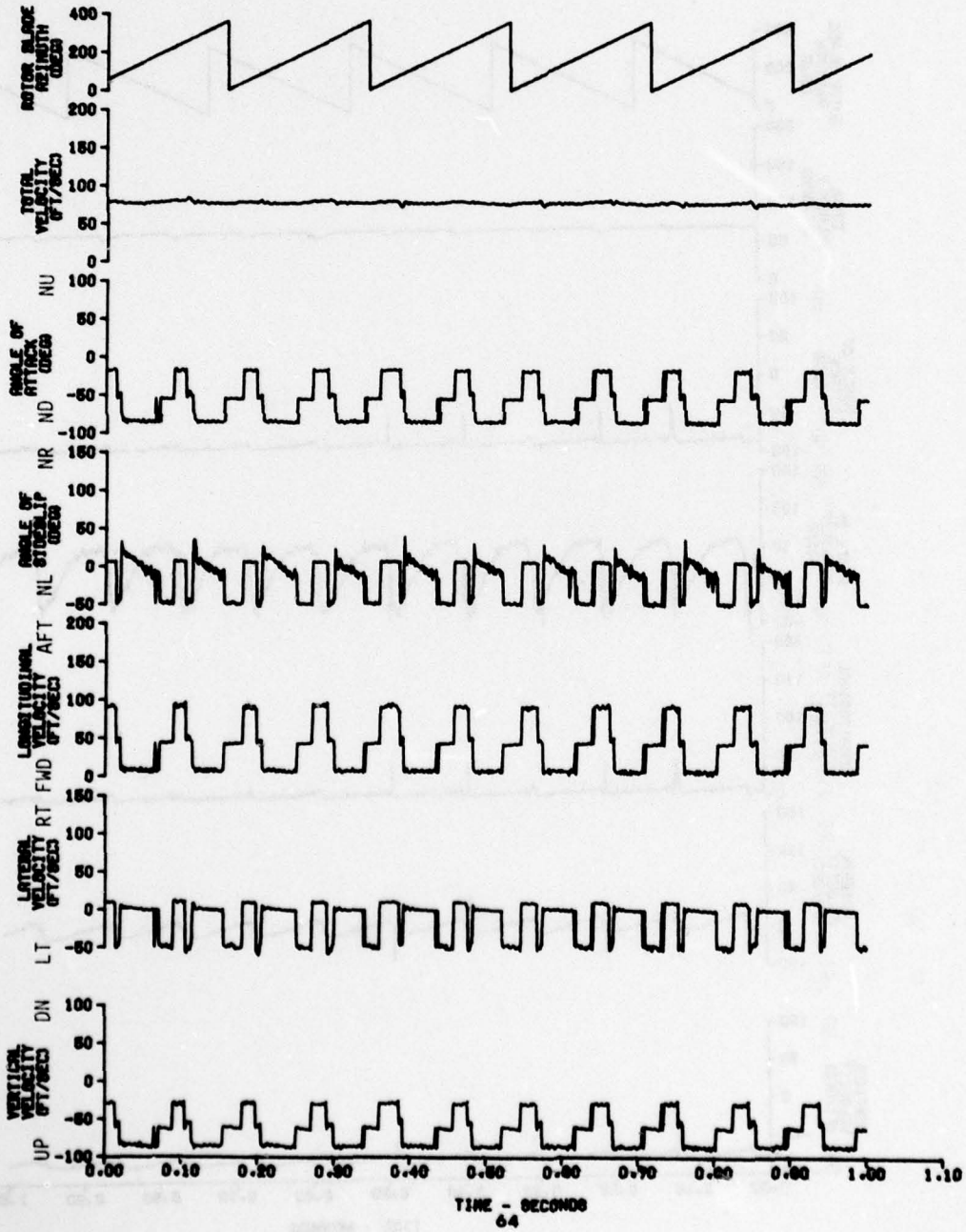

FIGURE 36
TRANSIENT AIRFLOW CHARACTERISTICS IN LEVEL FLIGHT
AH-1G UCR S/N 67-8844
RAKE POSITION NO. 2A (FS = 145, WL = 75)

PROBE NO. 3 (BL = 49)

FORWARD VELOCITY (ft/sec)	ADVANCE RATIO (μ)	THRUST COEFFICIENT (C_T)	ROTOR SPEED (RPM)
31.9	.0427	.00475	323.9

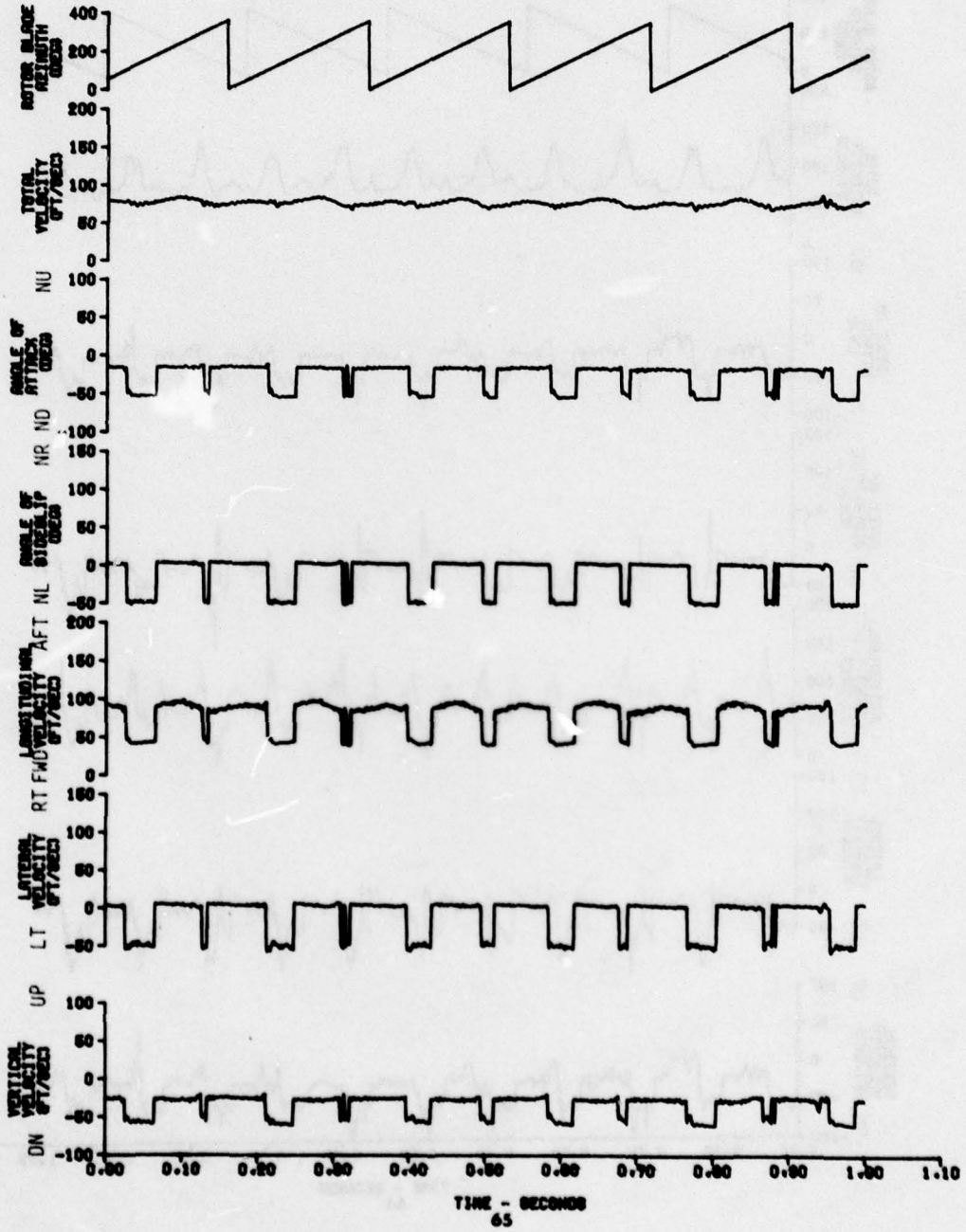

FIGURE 37
TRANSIENT AIRFLOW CHARACTERISTICS IN LEVEL FLIGHT
AH-1G USA S/N 67-8844
RAKE POSITION NO. 2A (FS = 145, WL = 75)

PROBE NO. 3 (BL = 49)

FORWARD VELOCITY (ft/sec)	ADVANCE RATIO (μ)	THRUST COEFFICIENT (C_T)	ROTOR SPEED (RPM)
41.5	.056	.00475	324.

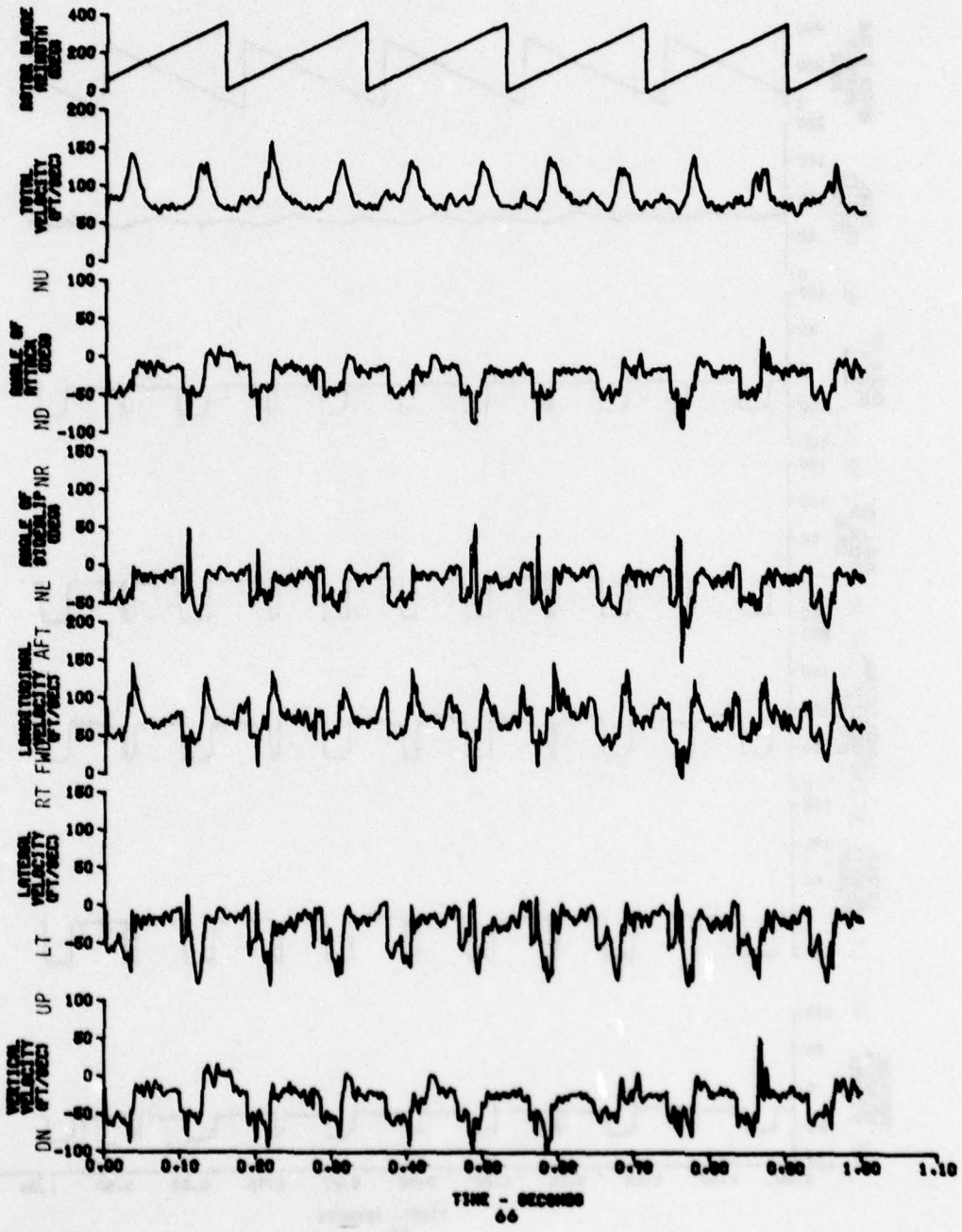

FIGURE 38
TRANSIENT AIRFLOW CHARACTERISTICS IN LEVEL FLIGHT
RH-1G USA S/N 67-8844
RAKE POSITION NO. 2A (FS = 145, WL = 75)

PROBE NO. 3 (BL = 49)

FORWARD VELOCITY (ft/sec)	ADVANCE RATIO (μ)	THRUST COEFFICIENT (C_T)	ROTOR SPEED (RPM)
56.3	.0701	.00473	323.9

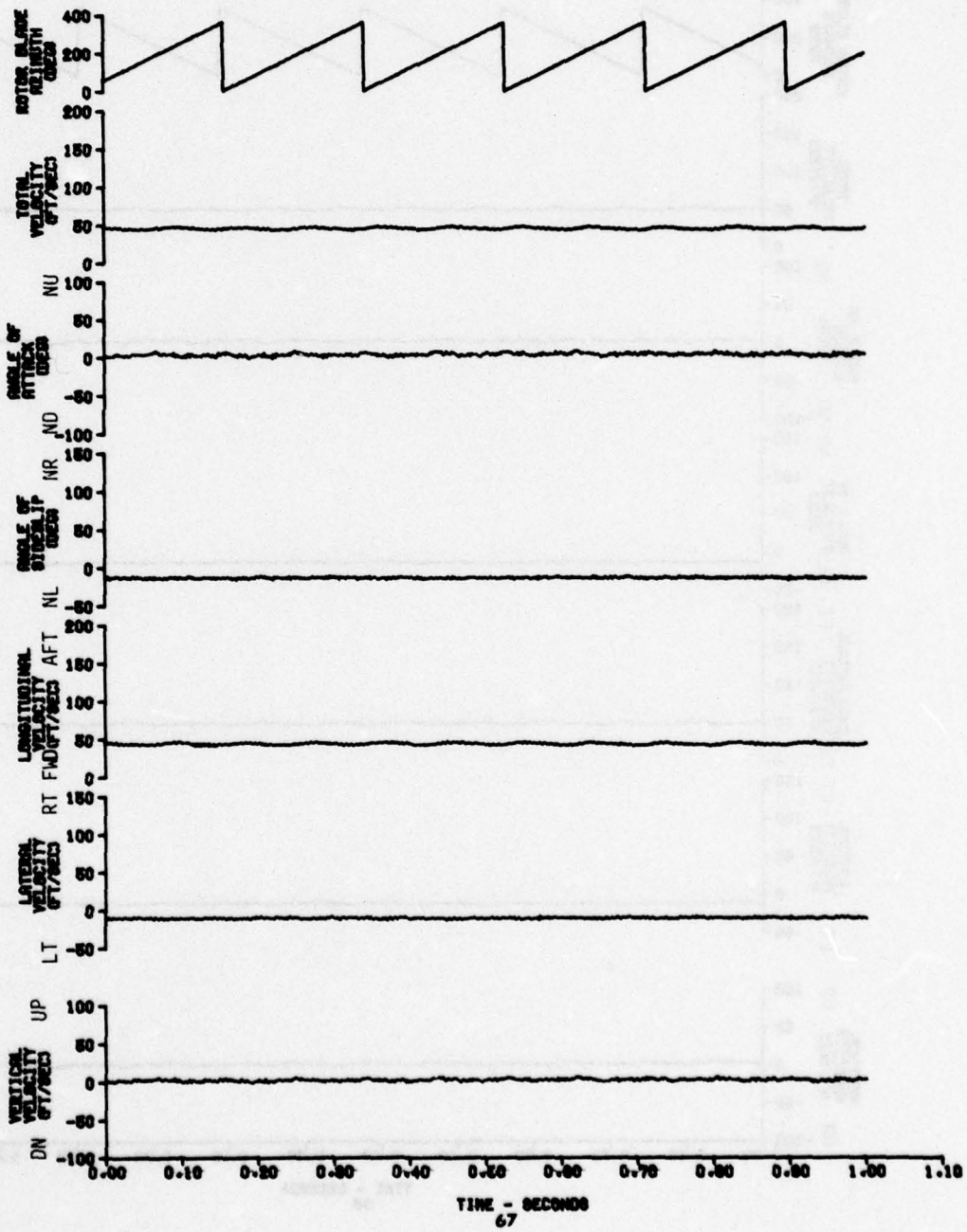

FIGURE 39
TRANSIENT AIRFLOW CHARACTERISTICS IN LEVEL FLIGHT
AH-1G UGR-S/N 67-0844
RAKE POSITION NO. 2A (FS = 145, WL = 75)

PROBE NO. 3 (BL = 49)

FORWARD VELOCITY (ft/sec)	ADVANCE RATIO (μ)	THRUST COEFFICIENT (C_T)	ROTOR SPEED (RPM)
56.2	.0753	.00473	323.8

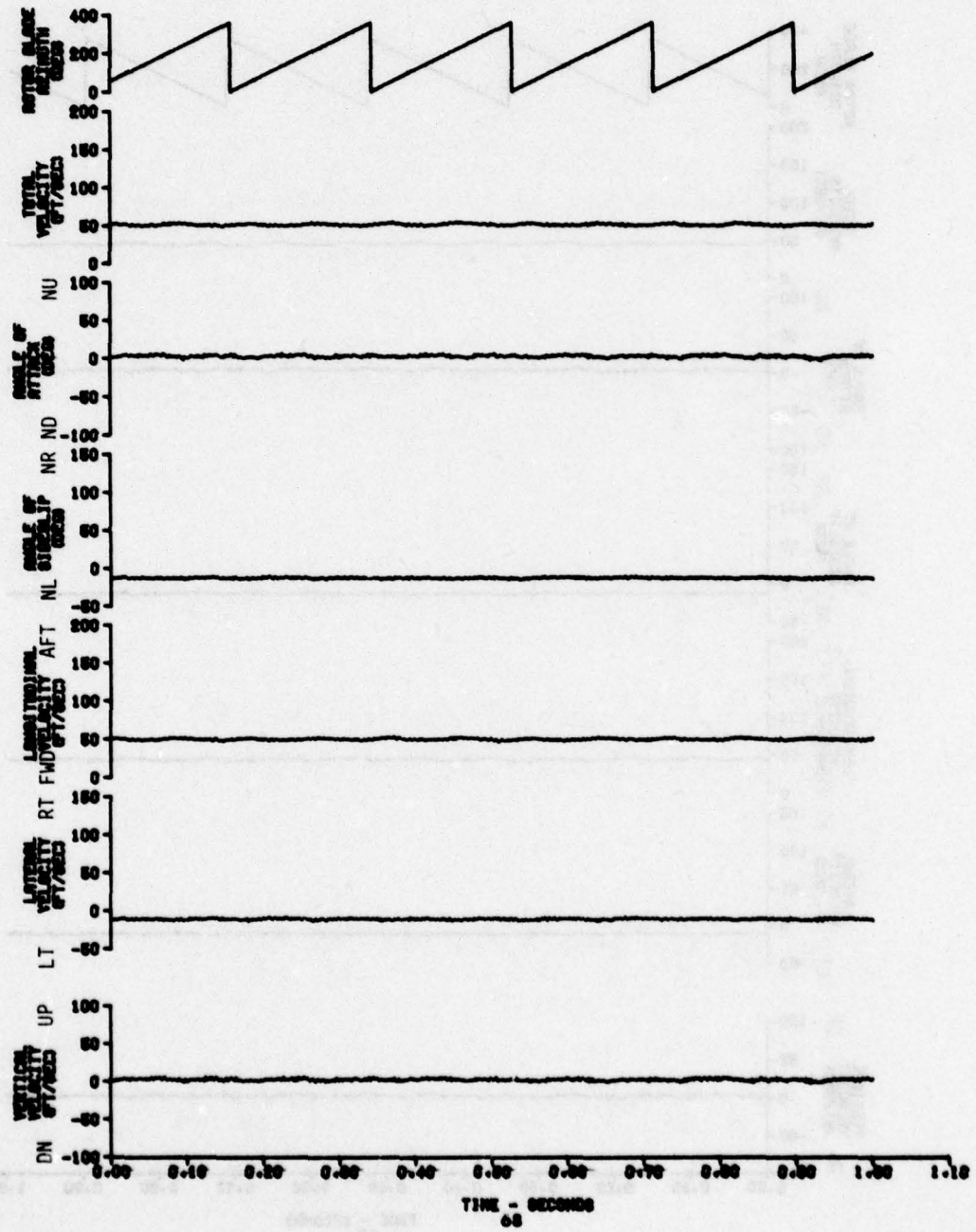

FIGURE 40
TRANSIENT AIRFLOW CHARACTERISTICS IN LEVEL FLIGHT
AH-1G USA S/N 67-8844
RAKE POSITION NO. 2A (FS = 145, WL = 75)

PROBE NO. 3 (BL = 49)

FORWARD VELOCITY (ft/sec)	ADVANCE RATIO (μ)	THRUST COEFFICIENT (C_T)	ROTOR SPEED (RPM)
94.8	.127	.00473	323.9

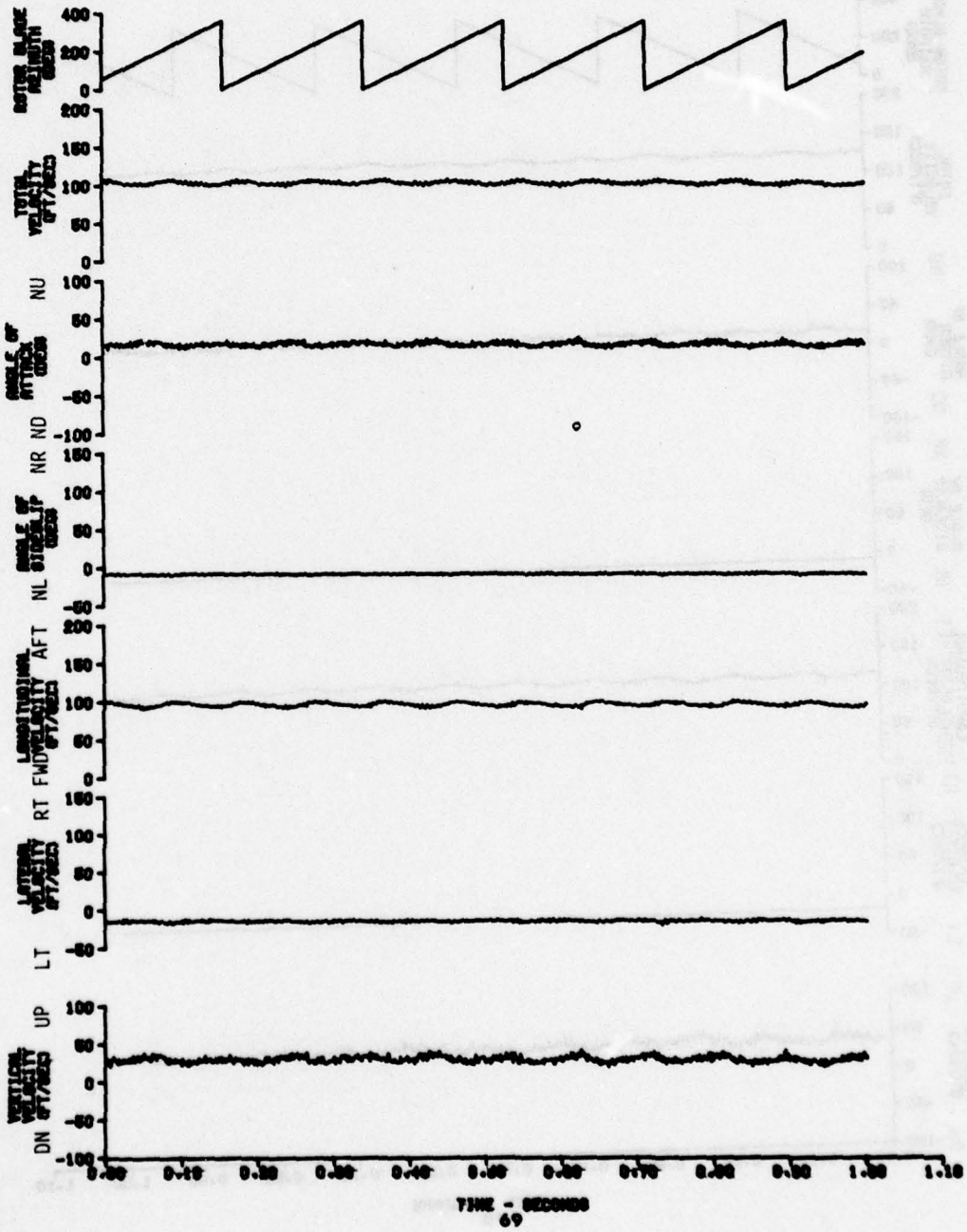

FIGURE 41
TRANSIENT AIRFLOW CHARACTERISTICS IN LEVEL FLIGHT
AH-1G USA S/N 67-0044
RAKE POSITION NO. 2A (FS = 145, WL = 75)

PROBE NO. 3 (BL = 49)

FORWARD VELOCITY (ft/sec)	ADVANCE RATIO (μ)	THRUST COEFFICIENT (C_T)	ROTOR SPEED (RPM)
116.0	.156	.00476	323.5

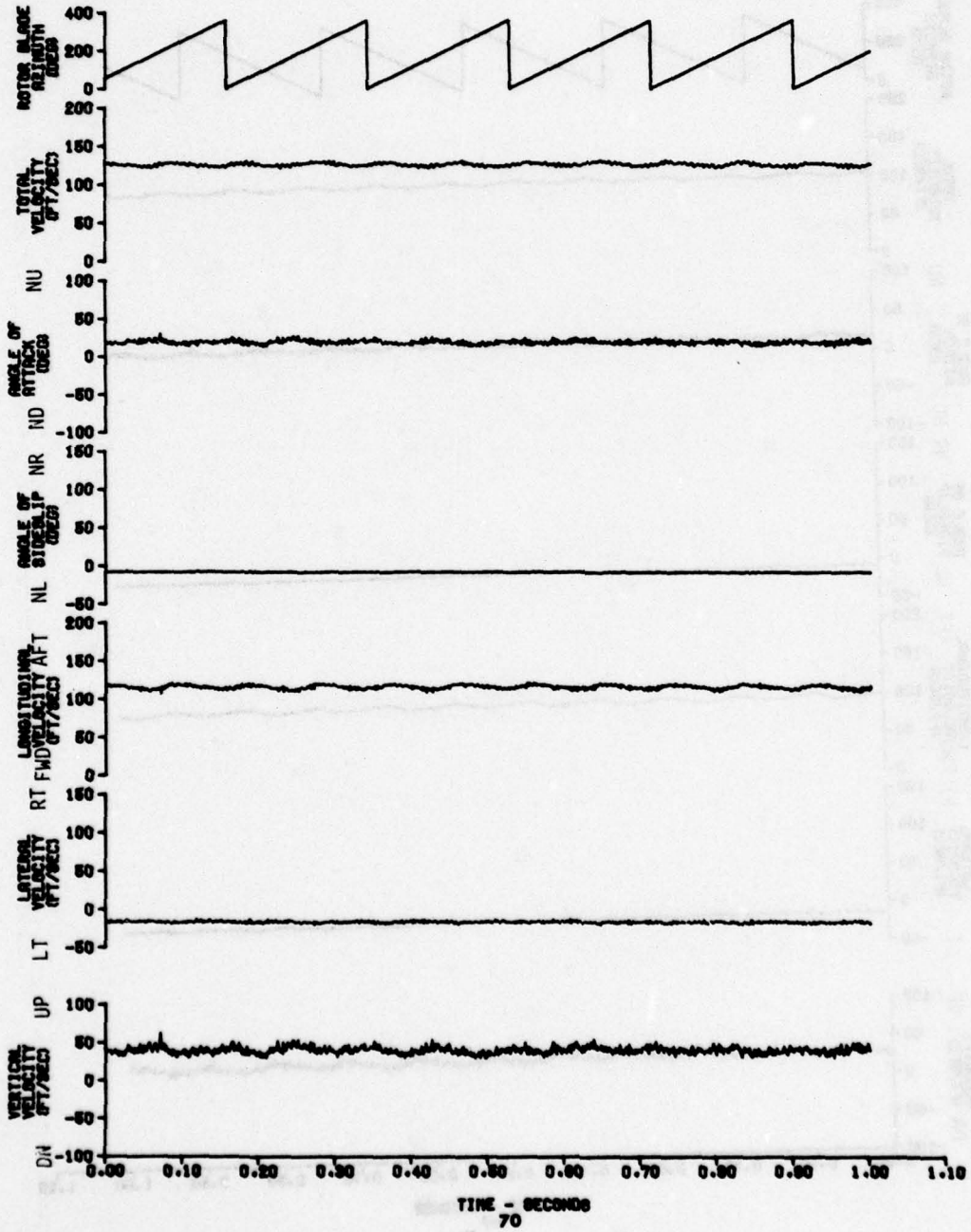

FIGURE 42
TRANSIENT AIRFLOW CHARACTERICTICS IN LEVEL FLIGHT
AH-1G USA S/N 67-0844
RAKE POSITION NO. 2A (FS = 145, WL = 75)

PROBE NO. 3 (BL = 49)

FORWARD VELOCITY (ft/sec)	ADVANCE RATIO (μ)	THRUST COEFFICIENT (C_T)	ROTOR SPEED (RPM)
119.4	.1601	.00476	323.8

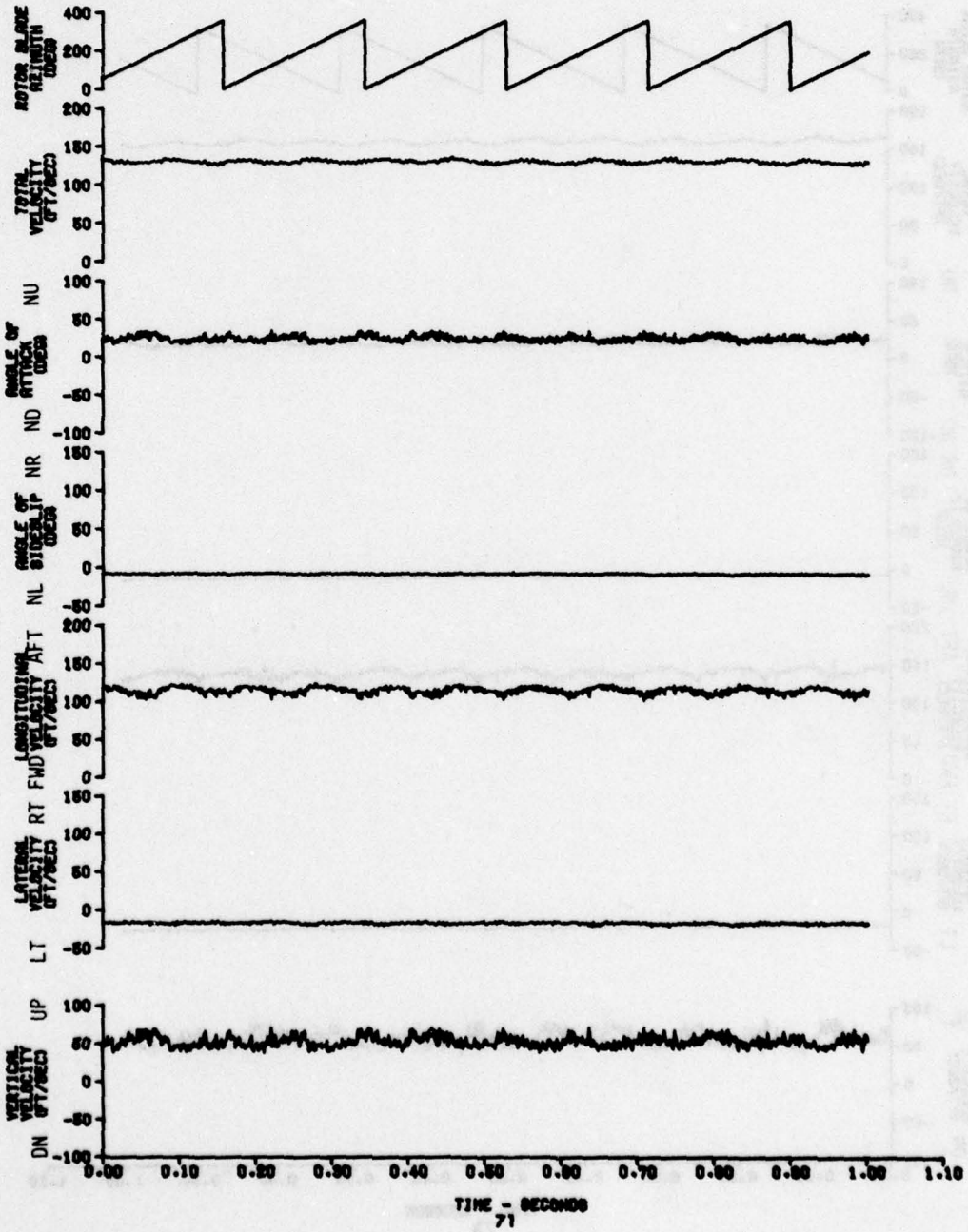

FIGURE 43
TRANSIENT AIRFLOW CHARACTERISTICS IN LEVEL FLIGHT
AH-1G USA S/N 67-0044
RAKE POSITION NO. 2A (FS = 145, WL = 75)

PROBE NO. 3 (BL = 49)

FORWARD VELOCITY (ft/sec)	ADVANCE RATIO (μ)	THRUST COEFFICIENT (C_T)	ROTOR SPEED (RPM)
152.	.204	.00476	323.9

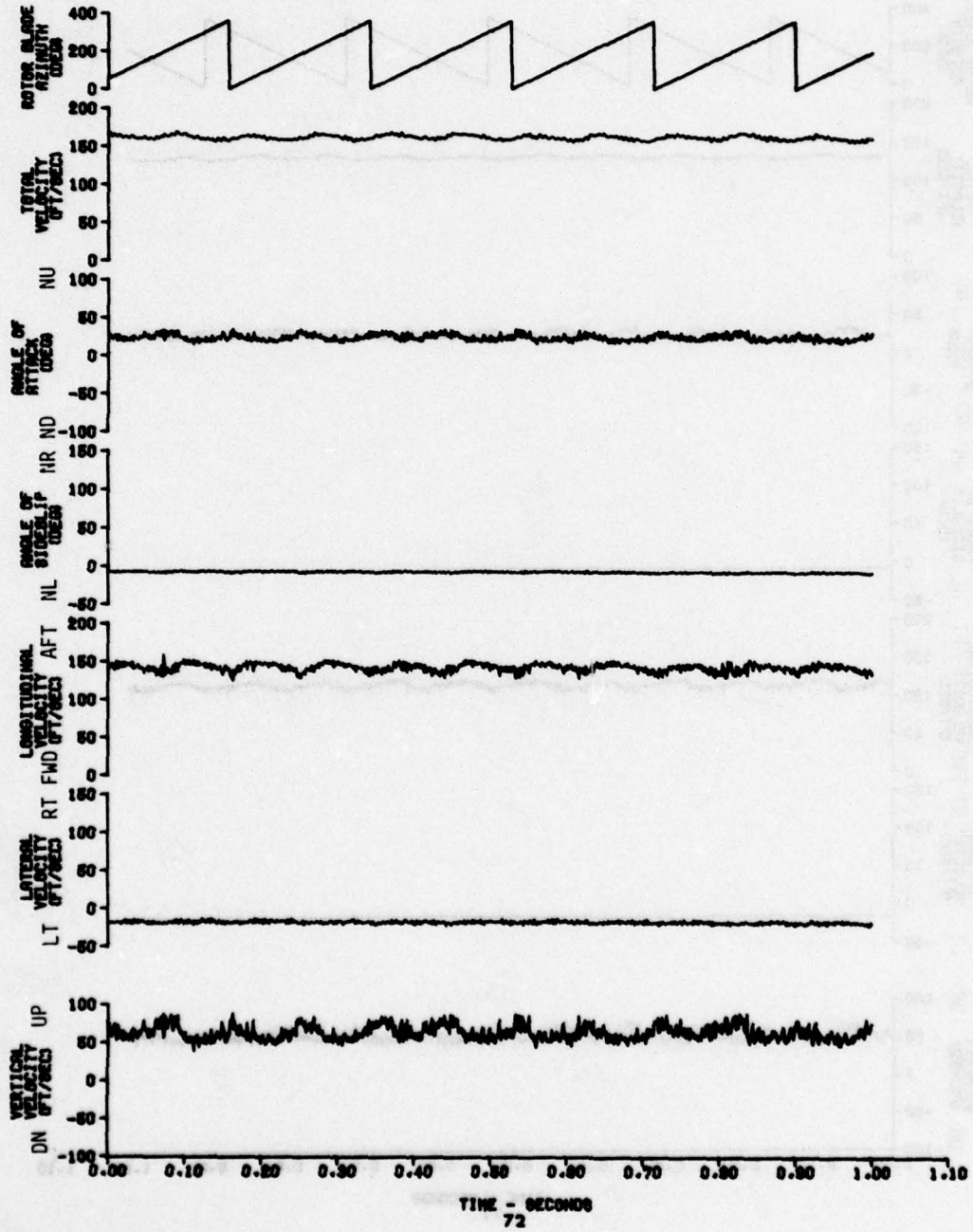

FIGURE 44
TRANSIENT AIRFLOW CHARACTERISTICS IN LEVEL FLIGHT
AH-1G USA S/N 67-0844
RAKE POSITION NO. 2A (FS = 145, WL = 75)

PROBE NO. 3 (BL = 49)

FORWARD VELCITY (ft/sec)	ADVANCE RATIO (μ)	THRUST COEFFICIENT (C_T)	ROTOR SPEED (RPM)
197.8	.265	.00473	323.9

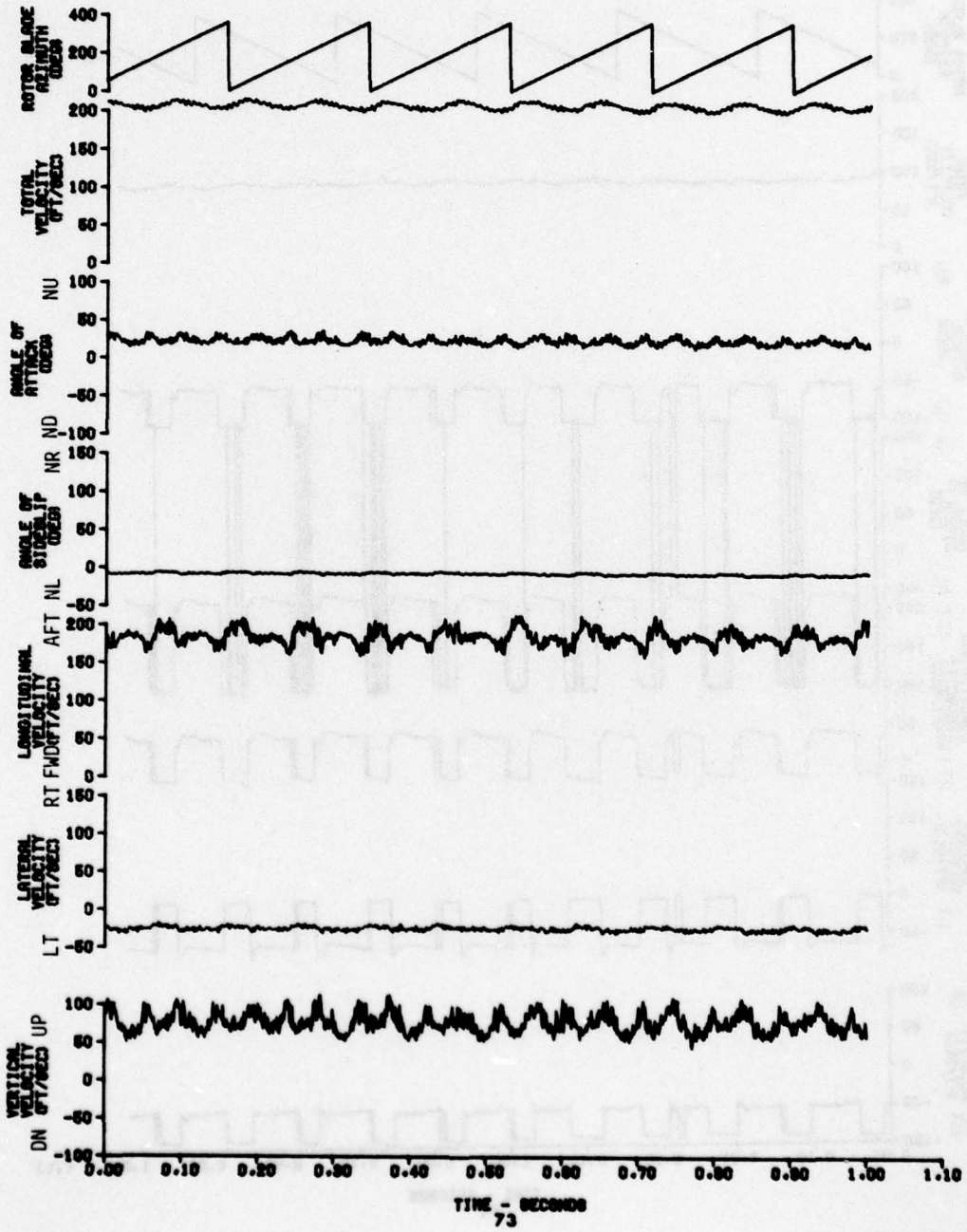

FIGURE 45
TRANSIENT AIRFLOW CHARACTERISTICS IN LEVEL FLIGHT
AH-1G USA S/N 67-6844
RAKE POSITION NO. 8A (FS = 37, WL = 75)

PROBE NO. 3 (BL = 49)

FORWARD VELOCITY (ft/sec)	ADVANCE RATIO (μ)	THRUST COEFFICIENT (C_T)	ROTOR SPEED (RPM)
0.	0. (HOVER)	.00475	324.3

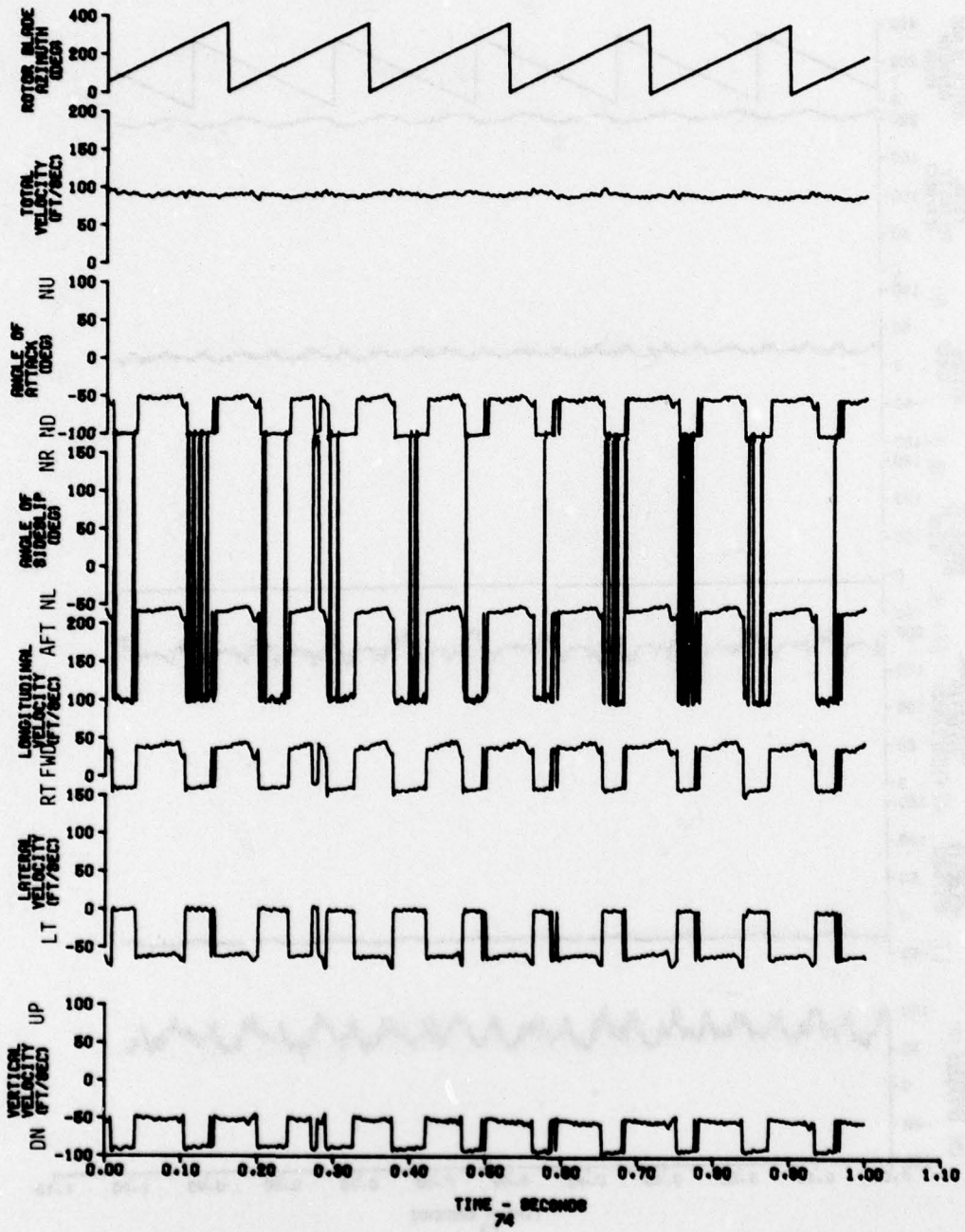

FIGURE 46
TRANSIENT AIRFLOW CHARACTERISTICS IN LEVEL FLIGHT
AH-1G USA S/N 67-8844
RAKE POSITION NO. 8A (FS = 37, WL = 75)

PROBE NO. 3 (BL = 49)

FORWARD VELOCITY (ft/sec)	ADVANCE RATIO (μ)	THRUST COEFFICIENT (C_T)	ROTOR SPEED (RPM)
13.7	.184	.00475	324.2

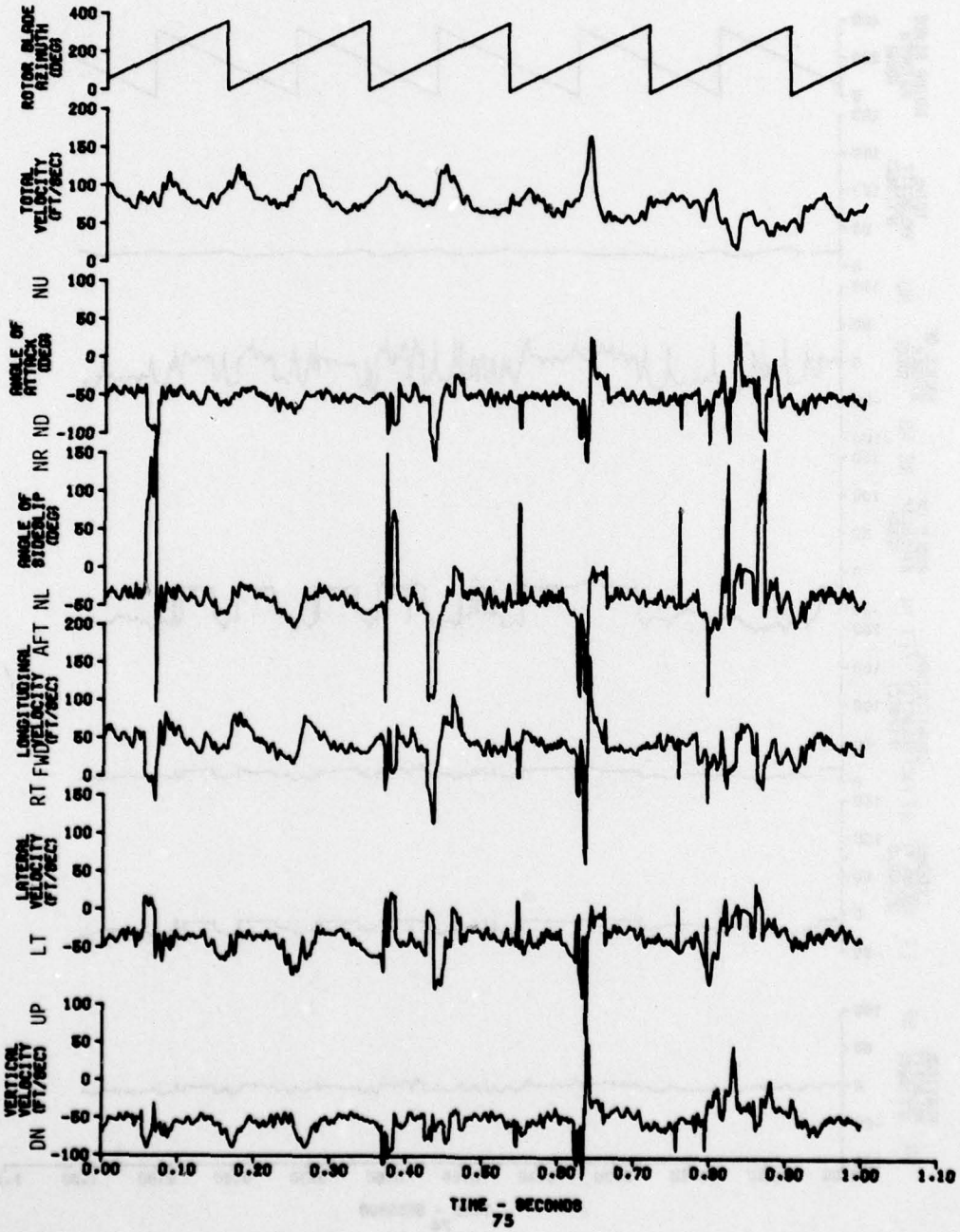

FIGURE 47
TRANSIENT AIRFLOW CHARACTERISTICS IN LEVEL FLIGHT
AH-1G USA S/N 67-8844
RAKE POSITION NO. 8A (FS = 37, WL = 75)

PROBE NO. 3 (BL = 49)

FORWARD VELOCITY (ft/sec)	ADVANCE RATIO (μ)	THRUST COEFFICIENT (C_T)	ROTOR SPEED (RPM)
25.2	.337	.00475	324.3

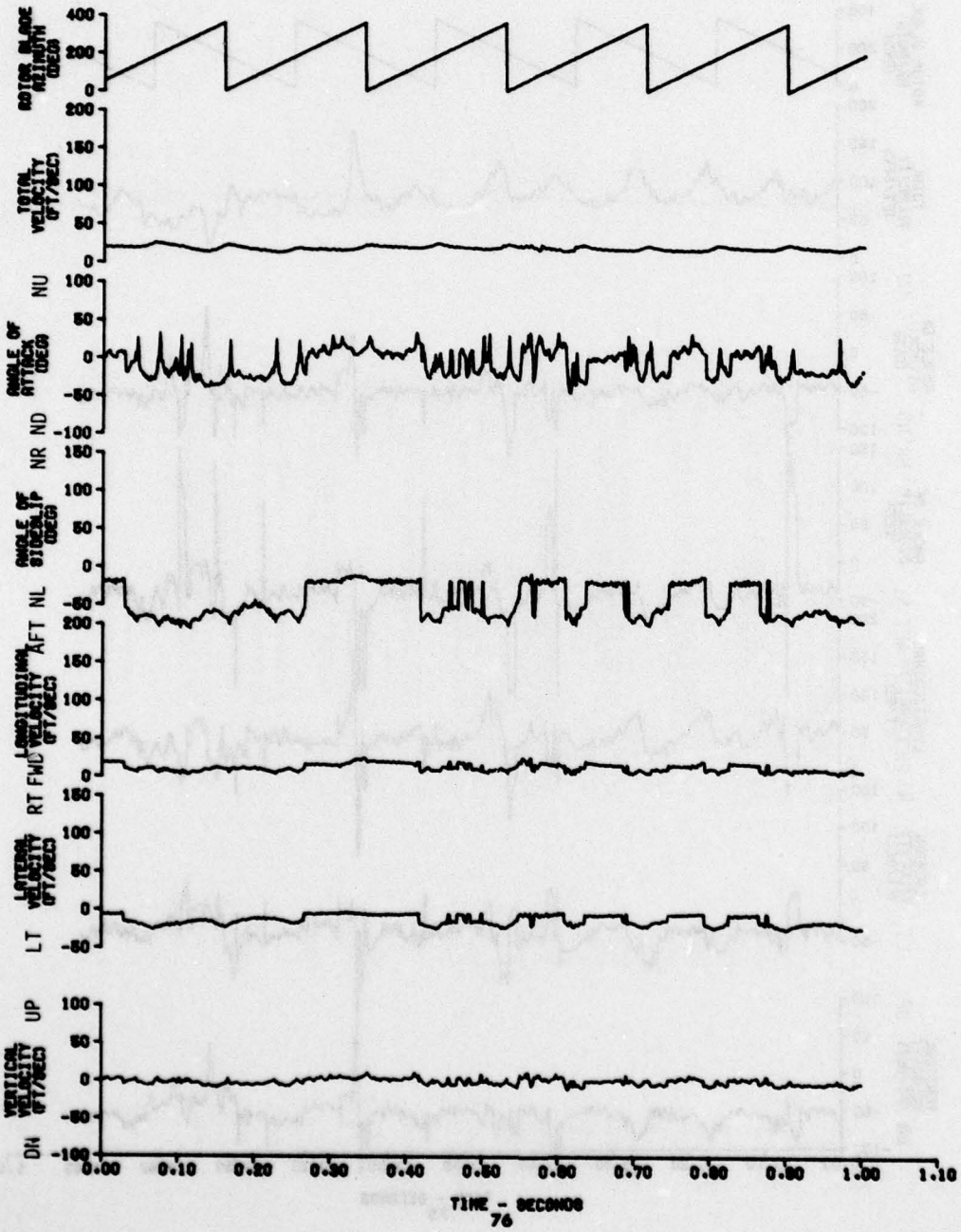

FIGURE 48
TRANSIENT AIRFLOW CHARACTERISTICS IN LEVEL FLIGHT
AH-1G USA S/N 67-0044
RAKE POSITION NO. 8A (FS = 37, WL = 75)

PROBE NO. 3 (BL = 49)

FORWARD VELOCITY (ft/sec)	ADVANCE RATIO (μ)	THRUST COEFFICIENT (C_T)	ROTOR SPEED (RPM)
33.4	.0446	.00475	325.1

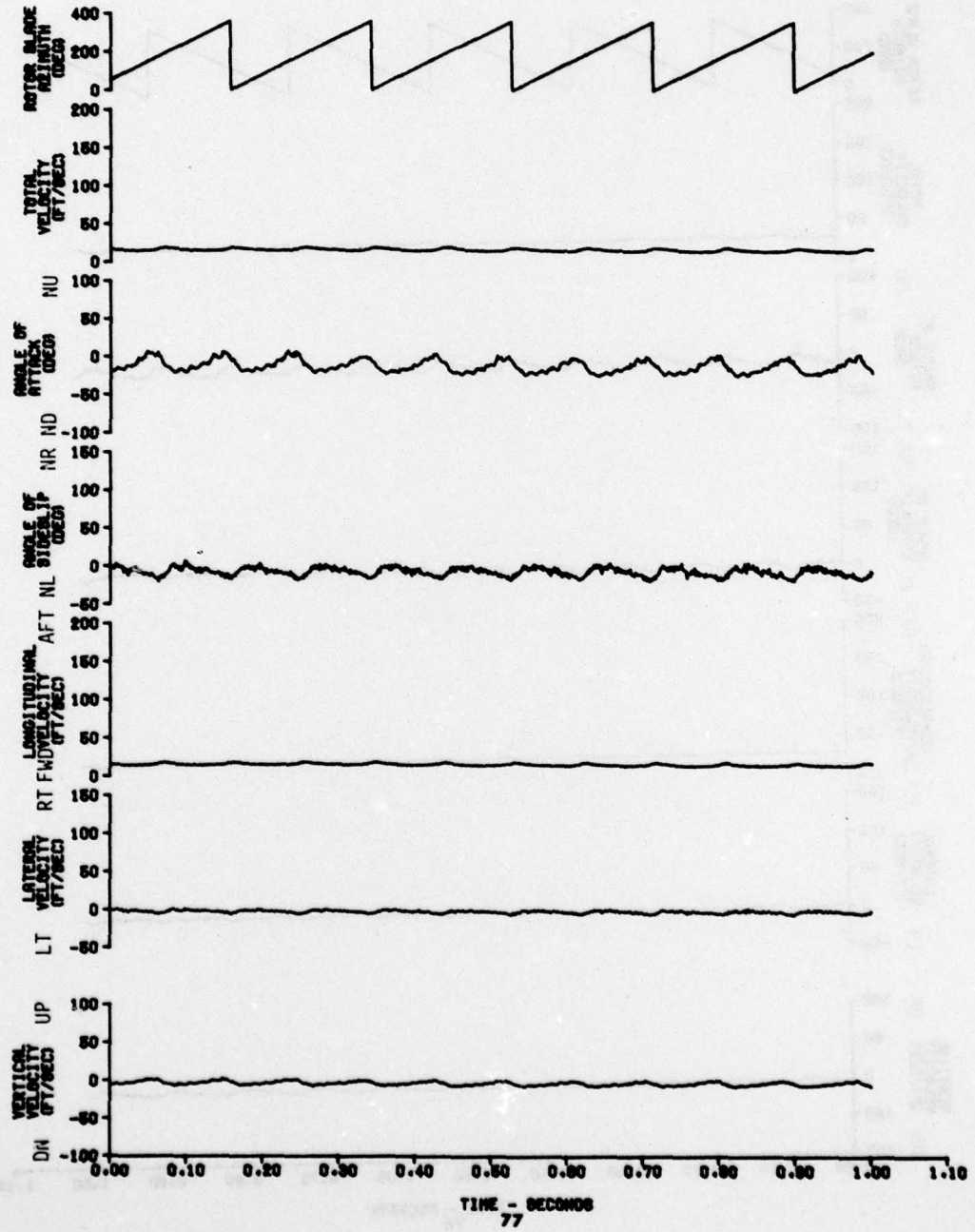

FIGURE 49
TRANSIENT AIRFLOW CHARACTERISTICS IN LEVEL FLIGHT
AH-1G USR S/N 67-6044
RAKE POSITION NO. 8A (FS = 37, WL = 75)

PROBE NO. 3 (BL = 49)

FORWARD VELOCITY (ft/sec)	ADVANCE RATIO (μ)	THRUST COEFFICIENT (C_T)	ROTOR SPEED (RPM)
42.9	.0574	.00475	324.8

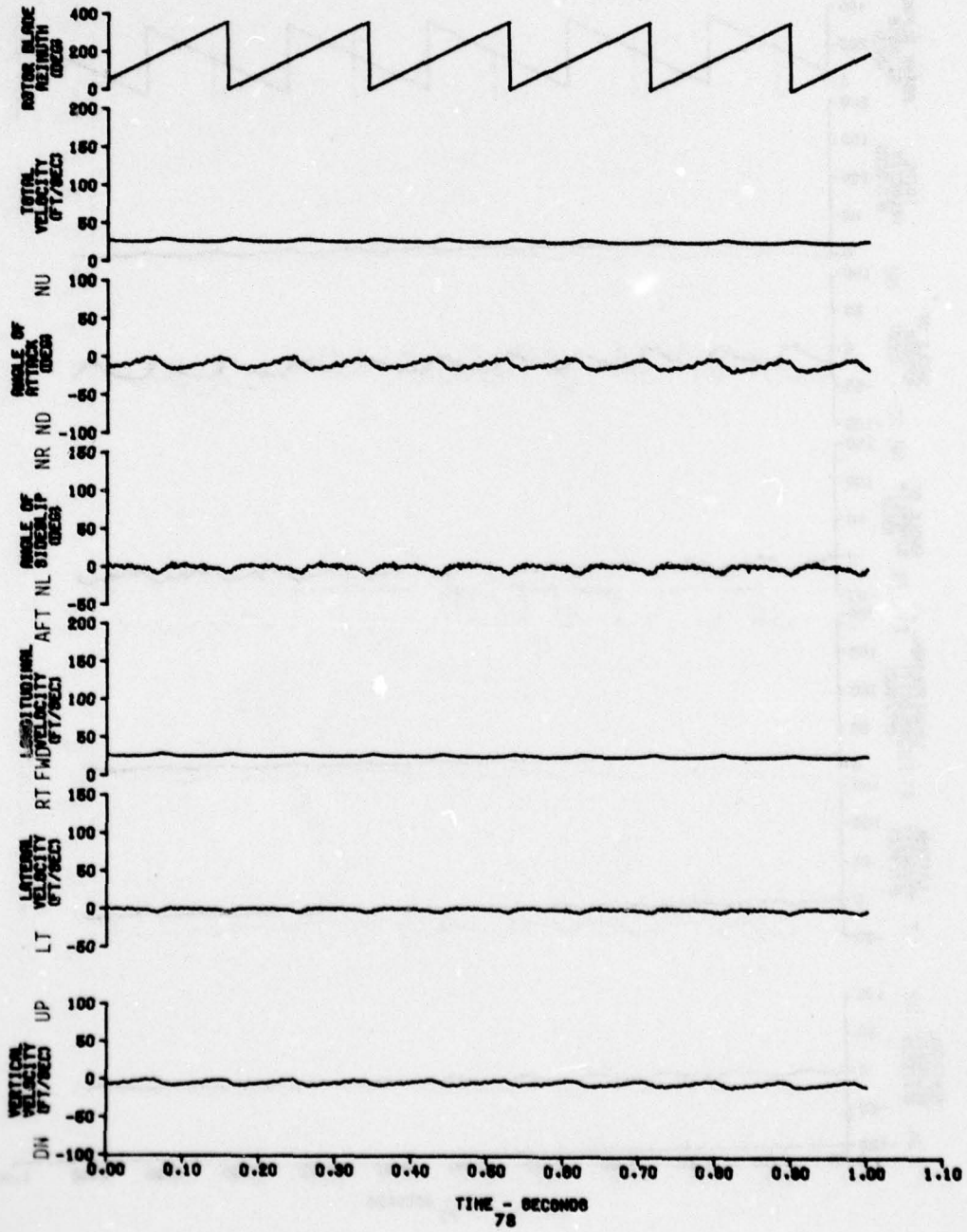

FIGURE 50
TRANSIENT AIRFLOW CHARACTERISTICS IN LEVEL FLIGHT
AH-1G USA S/N 67-0044
RAKE POSITION NO. 8A (FS = 37, WL = 75)

PROBE NO. 3 (BL = 49)

FORWARD VELOCITY (ft/sec)	ADVANCE RATIO (μ)	THRUST COEFFICIENT (C_T)	ROTOR SPEED (RPM)
53.8	.0719	.00475	324.7

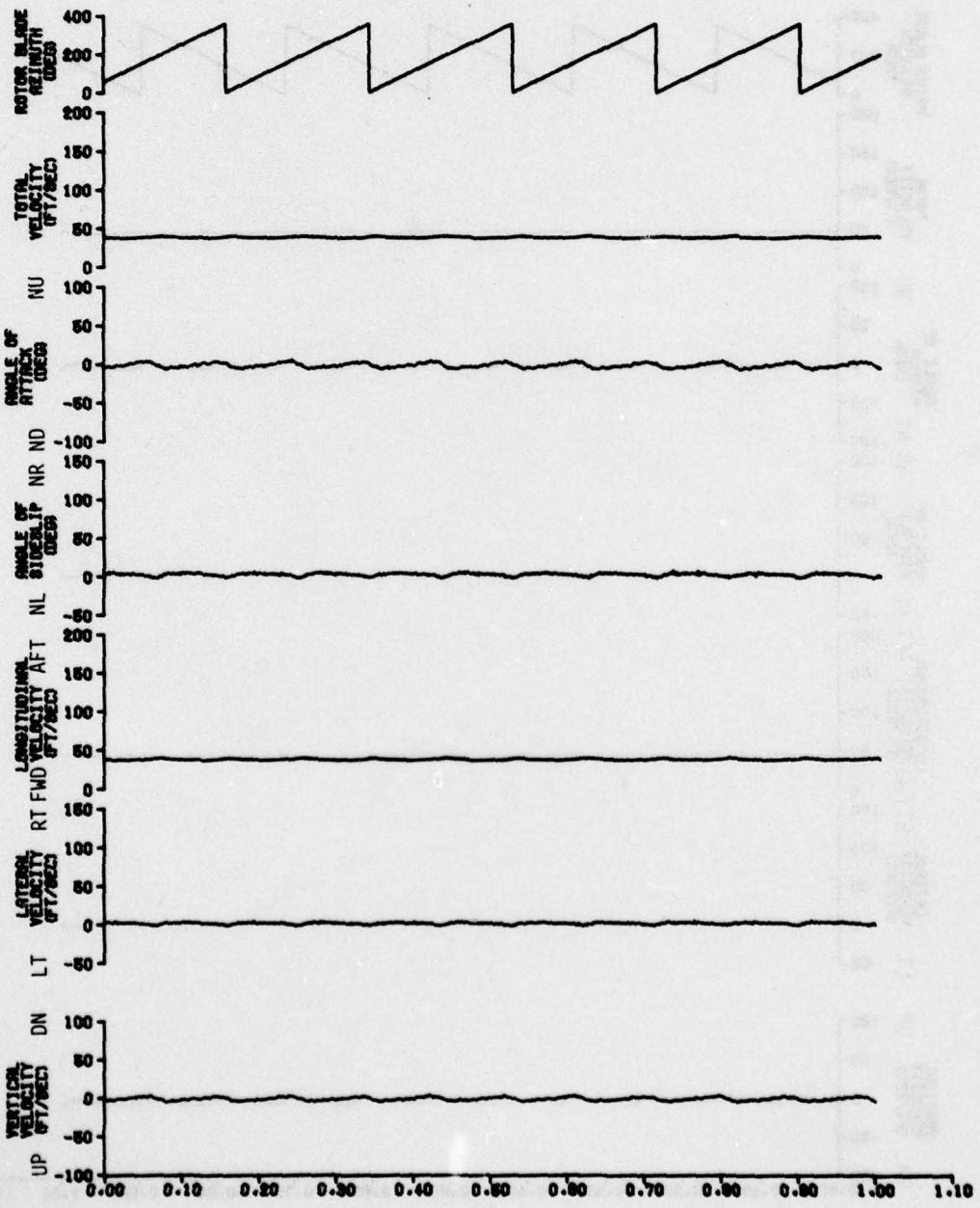

FIGURE 51
TRANSIENT AIRFLOW CHARACTERISTICS IN LEVEL FLIGHT
AH-1G USA S/N 67-0044
RAKE POSITION NO. 3A (FS = 37, WL = 75)

PROBE NO. 3 (BL = 75)

FORWARD VELOCITY (ft/sec)	ADVANCE RATIO (μ)	THRUST COEFFICIENT (C_T)	ROTOR SPEED (RPM)
		.00475	324.

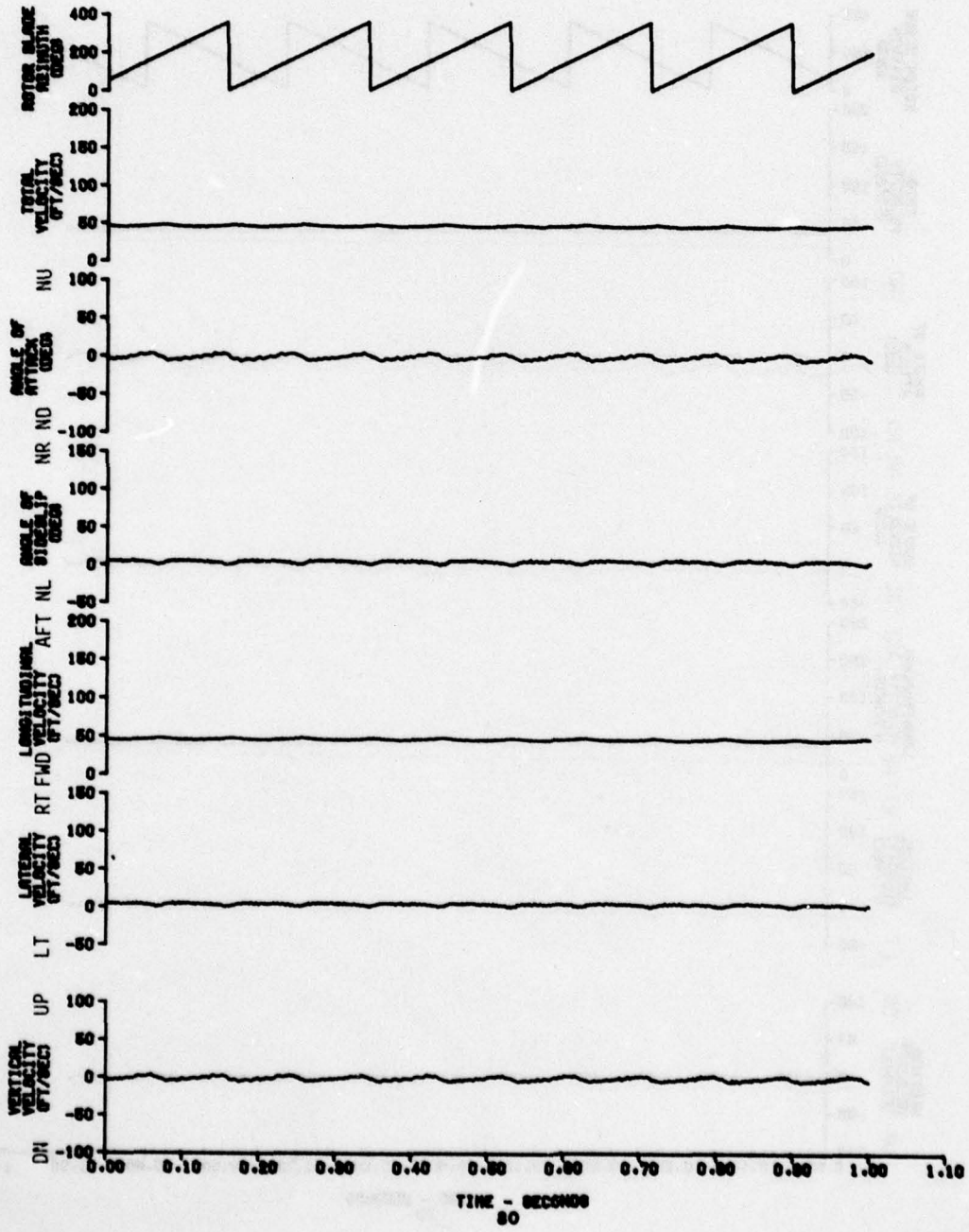

FIGURE 52
TRANSIENT AIRFLOW CHARACTERISTICS IN LEVEL FLIGHT
AH-1G USA S/N 67-6044
RAKE POSITION NO. 8A (FS = 37, WL = 75)

PROBE NO. 3 (BL = 49)

FORWARD VELOCITY (ft/sec)	ADVANCE RATIO (μ)	THRUST COEFFICIENT (C_T)	ROTOR SPEED (RPM)
101.6	.136	.00475	324.6

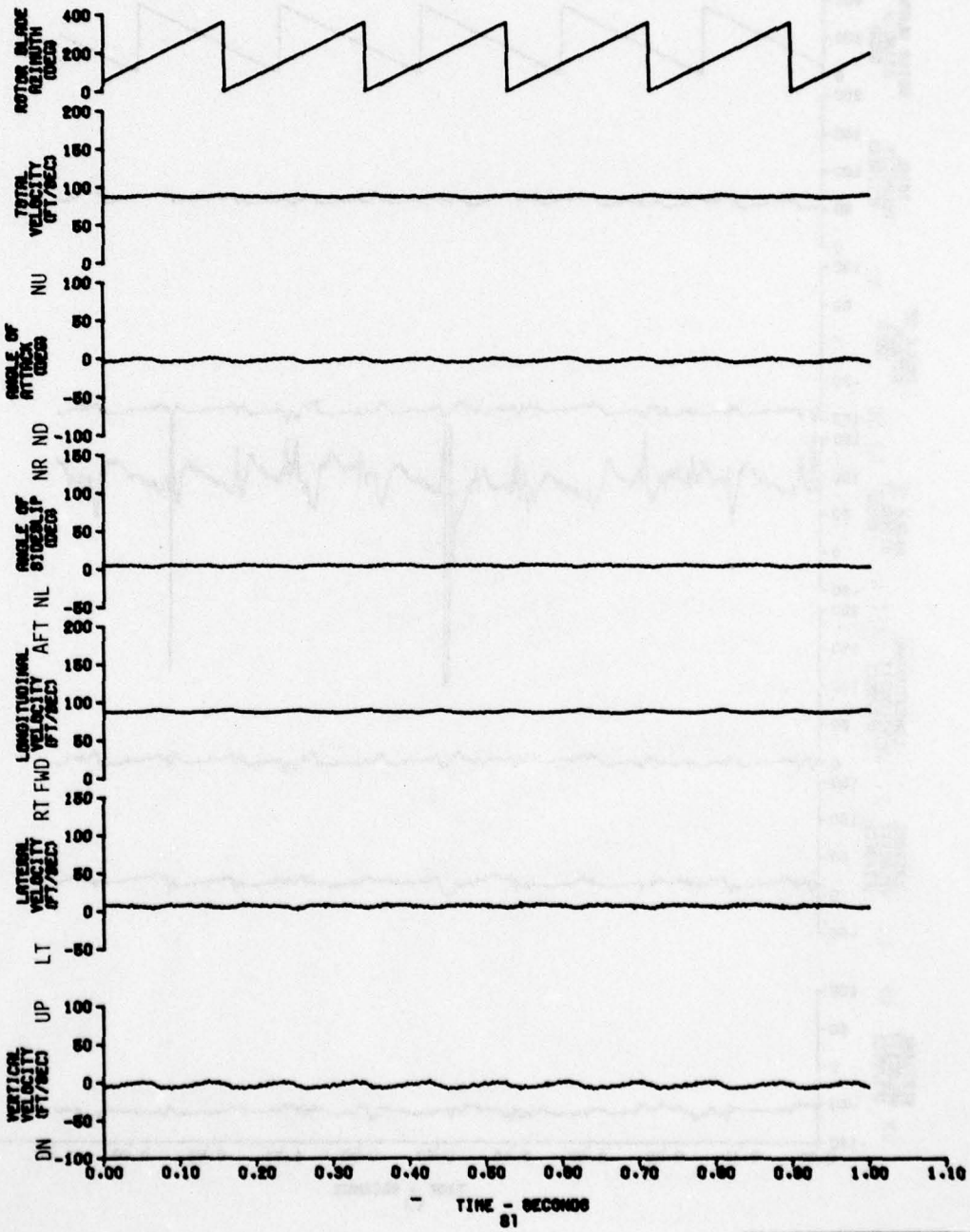

FIGURE 53
TRANSIENT AIRFLOW CHARACTERISTICS IN LEVEL FLIGHT
AH-1G USA S/N 67-GR44
RAKE POSITION NO. 1B (FS = 37, WL = 39)

PROBE NO. 3 (BL = 49)

ADVANCE RATIO (μ)	THRUST COEFFICIENT (C_T)	ROTOR SPEED (RPM)	ROTOR HEIGHTH (FT)
HOVER	.00469	324.3	OGE

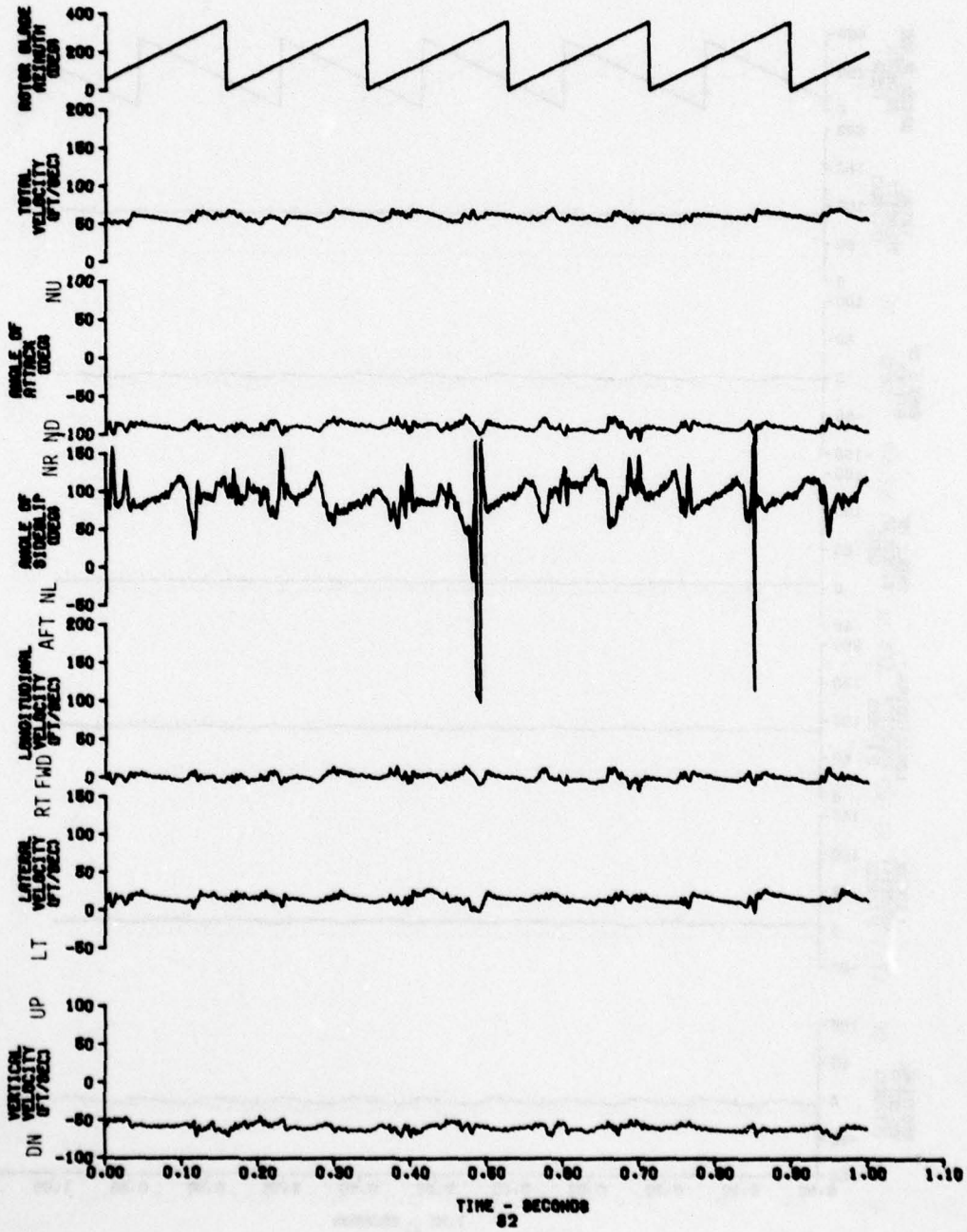

FIGURE 54
TRANSIENT AIRFLOW CHARACTERISTICS IN LEVEL FLIGHT
AH-1G USA S/N 67-0044
RAKE POSITION NO. 1B (FS = 37, WL = 39)

PROBE NO. 3 (BL = 49)

ADVANCE RATIO (μ)	THRUST COEFFICIENT (C_T)	ROTOR SPEED (RPM)	ROTOR HEIGHTH (FT)
HOVER	.00409	324.3	42.

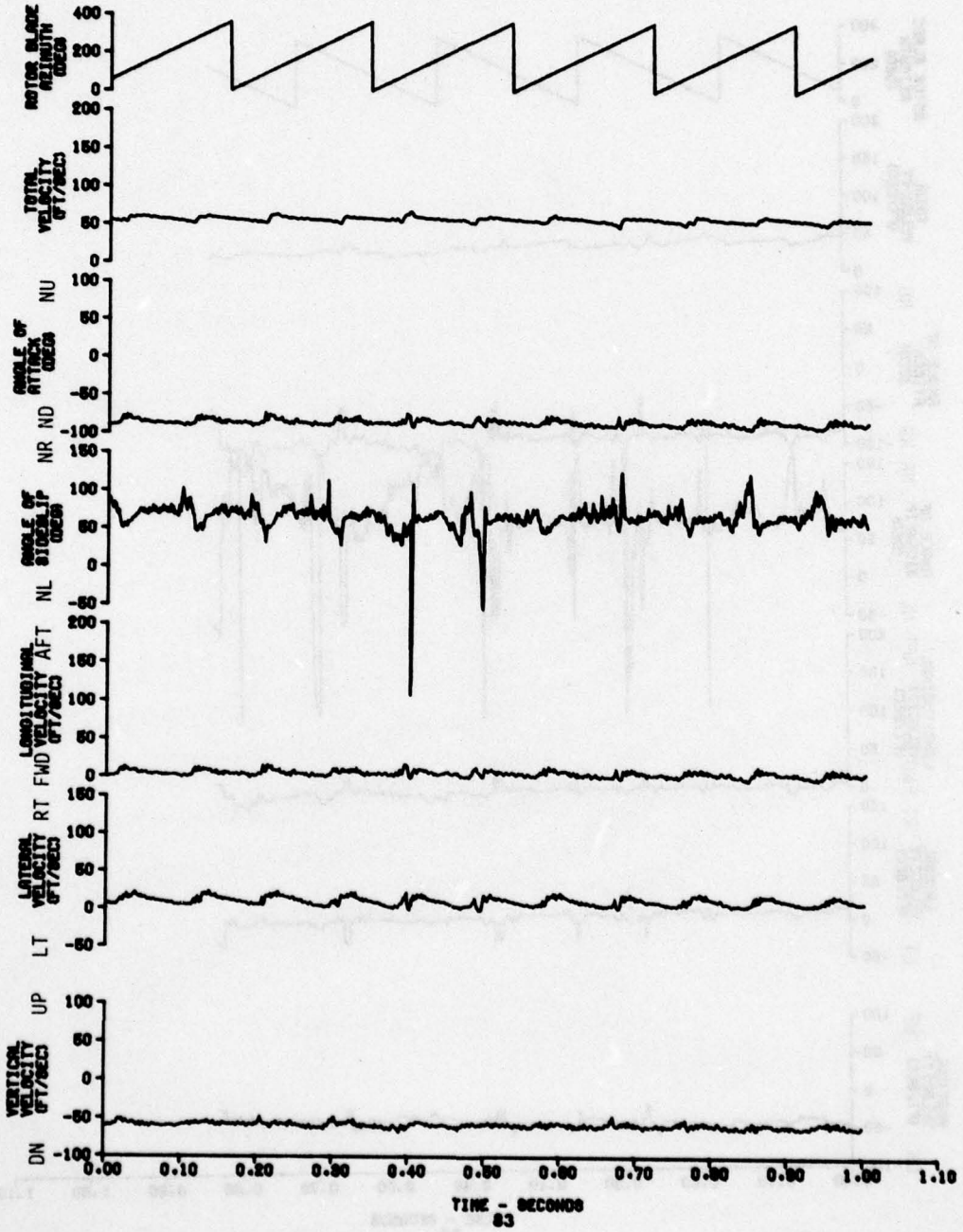

FIGURE 55
TRANSIENT AIRFLOW CHARACTERISTICS IN LEVEL FLIGHT
AH-1G USA S/N 67-0044
RAKE POSITION NO. 1B (FS = 37, WL = 39)

PROBE NO. 3 (BL = 49)

ADVANCE RATIO (μ)	THRUST COEFFICIENT (C_T)	ROTOR SPEED (RPM)	ROTOR HEIGHTH (FT)
HOVER	.00407	323.5	32.

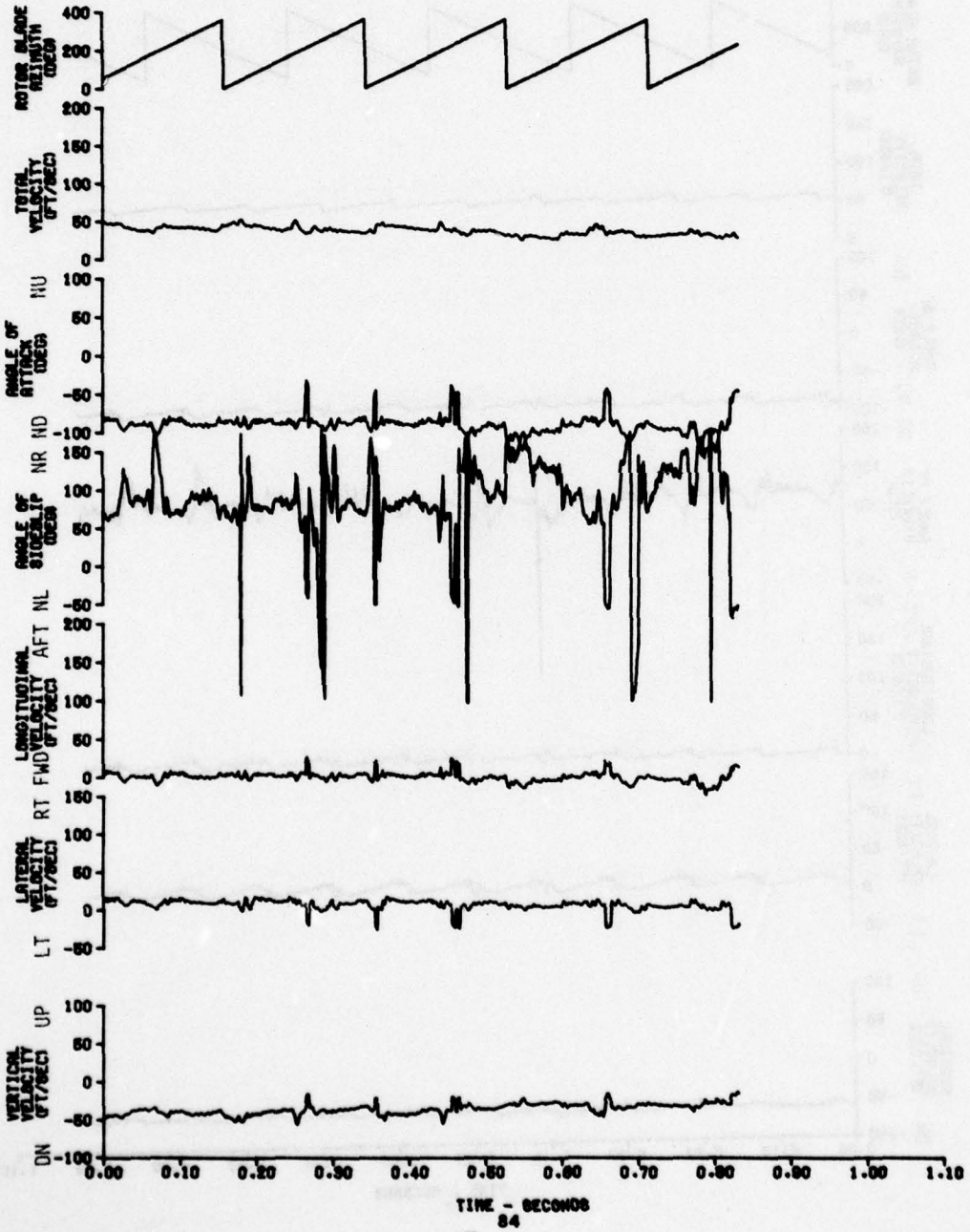

FIGURE 56
TRANSIENT AIRFLOW CHARACTERISTICS IN LEVEL FLIGHT
AH-1G USA S/N 67-6044
RAKE POSITION NO. 1B (FS = 37, WL = 39)

PROBE NO. 3 (BL = 49)

ADVANCE RATIO (μ)	THRUST COEFFICIENT (C_T)	ROTOR SPEED (RPM)	ROTOR HEIGHTH (FT)
HOVER	.00406	323.6	22

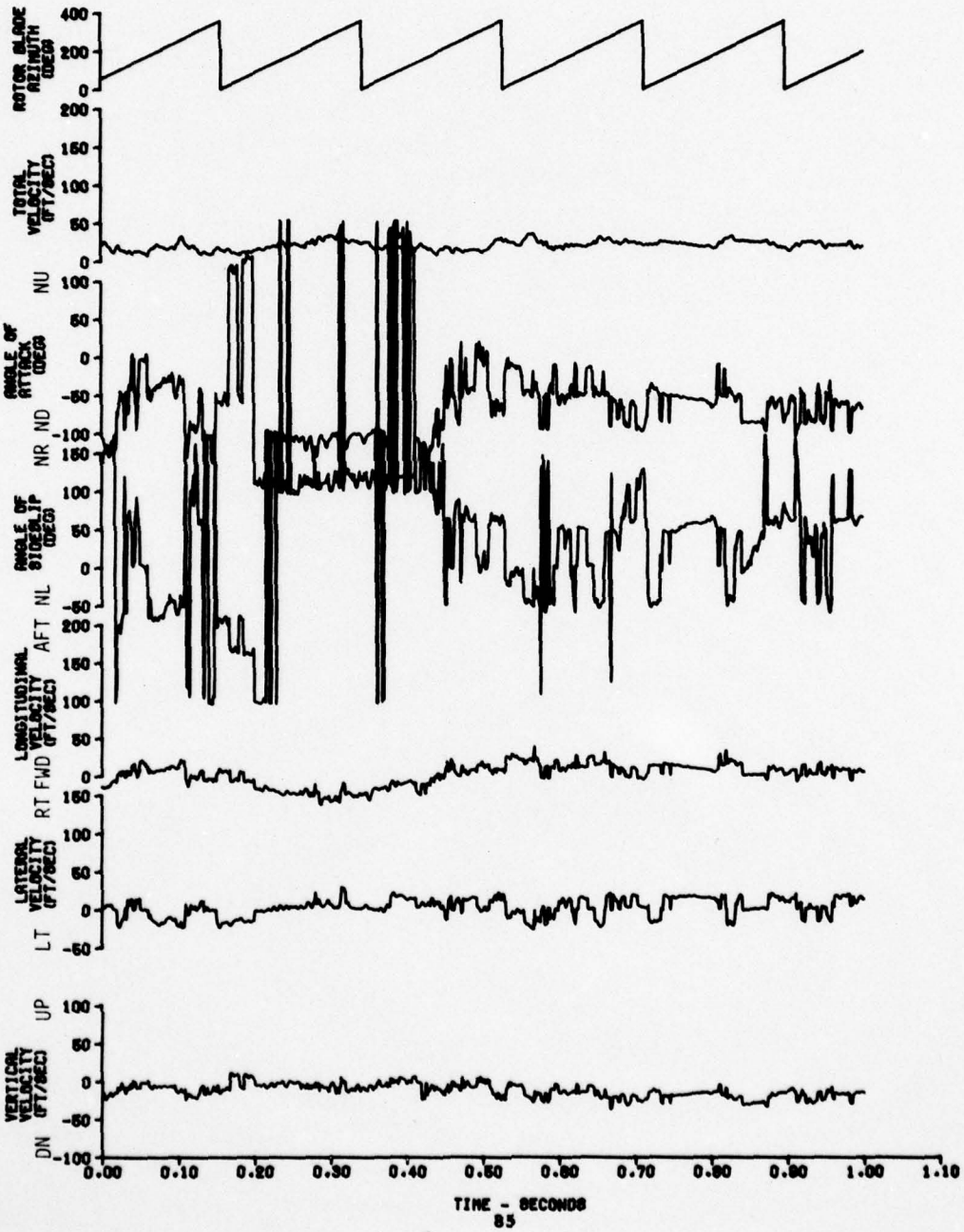

DISTRIBUTION

Director of Defense Research and Engineering	2
Deputy Director of Test and Evaluation, OSD (OAD(SSST&E))	1
Assistant Secretary of the Army (R&D), Deputy for Aviation	1
Deputy Chief of Staff for Research, Development, and Acquisition (DAMA-WSA, DAMA-RA, DAMA-PPM-T)	2
US Army Materiel Development and Readiness Command DRCPM-AAH-TM-T, DRCPM-CO, DRCSF-A, DRCQA)	12
US Army Aviation Research and Development Command (DRDAV-EQ)	12
US Army Training and Doctrine Command (ATCD-CM-C)	1
US Army Materiel Systems Analysis Activity (DRXSY-CM)	2
US Army Test and Evaluation Command (DRSTE-AV, USMC LnO)	3
US Army Electronics Command (AMSEL-VL-D)	1
US Army Forces Command (AFOP-AV)	1
US Army Armament Command (SARRI-LW)	2
US Army Missile Command (DRSMI-QT)	1
Director, Research & Technology Laboratories/Ames	2
Research & Technology Laboratory/Aeromechanics	2
Research & Technology Laboratory/Propulsion	2
Research & Technology Laboratory/Structures	2
US Army Air Mobility Laboratory, Applied Technology Lab	1
Human Engineering Laboratory (DRXHE-HE)	1
US Army Aeromedical Research Laboratory	1
US Army Infantry School (ATSH-TSM-BH)	1
US Army Aviation Center (ATZO-D-MT)	3
US Army Aviation Test Board (ATZQ-OT-C)	2
US Army Aviation School (ATZQ-AS, ATST-CTD-DPS)	3
US Army Aircraft Development Test Activity (PROV) (STEGB-CO-T, STEBG-PO, STEBG-MT)	5
US Army Agency for Aviation Safety (IGAR-TA, IGAR-Library)	2

US Army Maintenance Management Center (DRXMD-EA)	1
US Army Transportation School (ATSP-CD-MS)	1
US Army Logistics Management Center	1
US Army Foreign Science and Technology Center (AMXST-WS4)	1
US Military Academy	3
US Marine Corps Development and Education Command	2
US Naval Air Test Center	1
US Air Force Aeronautical Division (ASD-ENFTA)	1
US Air Force Flight Dynamics Laboratory (TST/Library)	1
US Air Force Flight Test Center (SSD/Technical Library (DOEE)	3
US Air Force Electronic Warfare Center (SURP)	1
Department of Transportation Library	1
US Army Bell Plan Activity (DAVBE-ES)	5
Bell Helicopter Textron	5
Thermo-Systems, Inc.	1
Defense Documentation Center	12